US 20110259544A1

(19) **United States**

(12) **Patent Application Publication**

Neti et al.

(10) **Pub. No.: US 2011/0259544 A1**

(43) **Pub. Date: Oct. 27, 2011**

(54) **ENCAPSULATED PHASE CHANGE APPARATUS FOR THERMAL ENERGY STORAGE**

(75) Inventors: **Sudhakar Neti**, Bethlehem, PA (US); **John C. Chen**, Bethlehem, PA (US); **Wojciech Z. Misiolek**, Hatfield, PA (US); **Alparslan Oztekin**, Allentown, PA (US); **Kemal Tuzla**, Allentown, PA (US)

(73) Assignee: **LEHIGH UNIVERSITY**, Bethlehem, PA (US)

(21) Appl. No.: **13/090,530**

(22) Filed: **Apr. 20, 2011**

Related U.S. Application Data

(60) Provisional application No. 61/326,412, filed on Apr. 21, 2010.

Publication Classification

(51) **Int. Cl.**
F28D 20/00 (2006.01)

(52) **U.S. Cl.** **165/10**

(57) **ABSTRACT**

Provided are apparatus and methods for storing thermal energy. For example, an apparatus including comprising at least one phase change material, and a capsule containing the at least one phase change material. The capsule may be permanently or temporarily sealed to contain the encapsulation material. The encapsulation material includes at least one material that is chemically and physically distinct from the phase change material. The encapsulation material and phase change material are selected to store and discharge thermal energy at temperatures of greater than 400° C. without capsule failure.

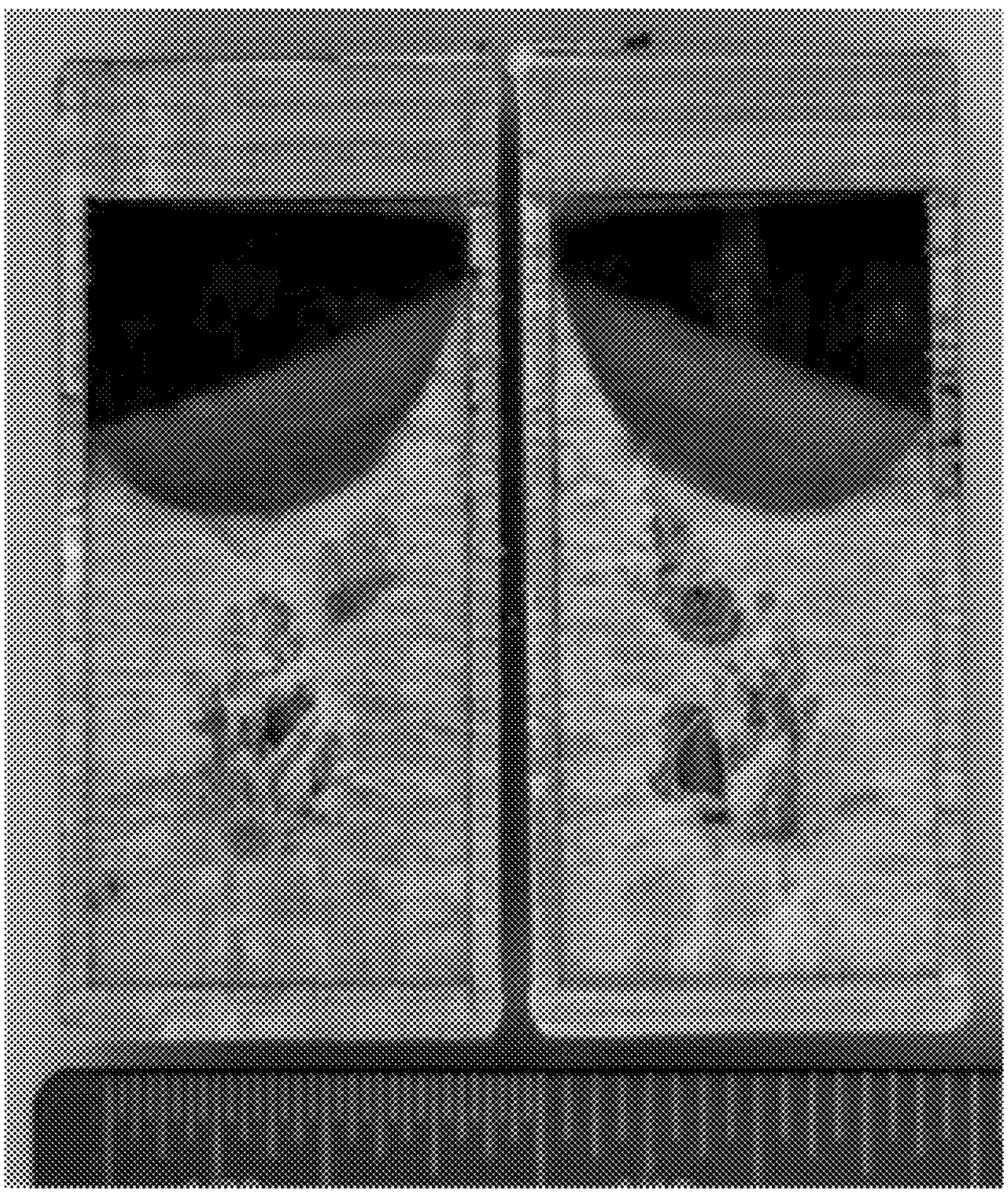

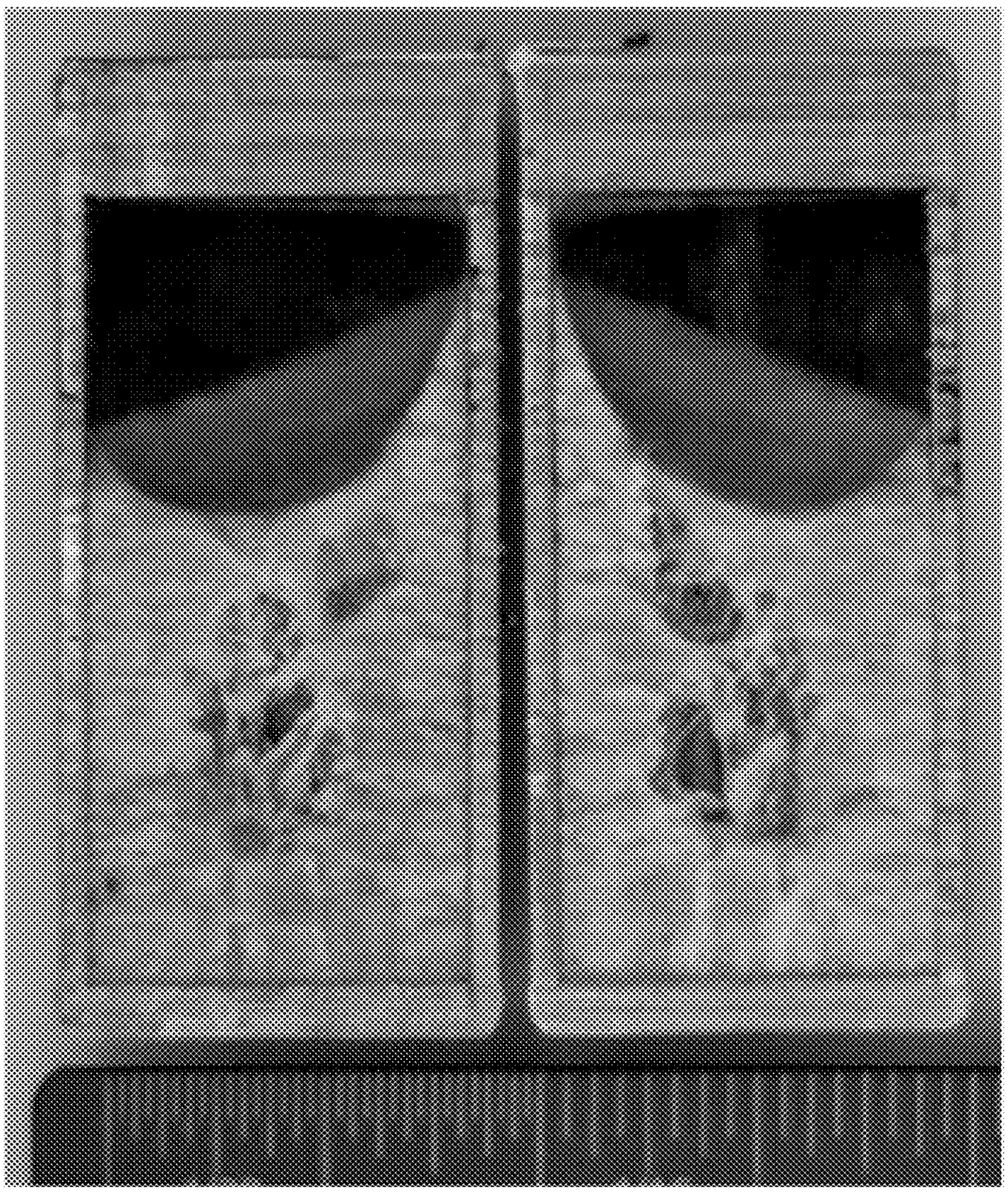

Figure 1

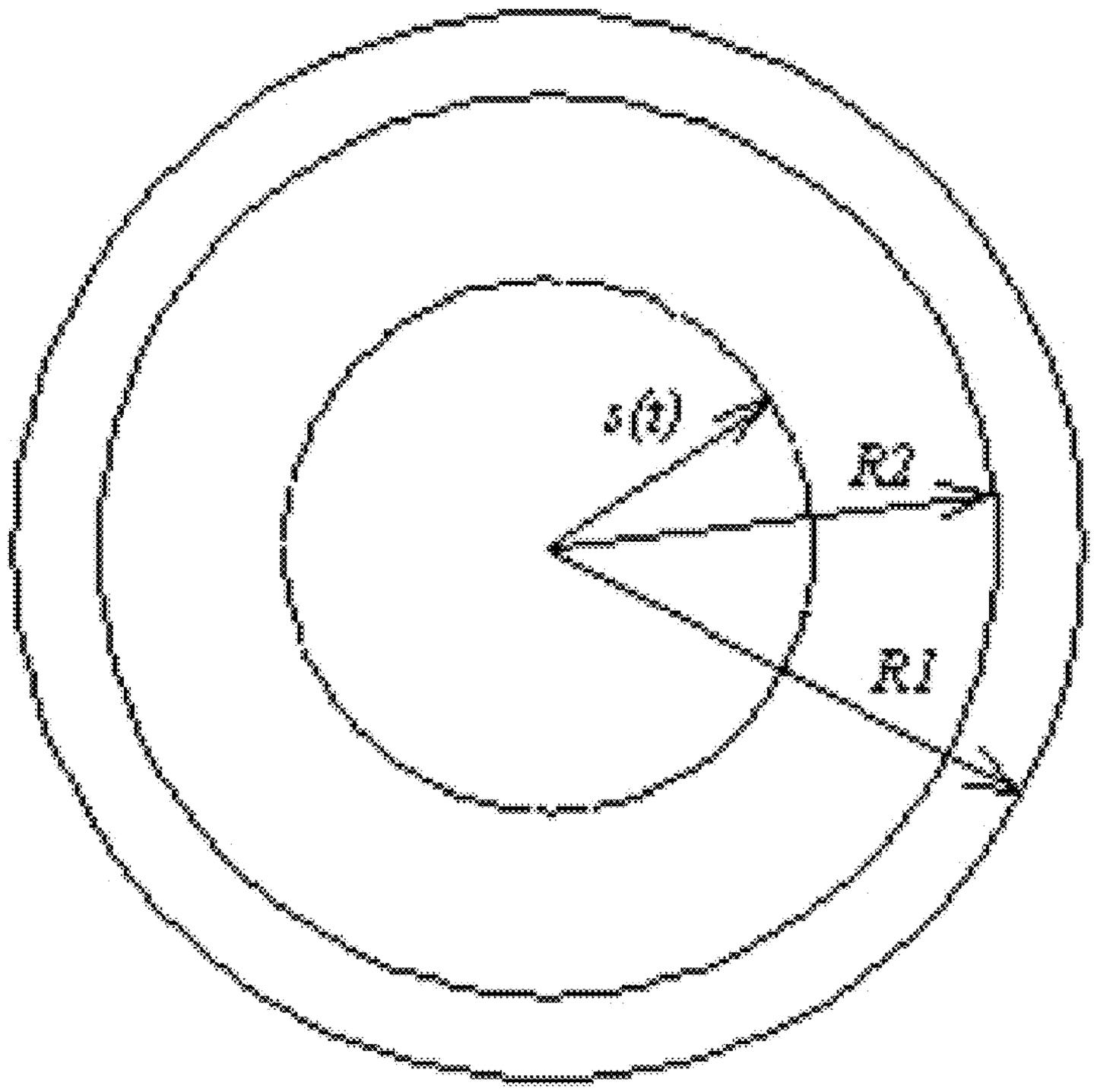

Figure 2

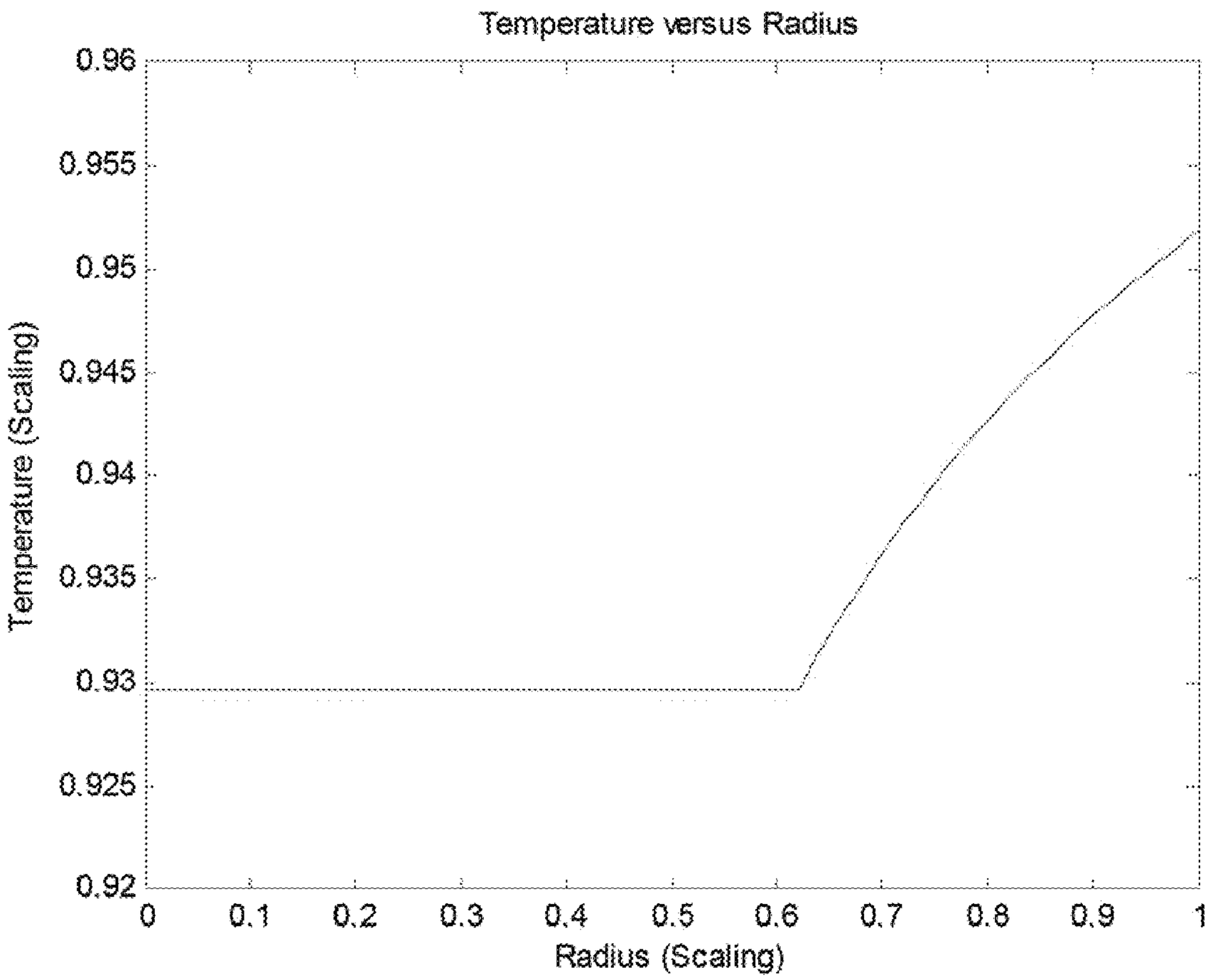
Temperature versus Radius
Temperature (Scaling)
Radius (Scaling)
0.96
0.955
0.95
0.945
0.94
0.935
0.93
0.925
0.92
0
0.1
0.2
0.3
0.4
0.5
0.6
0.7
0.8
0.9
1

Figure 3

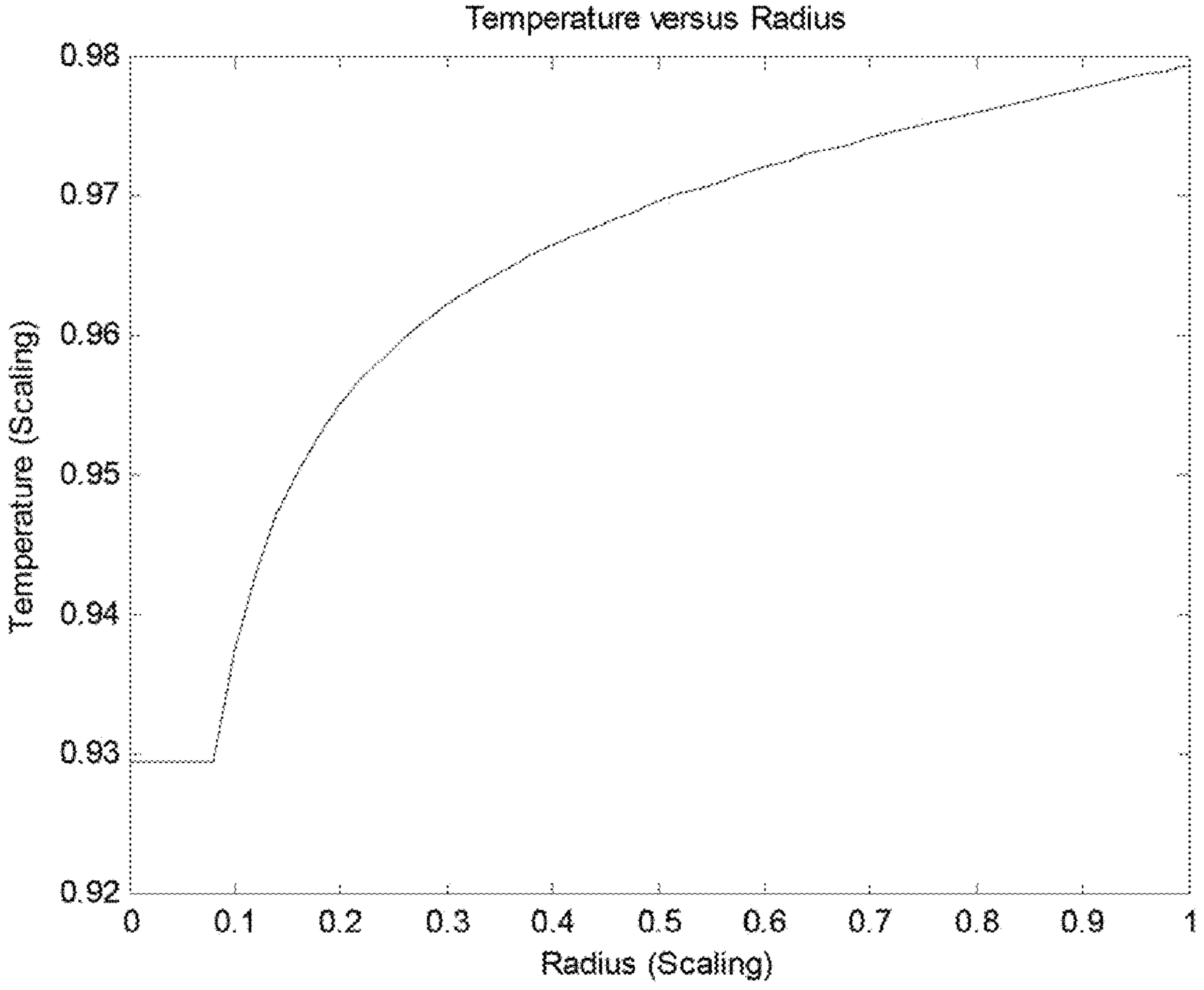
Temperature versus Radius
Temperature (Scaling)
0.98
0.97
0.96
0.95
0.94
0.93
0.92
0
0.1
0.2
0.3
0.4
0.5
0.6
0.7
0.8
0.9
1
Radius (Scaling)

Figure 4

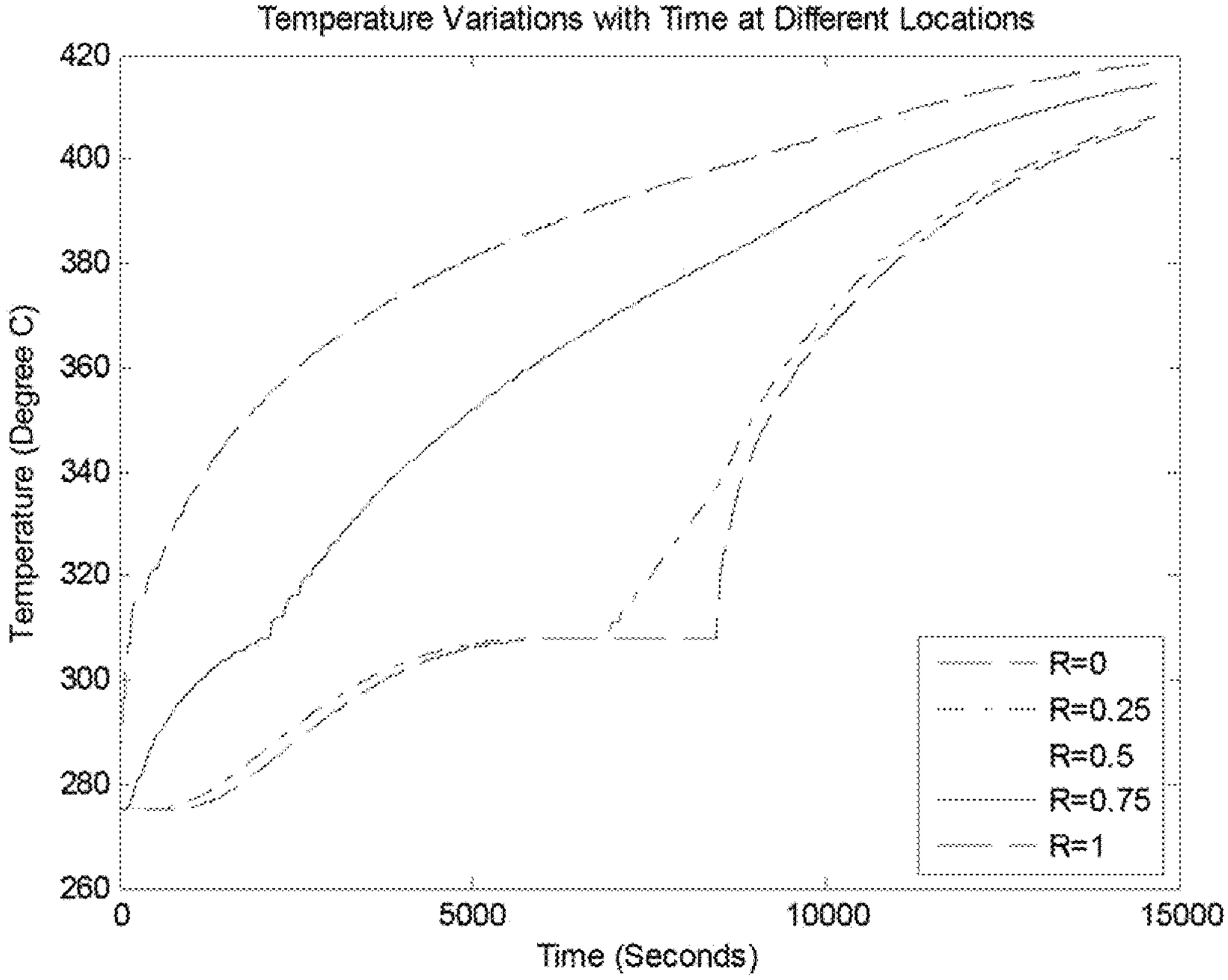
Temperature Variations with Time at Different Locations
Temperature (Degree C)
420
400
380
360
340
320
300
280
260
0
5000
10000
15000
Time (Seconds)
R=0
R=0.25
R=0.5
R=0.75
R=1

Figure 5

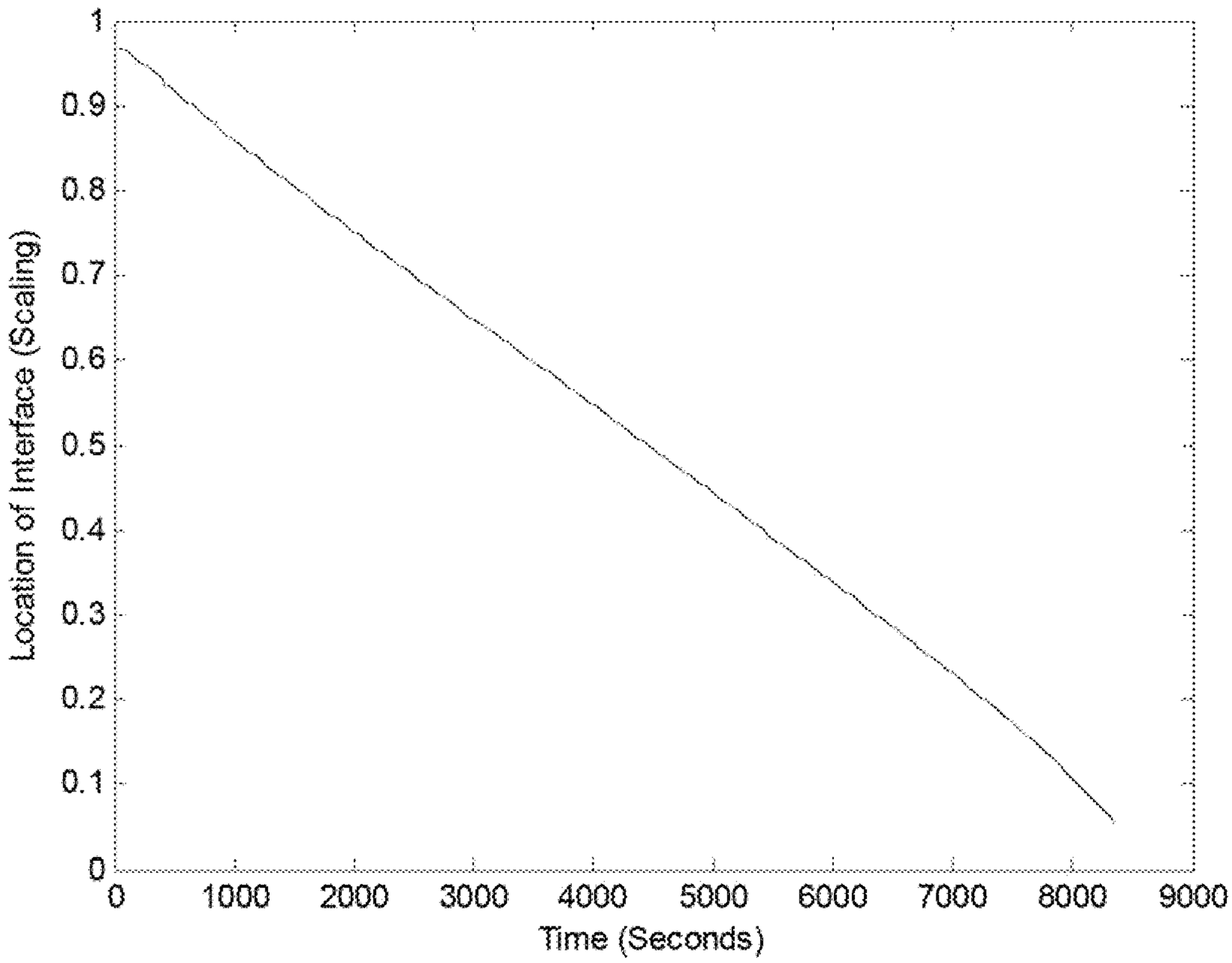
Location of Interface (Scaling)
Time (Seconds)
0
0.1
0.2
0.3
0.4
0.5
0.6
0.7
0.8
0.9
1
0
1000
2000
3000
4000
5000
6000
7000
8000
9000

Figure 6

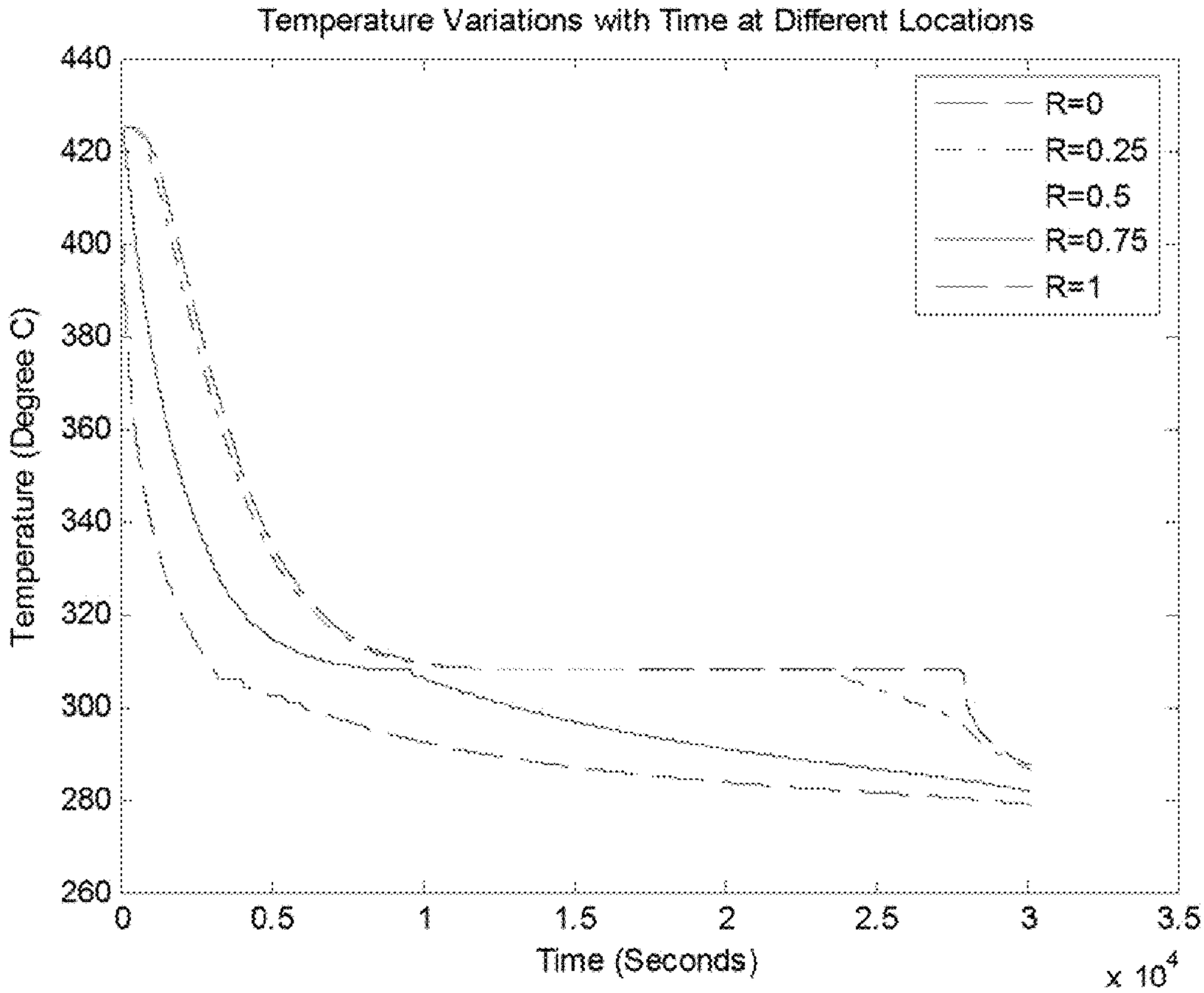
Temperature Variations with Time at Different Locations
Temperature (Degree C)
440
420
400
380
360
340
320
300
280
260
0
0.5
1
1.5
2
2.5
3
3.5
x 10^4
Time (Seconds)
R=0
R=0.25
R=0.5
R=0.75
R=1

Figure 7

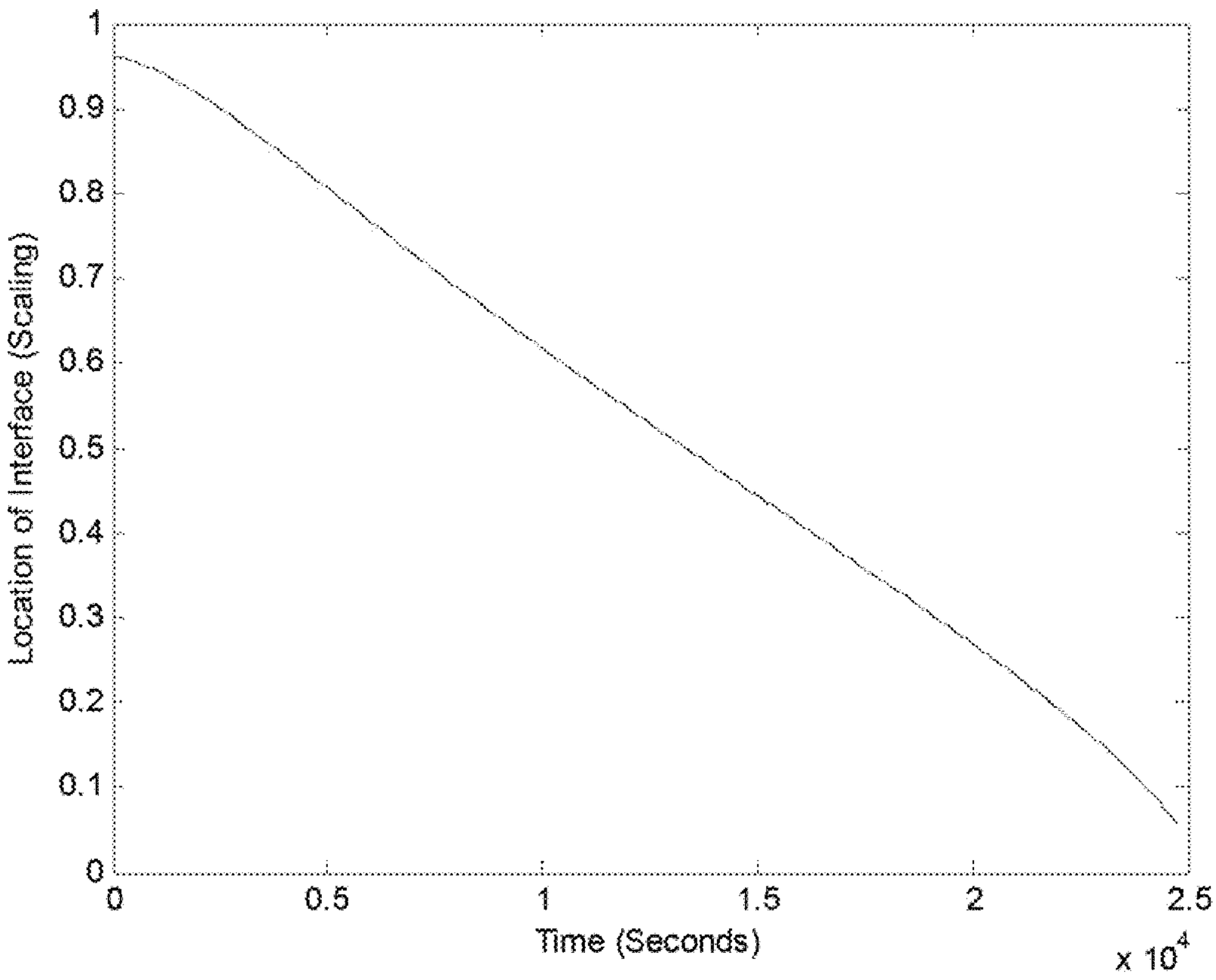
Location of Interface (Scaling)
0
0.1
0.2
0.3
0.4
0.5
0.6
0.7
0.8
0.9
1
0
0.5
1
1.5
2
2.5
Time (Seconds)
x 10^4

Figure 8

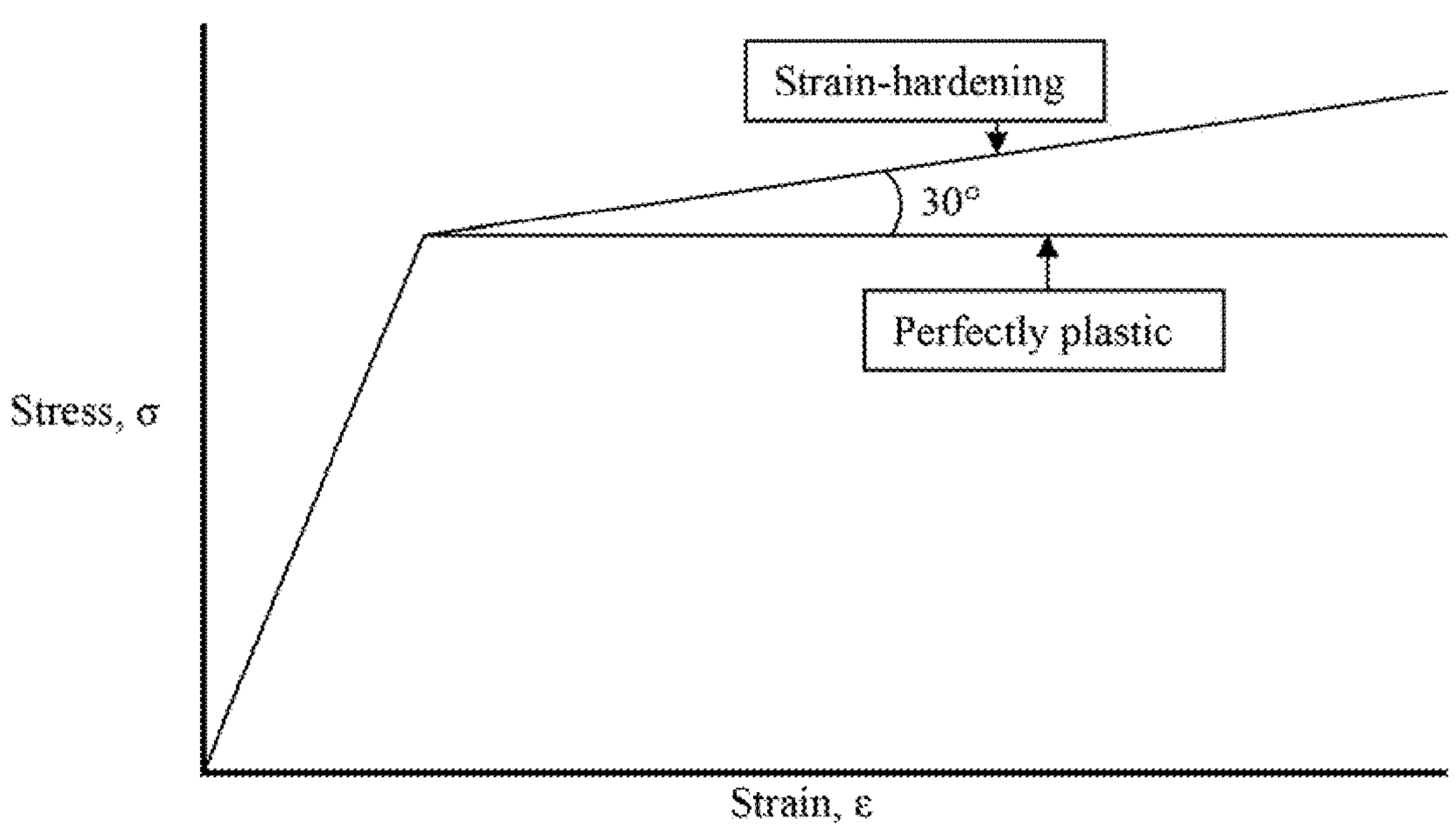

Figure 9

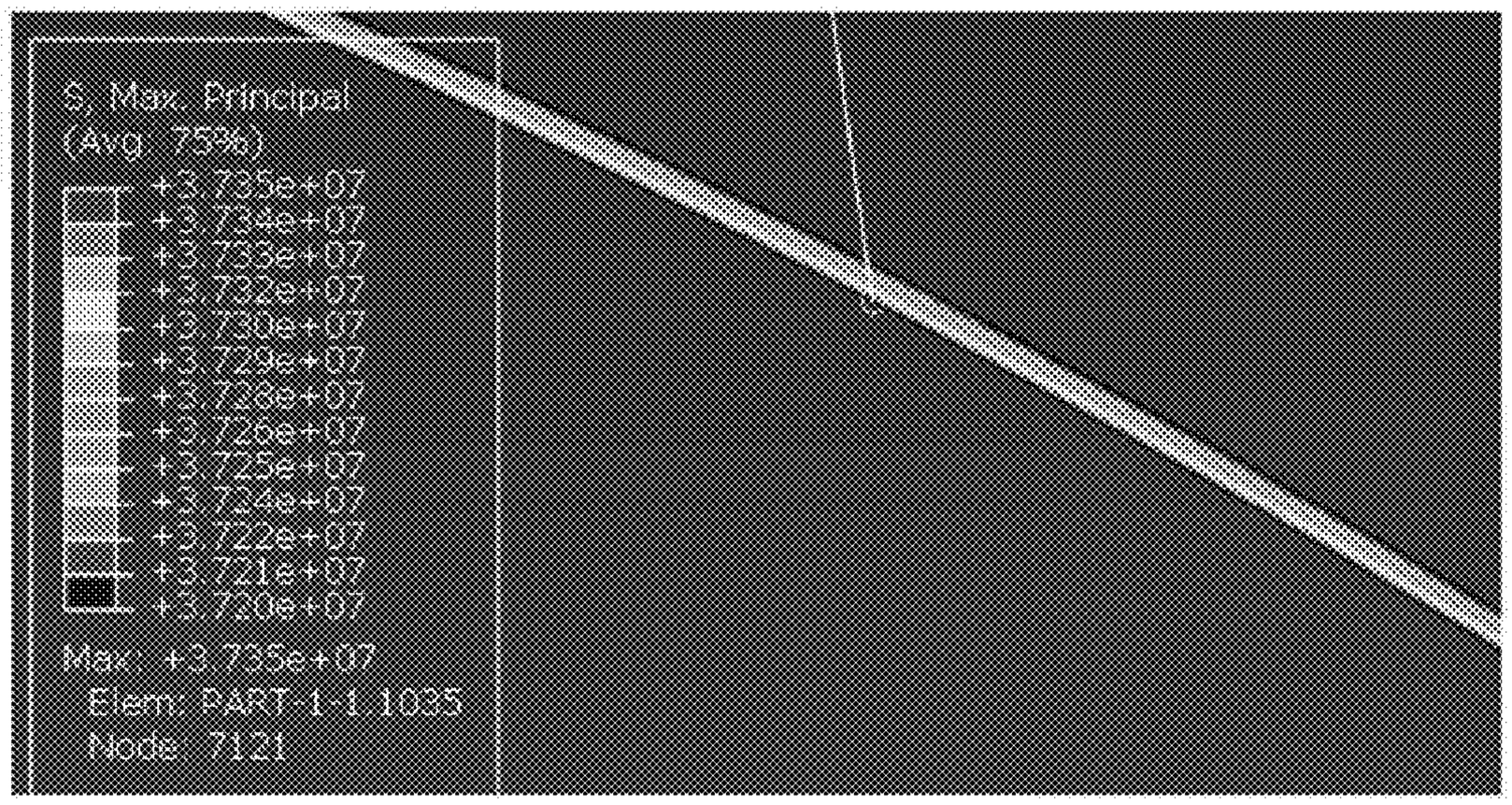
S, Max. Principal
(Avg: 75%)
+3.735e+07
+3.734e+07
+3.733e+07
+3.732e+07
+3.730e+07
+3.729e+07
+3.728e+07
+3.726e+07
+3.725e+07
+3.724e+07
+3.722e+07
+3.721e+07
+3.720e+07
Max: +3.735e+07
Elem: PART-1-1.1035
Node: 7121

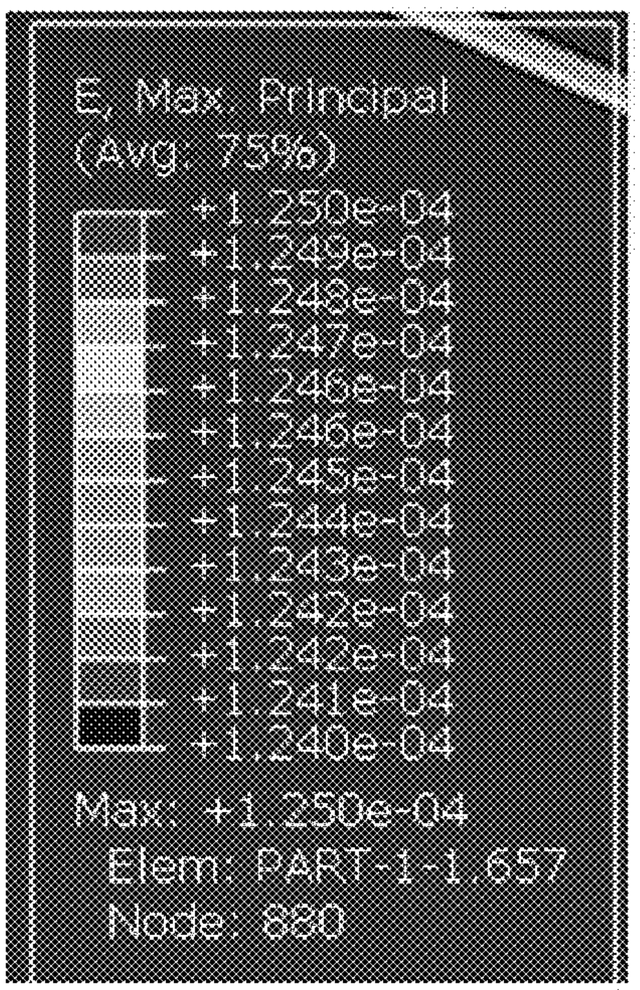
E, Max. Principal
(Avg: 75%)
+1.250e-04
+1.249e-04
+1.248e-04
+1.247e-04
+1.246e-04
+1.246e-04
+1.245e-04
+1.244e-04
+1.243e-04
+1.242e-04
+1.242e-04
+1.241e-04
+1.240e-04
Max: +1.250e-04
Elem: PART-1-1.657
Node: 880

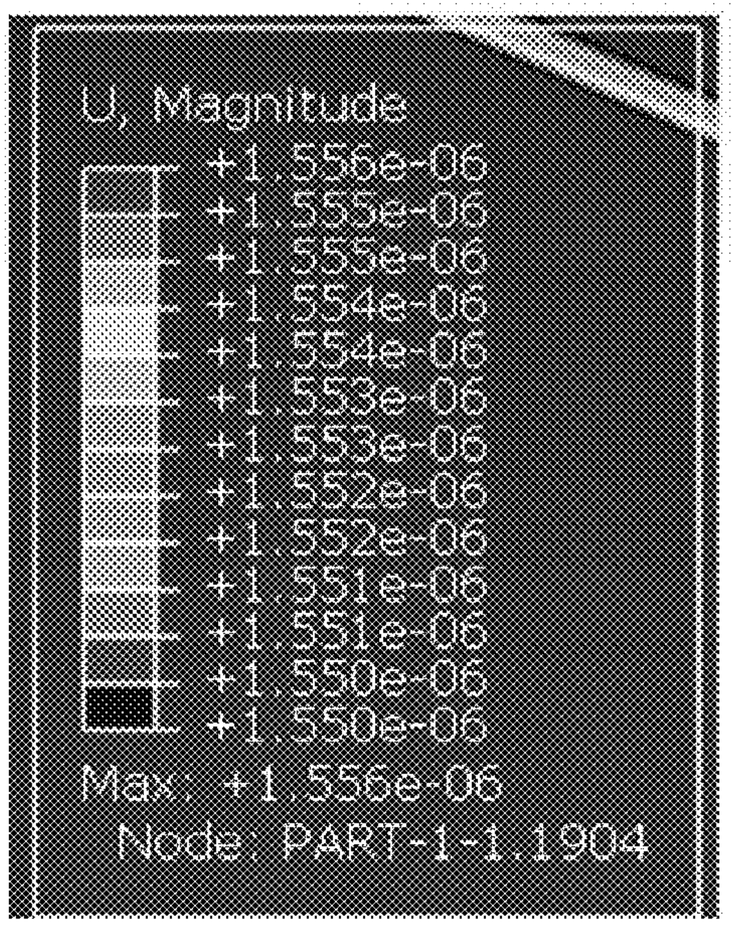
U, Magnitude
+1.556e-06
+1.555e-06
+1.555e-06
+1.554e-06
+1.554e-06
+1.553e-06
+1.553e-06
+1.552e-06
+1.552e-06
+1.551e-06
+1.551e-06
+1.550e-06
+1.550e-06
Max: +1.556e-06
Node: PART-1-1.1904

Figure 10

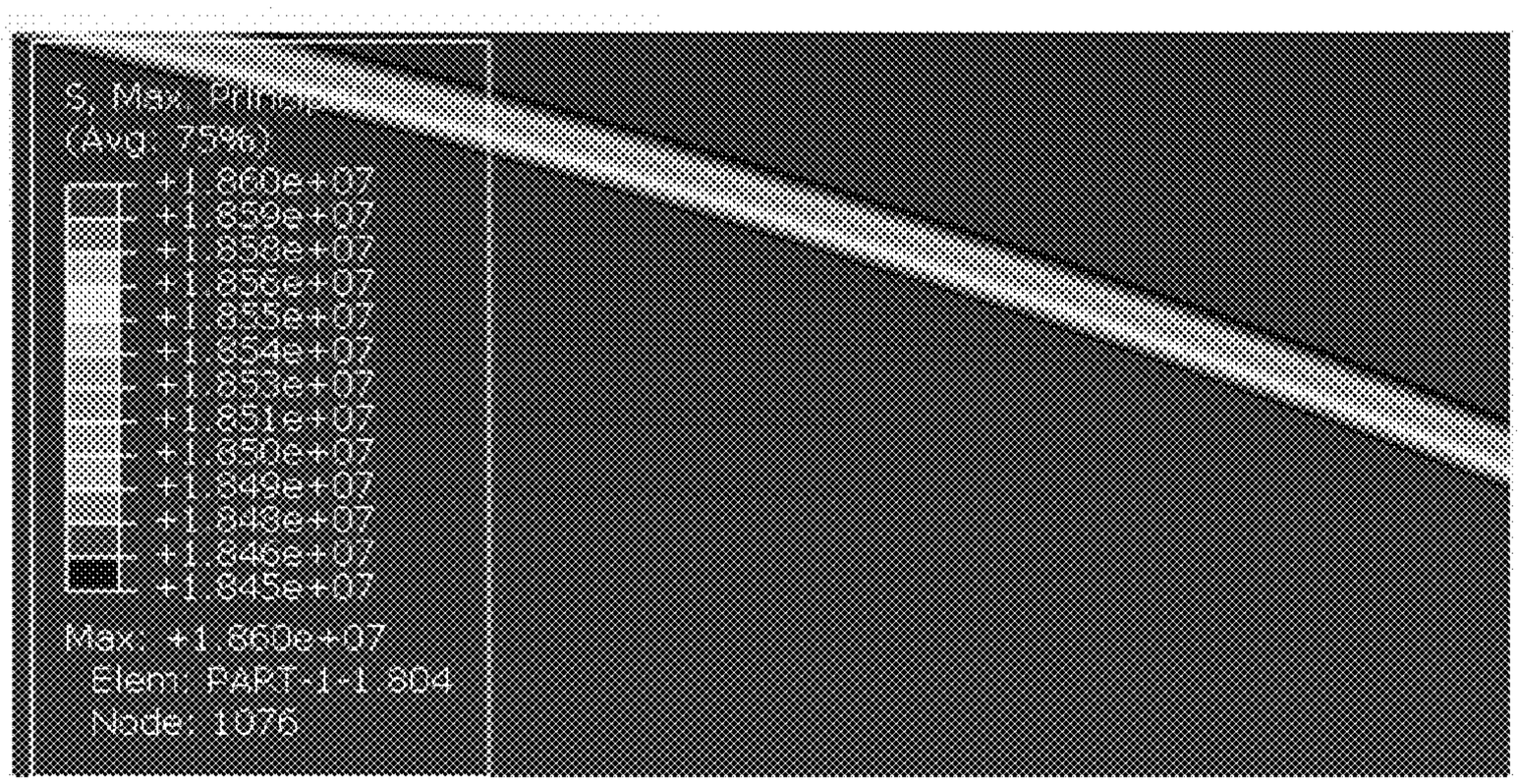
S, Max. Princ
(Avg: 75%)
+1.860e+07
+1.859e+07
+1.858e+07
+1.856e+07
+1.855e+07
+1.854e+07
+1.853e+07
+1.851e+07
+1.850e+07
+1.849e+07
+1.848e+07
+1.846e+07
+1.845e+07
Max: +1.860e+07
Elem: PART-1-1.804
Node: 1076

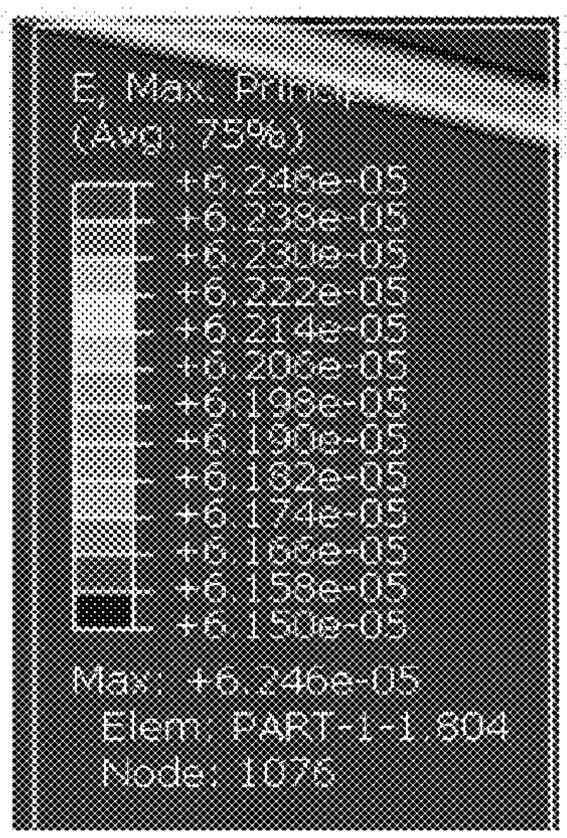
E, Max. Princ
(Avg: 75%)
+6.246e-05
+6.238e-05
+6.230e-05
+6.222e-05
+6.214e-05
+6.206e-05
+6.198e-05
+6.190e-05
+6.182e-05
+6.174e-05
+6.166e-05
+6.158e-05
+6.150e-05
Max: +6.246e-05
Elem: PART-1-1.804
Node: 1076

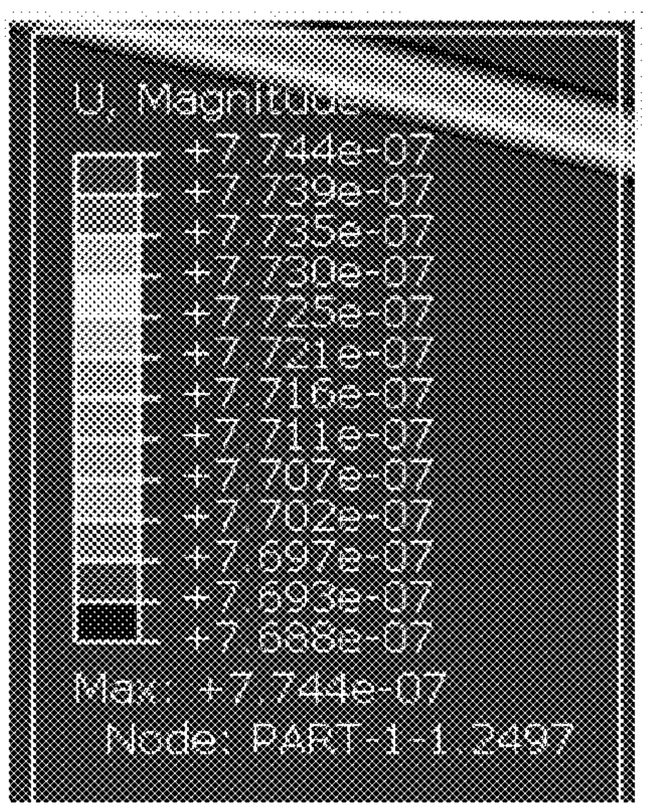
U, Magnitude
+7.744e-07
+7.739e-07
+7.735e-07
+7.730e-07
+7.725e-07
+7.721e-07
+7.716e-07
+7.711e-07
+7.707e-07
+7.702e-07
+7.697e-07
+7.693e-07
+7.688e-07
Max: +7.744e-07
Node: PART-1-1.2497

Figure 11

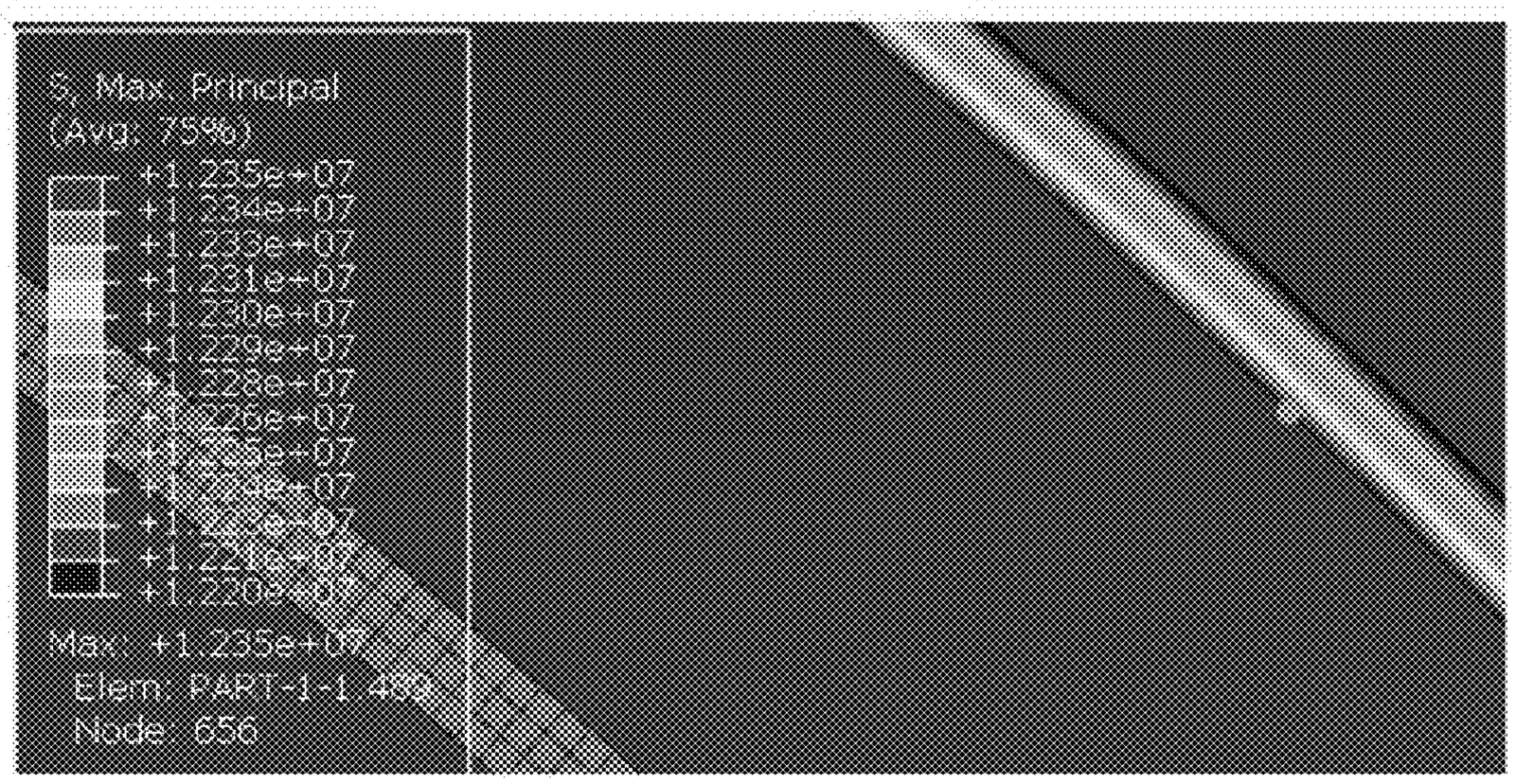
S, Max. Principal
(Avg: 75%)
+1.235e+07
+1.234e+07
+1.233e+07
+1.231e+07
+1.230e+07
+1.229e+07
+1.228e+07
+1.226e+07
+1.225e+07
+1.224e+07
+1.223e+07
Max: +1.235e+07
Elem: PART-1-1.493
Node: 656

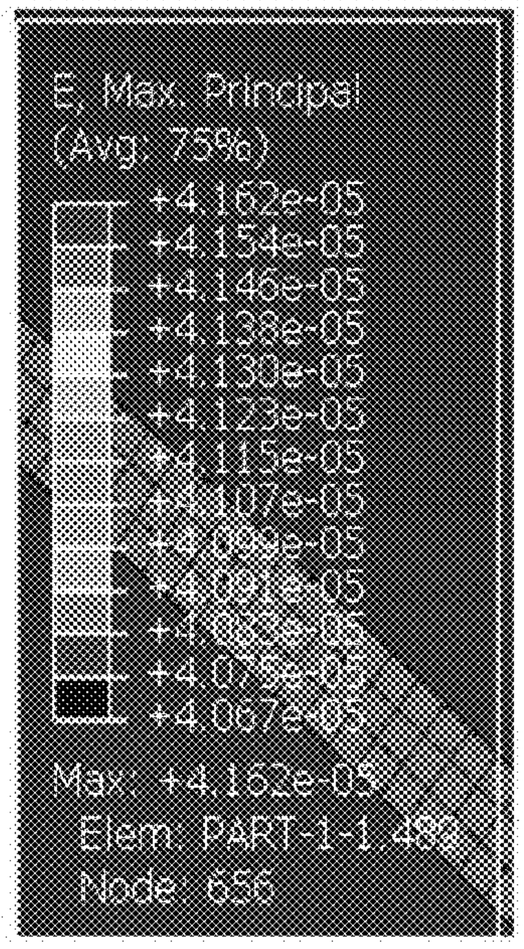
E, Max. Principal
(Avg: 75%)
+4.162e-05
+4.154e-05
+4.146e-05
+4.138e-05
+4.130e-05
+4.123e-05
+4.115e-05
+4.107e-05
+4.099e-05
+4.091e-05
+4.083e-05
+4.075e-05
+4.067e-05
Max: +4.162e-05
Elem: PART-1-1.493
Node: 656

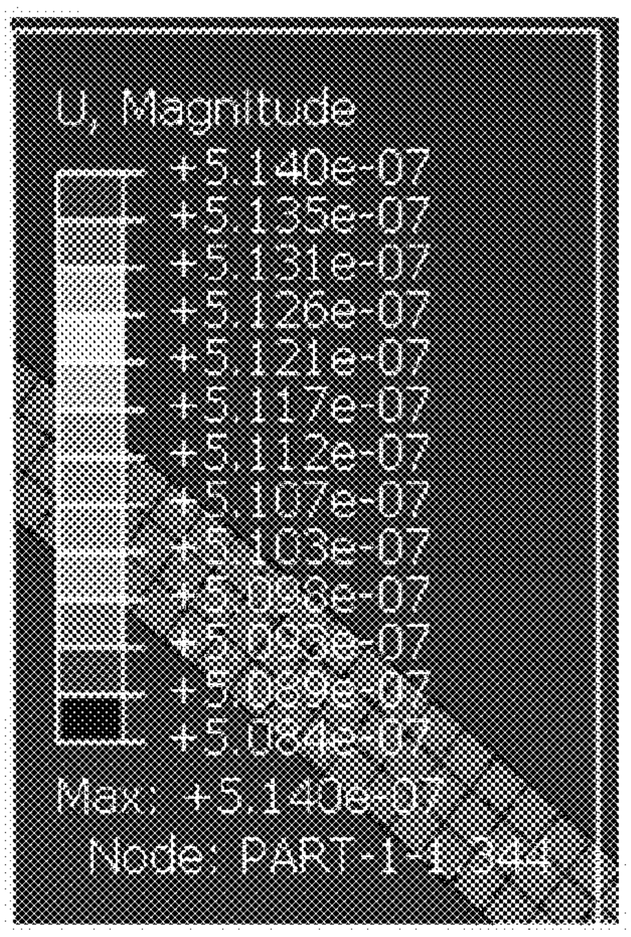
U, Magnitude
+5.140e-07
+5.135e-07
+5.131e-07
+5.126e-07
+5.121e-07
+5.117e-07
+5.112e-07
+5.107e-07
+5.103e-07
+5.098e-07
+5.093e-07
+5.089e-07
+5.084e-07
Max: +5.140e-07
Node: PART-1-1.244

Figure 12

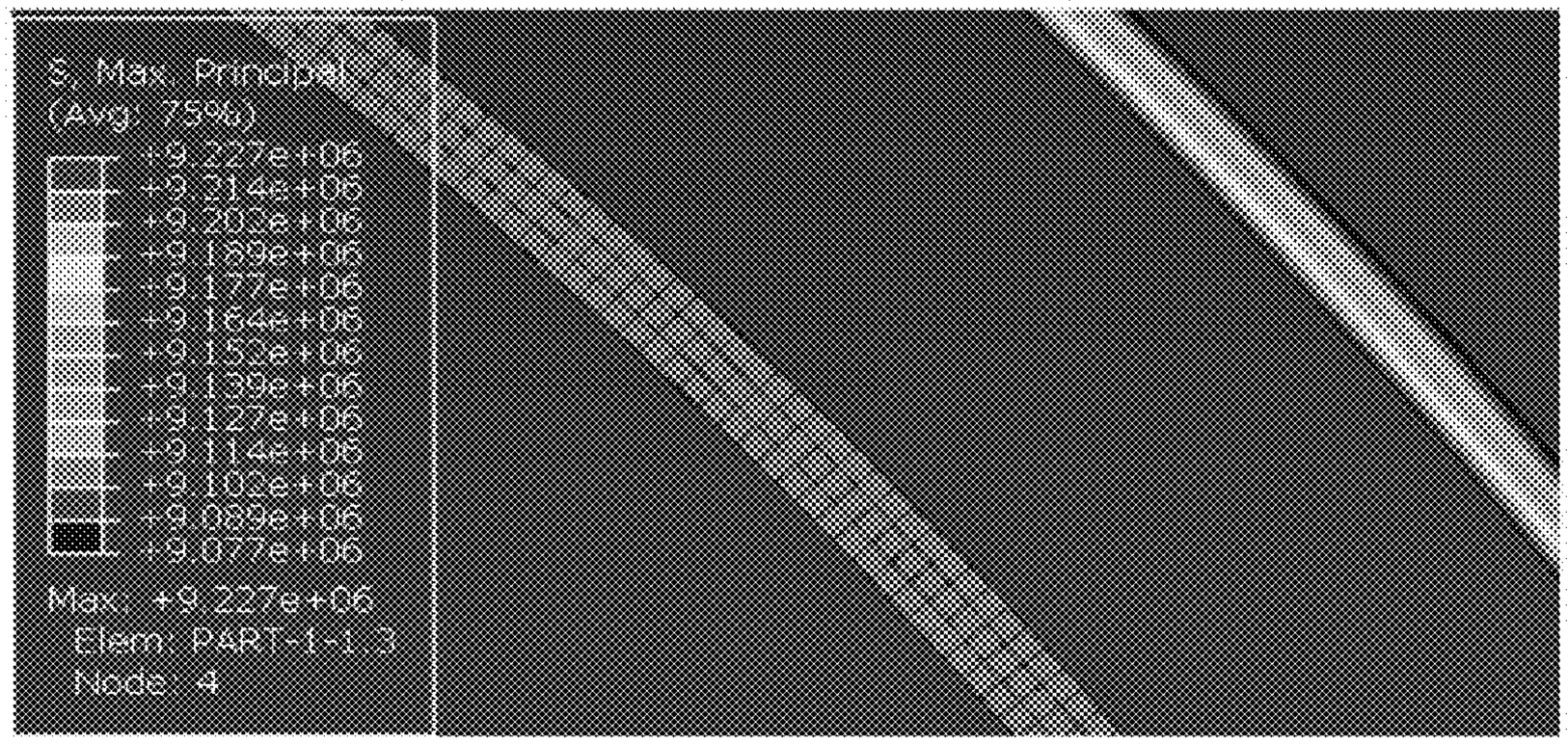
S, Max. Principal
(Avg: 75%)
+9.227e+06
+9.214e+06
+9.202e+06
+9.189e+06
+9.177e+06
+9.164e+06
+9.152e+06
+9.139e+06
+9.127e+06
+9.114e+06
+9.102e+06
+9.089e+06
+9.077e+06
Max: +9.227e+06
Elem: PART-1-1.3
Node: 4

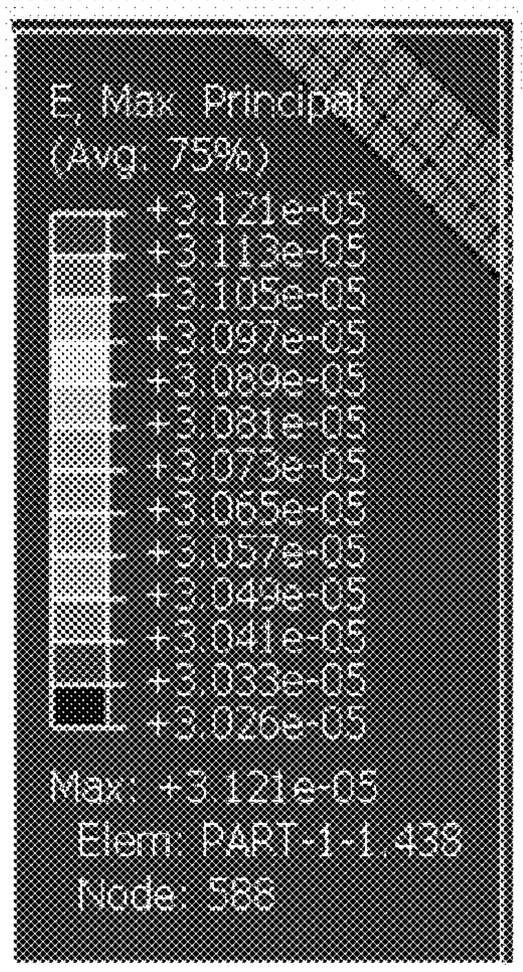
E, Max. Principal
(Avg: 75%)
+3.121e-05
+3.113e-05
+3.105e-05
+3.097e-05
+3.089e-05
+3.081e-05
+3.073e-05
+3.065e-05
+3.057e-05
+3.049e-05
+3.041e-05
+3.033e-05
+3.026e-05
Max: +3.121e-05
Elem: PART-1-1.438
Node: 586

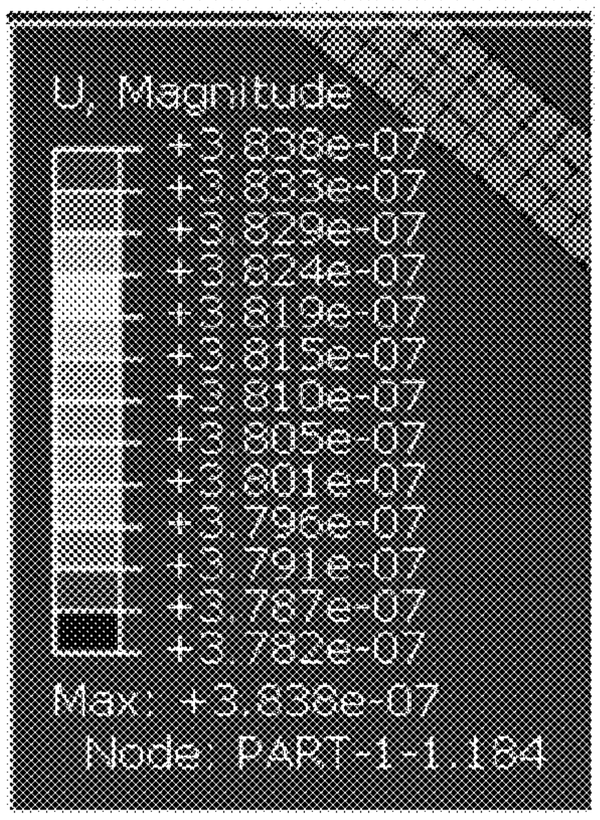
U, Magnitude
+3.838e-07
+3.833e-07
+3.829e-07
+3.824e-07
+3.819e-07
+3.815e-07
+3.810e-07
+3.805e-07
+3.801e-07
+3.796e-07
+3.791e-07
+3.787e-07
+3.782e-07
Max: +3.838e-07
Node: PART-1-1.184

Figure 13

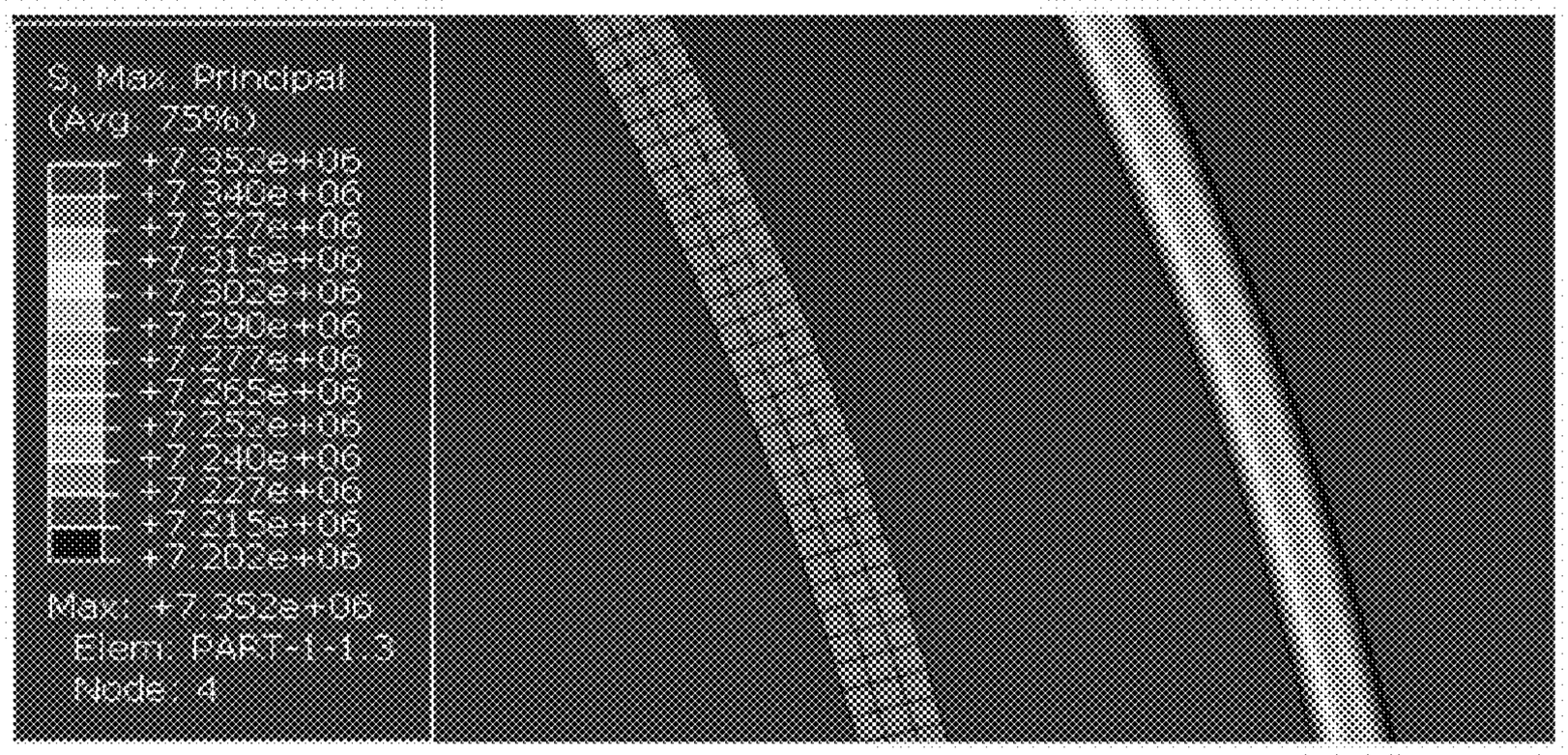
S, Max. Principal
(Avg: 75%)
+7.352e+05
+7.340e+06
+7.327e+06
+7.315e+06
+7.302e+06
+7.290e+06
+7.277e+06
+7.265e+06
+7.252e+06
+7.240e+06
+7.227e+06
+7.215e+06
+7.203e+06
Max: +7.352e+05
Elem: PART-1-1.3
Node: 4

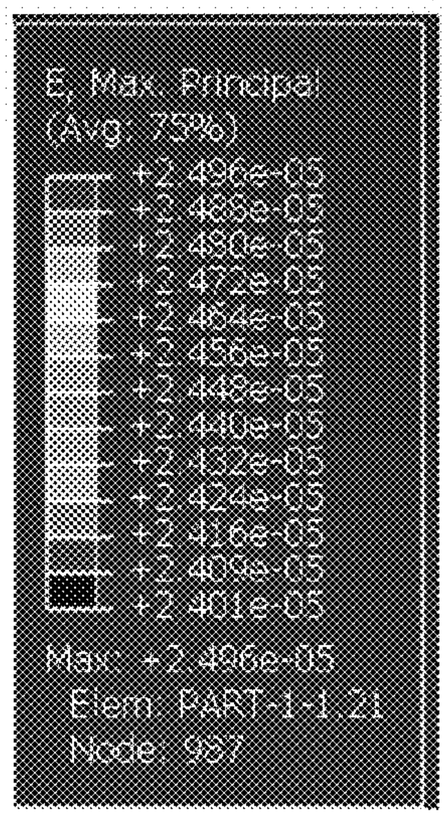
E, Max. Principal
(Avg: 75%)
+2.496e-05
+2.488e-05
+2.480e-05
+2.472e-05
+2.464e-05
+2.456e-05
+2.448e-05
+2.440e-05
+2.432e-05
+2.424e-05
+2.416e-05
+2.409e-05
+2.401e-05
Max: +2.496e-05
Elem: PART-1-1.21
Node: 987

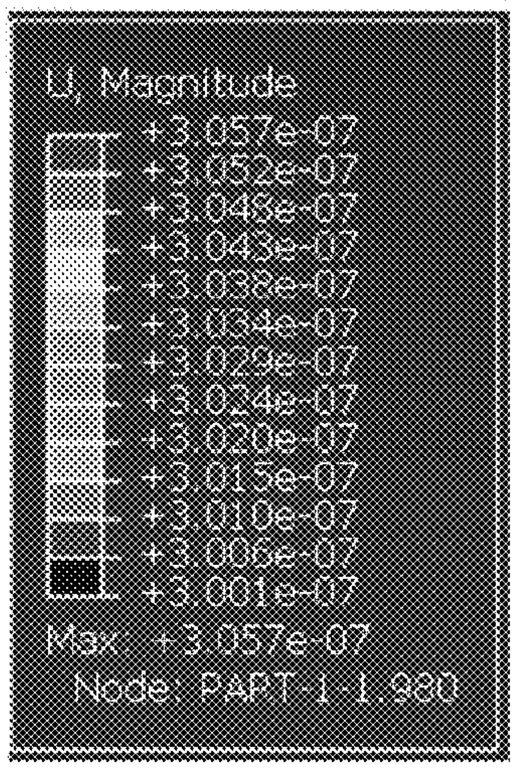
U, Magnitude
+3.057e-07
+3.052e-07
+3.048e-07
+3.043e-07
+3.038e-07
+3.034e-07
+3.029e-07
+3.024e-07
+3.020e-07
+3.015e-07
+3.010e-07
+3.006e-07
+3.001e-07
Max: +3.057e-07
Node: PART-1-1.980

Figure 14

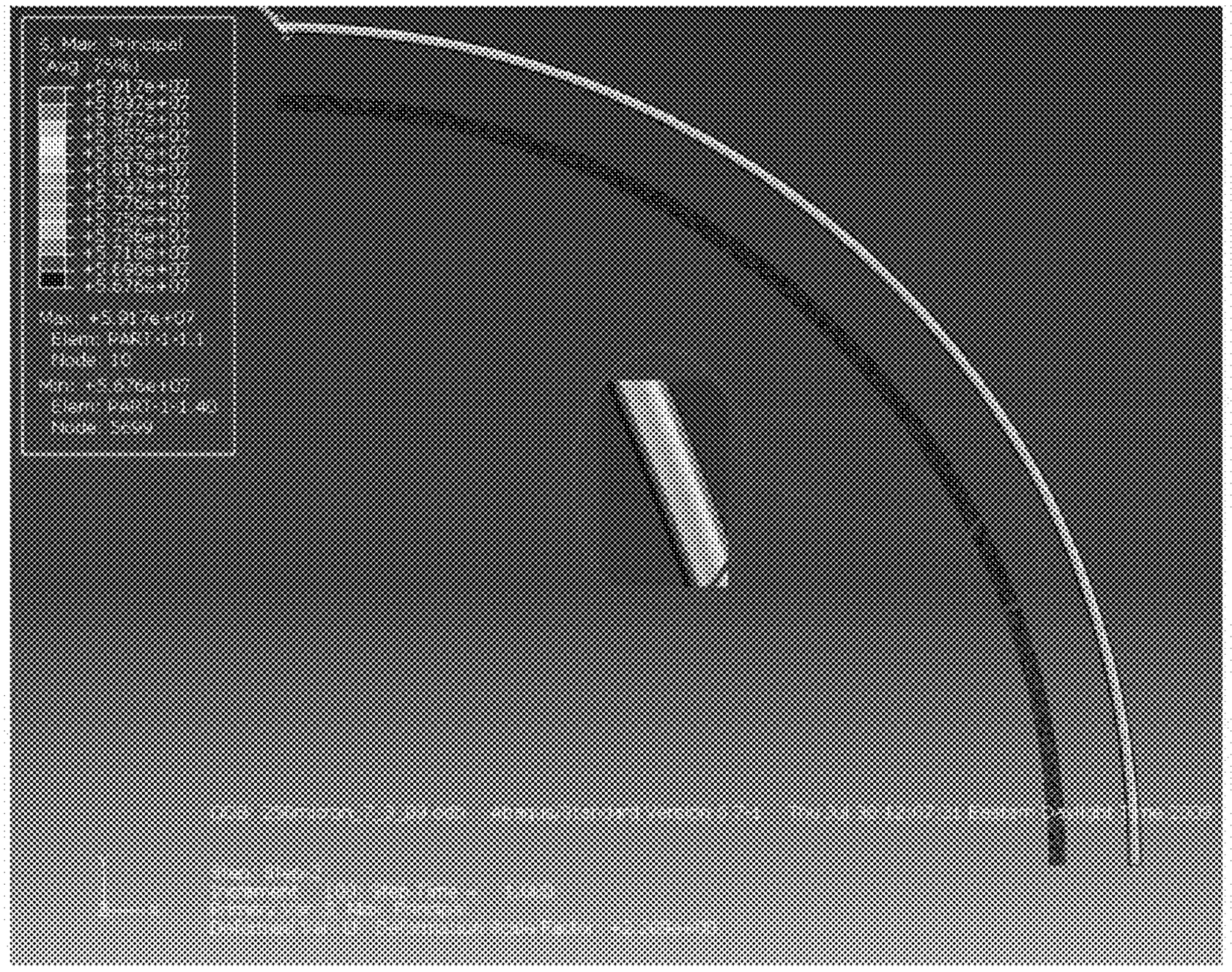
S, Max. Principal
Avg: 75%
+5.912e+07
+5.693e+07
+5.474e+07
+5.255e+07
+5.036e+07
+4.817e+07
+4.598e+07
+4.379e+07
+4.160e+07
+3.941e+07
+3.722e+07
+3.503e+07
+3.284e+07
+3.065e+07
+2.846e+07
+2.627e+07
Max: +5.912e+07
Elem: Part1-3-1-1
Node: 10
Min: +2.627e+07
Elem: Part1-1-1-48
Node: 3409

Figure 15

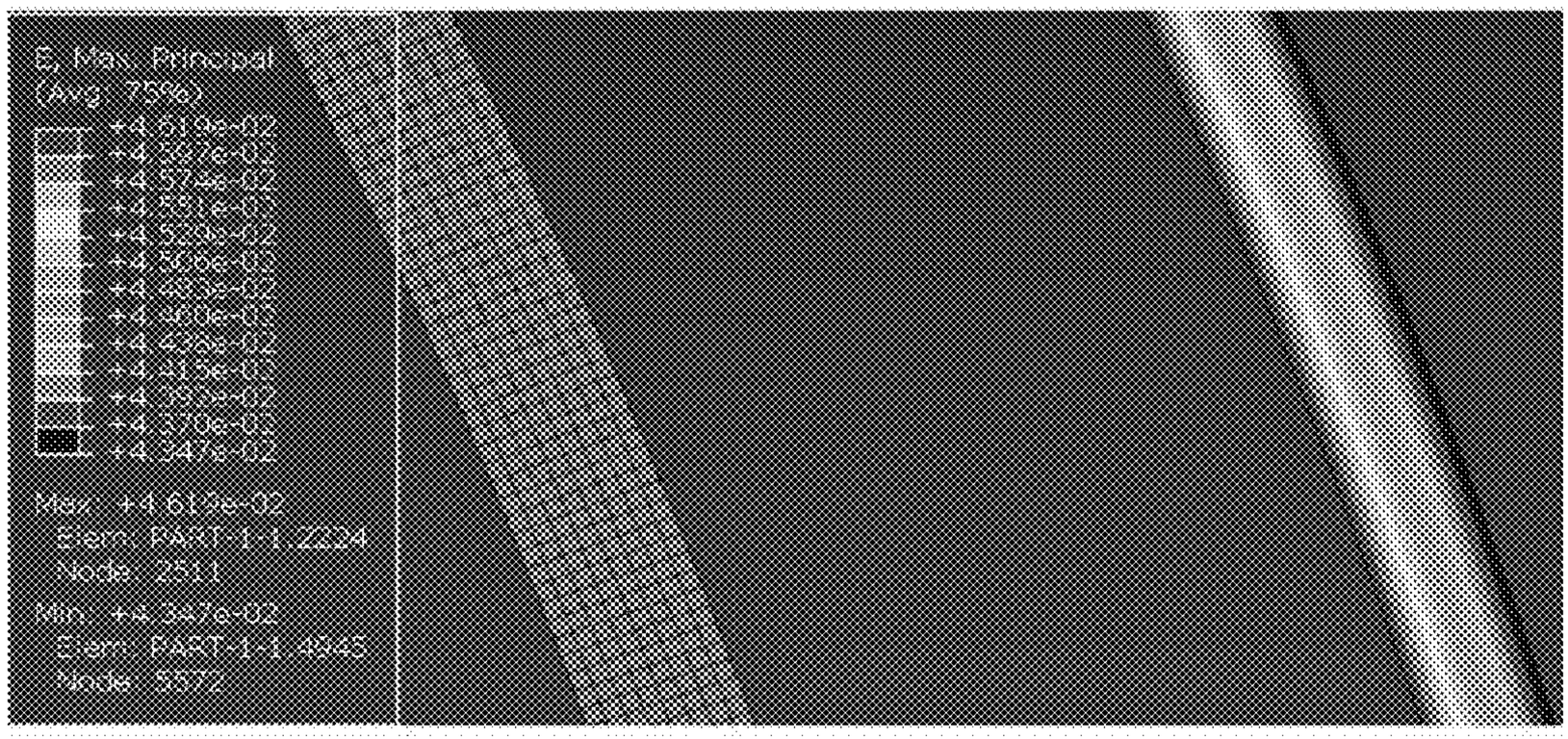

Figure 16

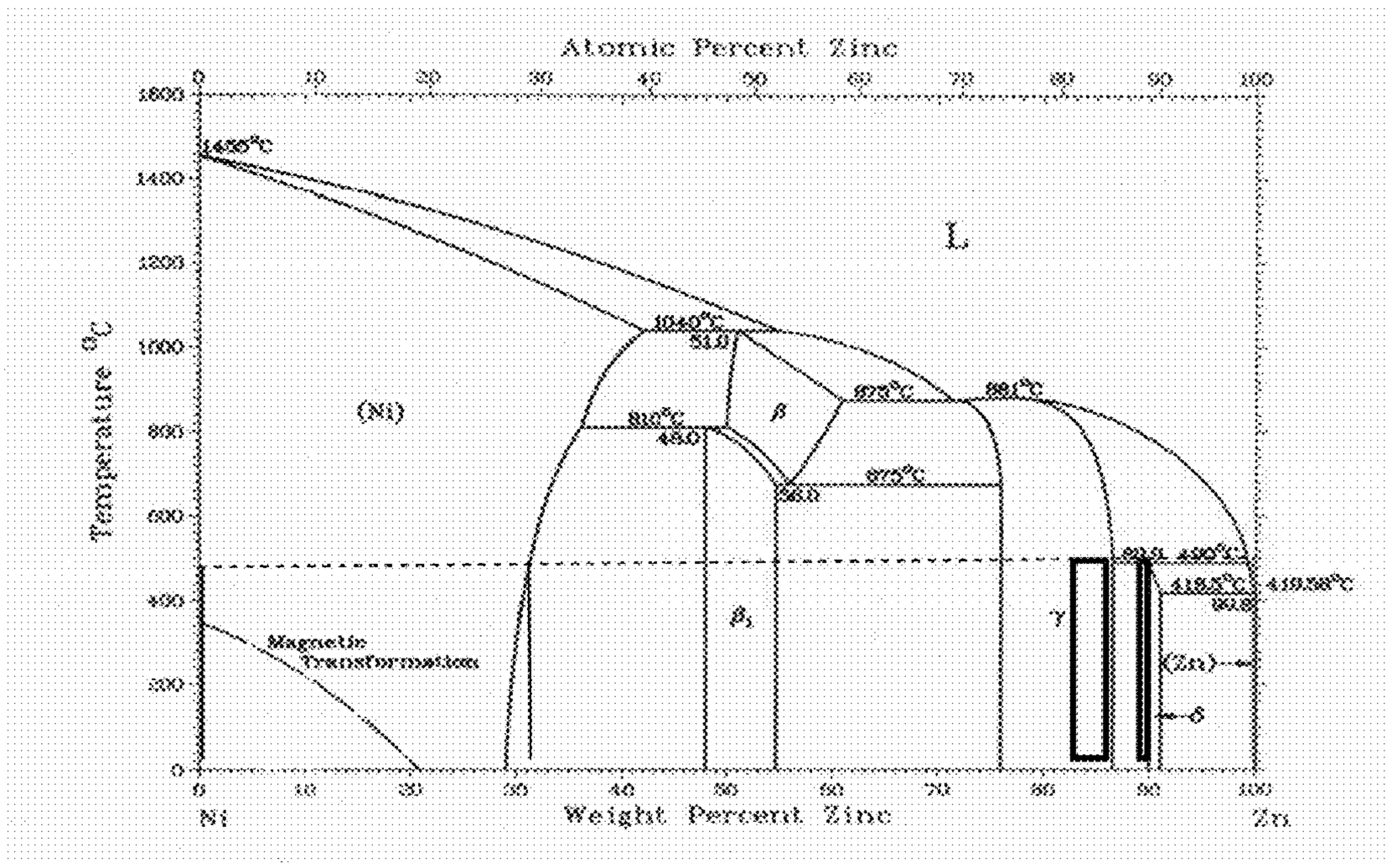

Figure 17

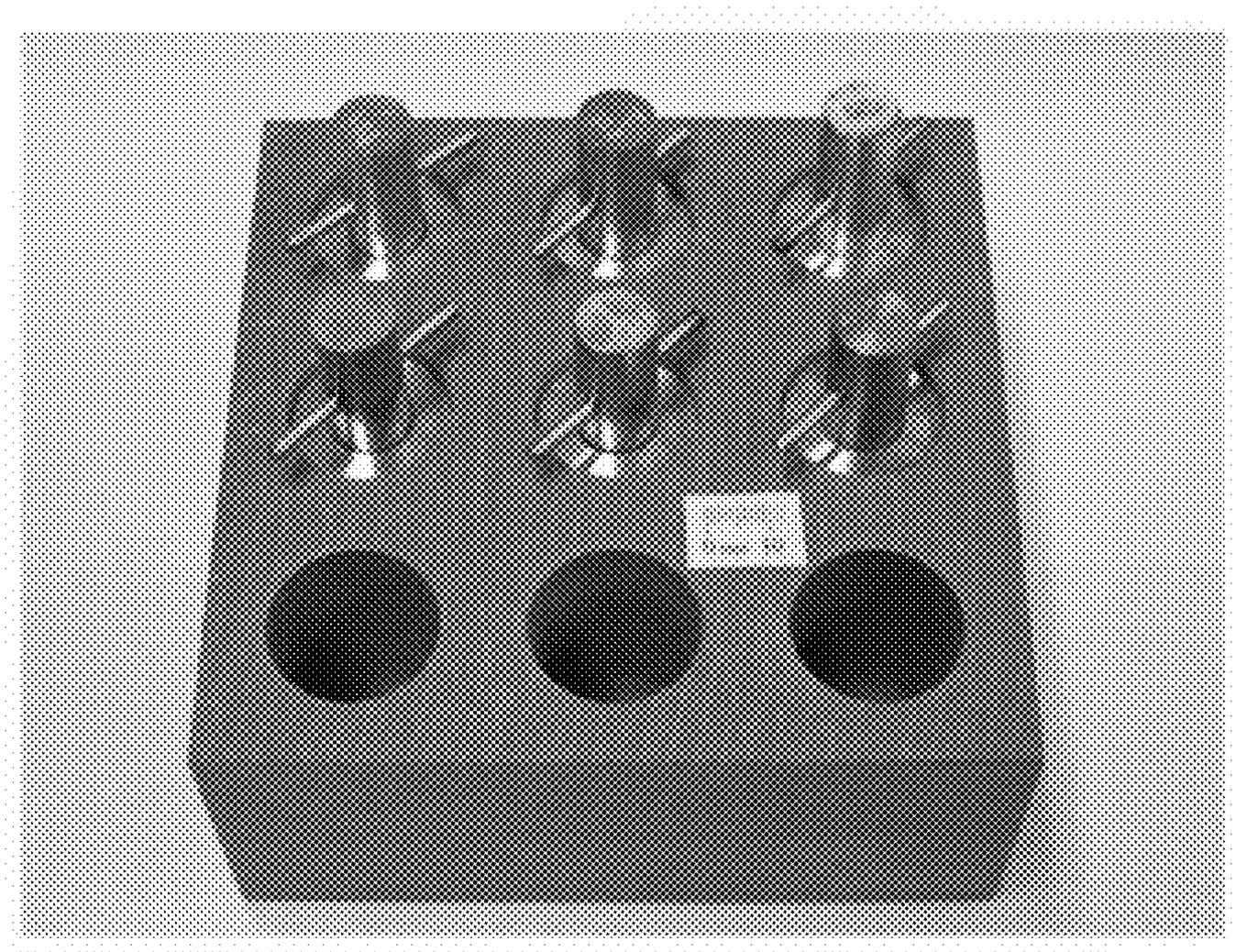

Figure 18

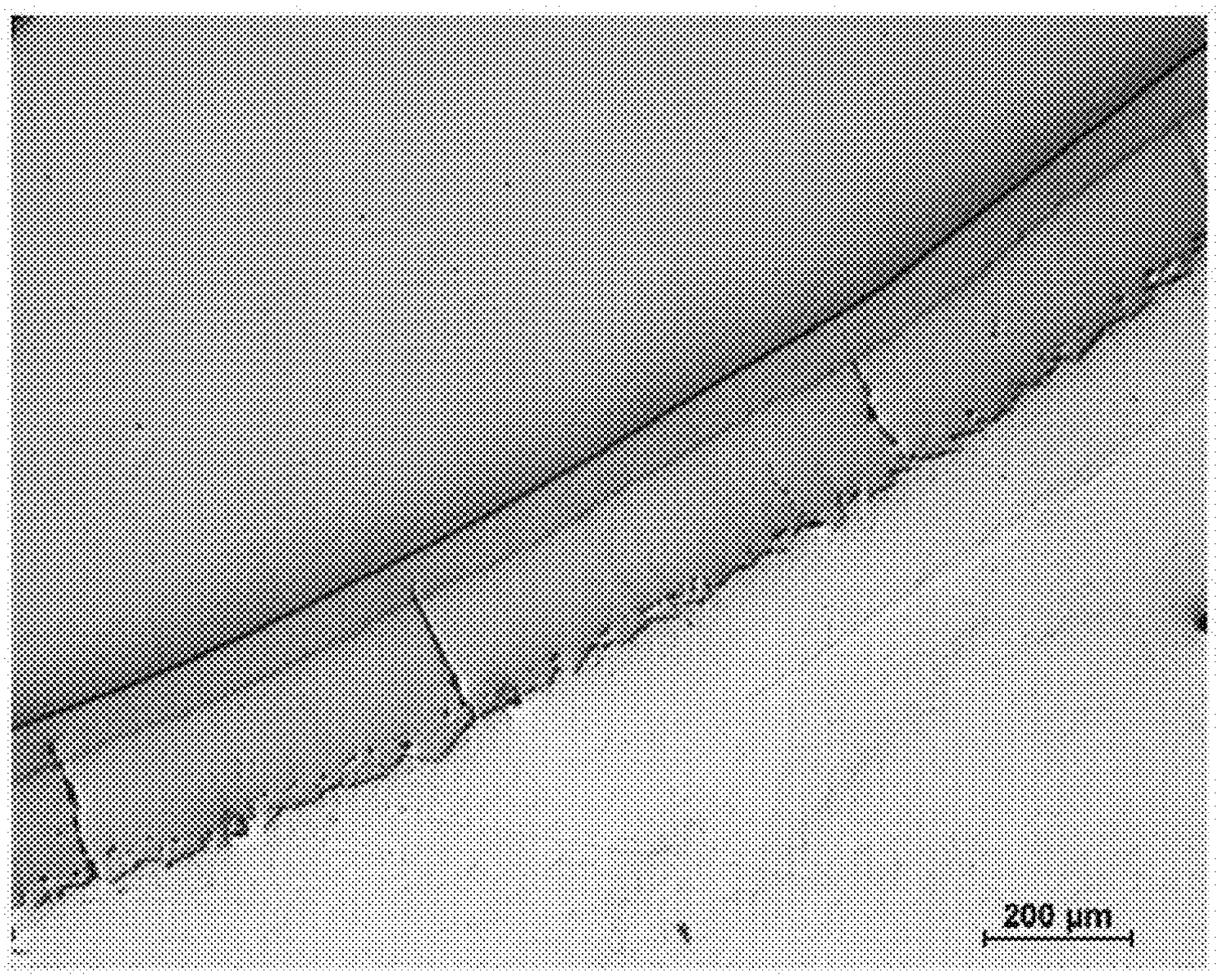

Figure 19

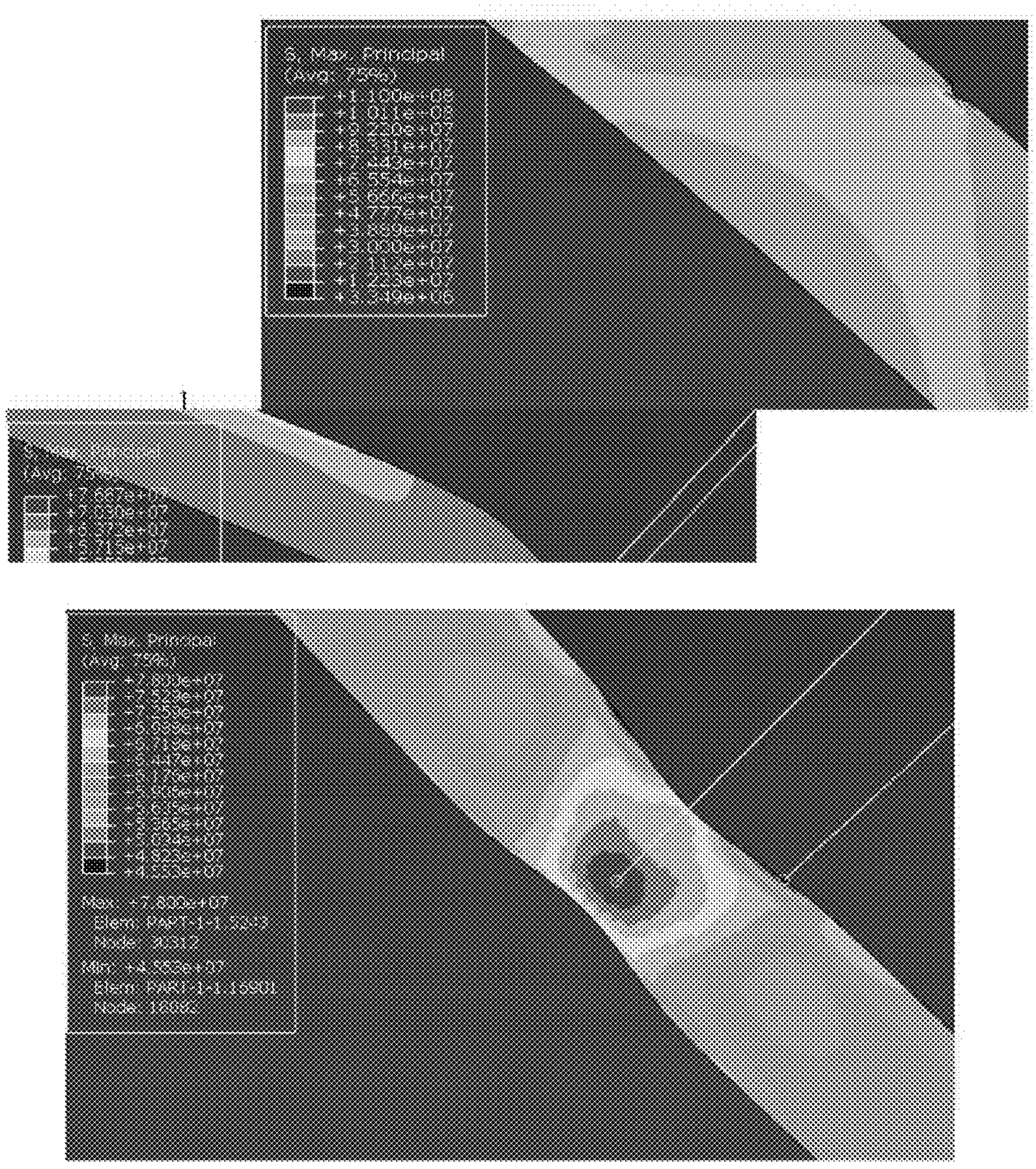
S, Max. Principal
(Avg: 75%)
+1.100e+08
+1.011e+08
+9.220e+07
+8.331e+07
+7.442e+07
+6.554e+07
+5.665e+07
+4.777e+07
+3.888e+07
+3.000e+07
+2.111e+07
+1.222e+07
+3.334e+06
S, Max. Principal
(Avg: 75%)
+7.667e+07
+7.556e+07
+7.445e+07
+7.334e+07
S, Max. Principal
(Avg: 75%)
+7.800e+07
+7.689e+07
+7.578e+07
+7.467e+07
+7.356e+07
+7.245e+07
+7.134e+07
+7.023e+07
+6.912e+07
+6.801e+07
+6.690e+07
+6.579e+07
+6.468e+07
+6.357e+07
+6.246e+07
+6.135e+07
+6.024e+07
+5.913e+07
Max: +7.800e+07
Elem: PART-1-1.53512
Node: 53512
Min: +5.802e+07
Elem: PART-1-1.16901
Node: 16902

Figure 20

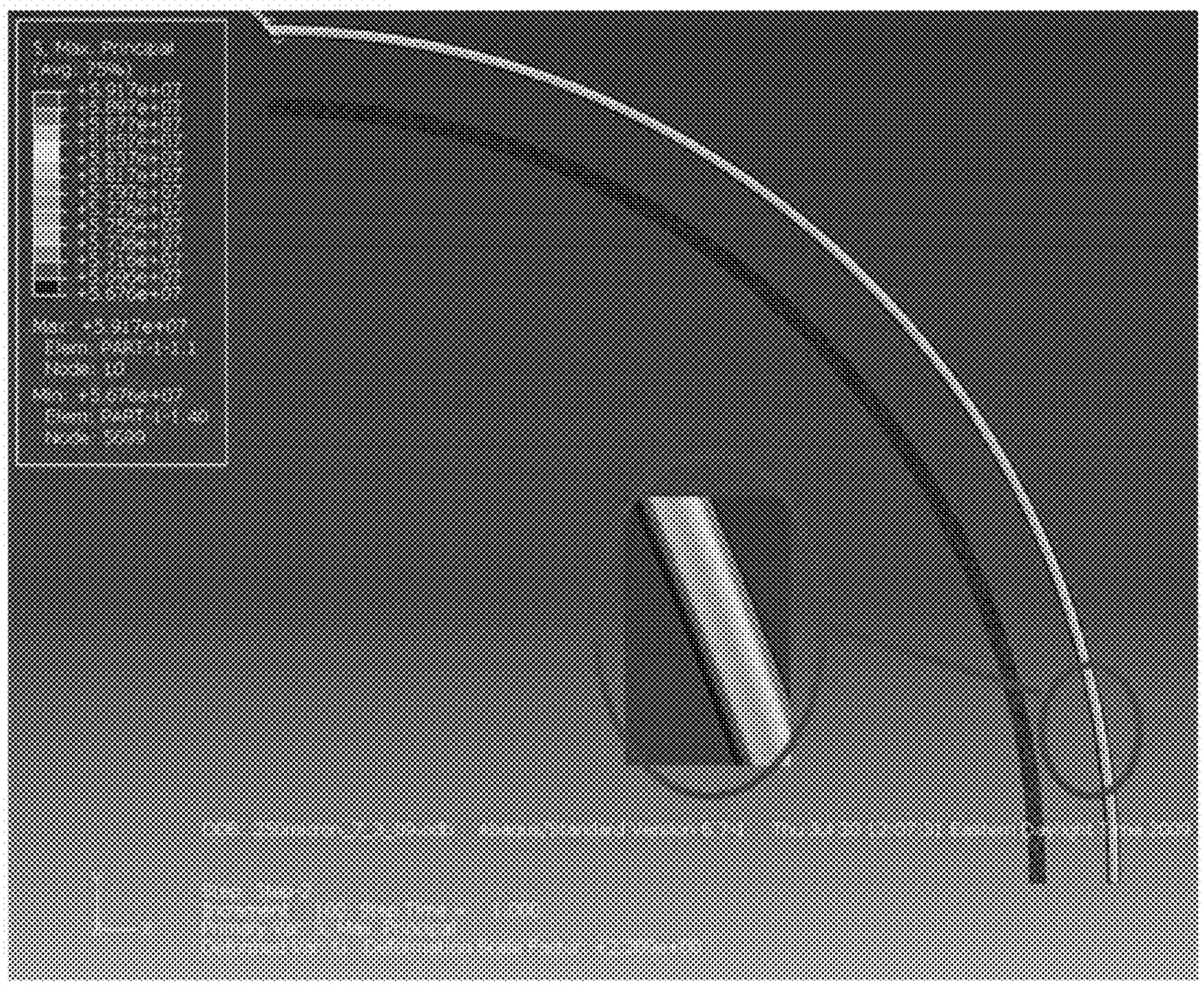

Figure 21

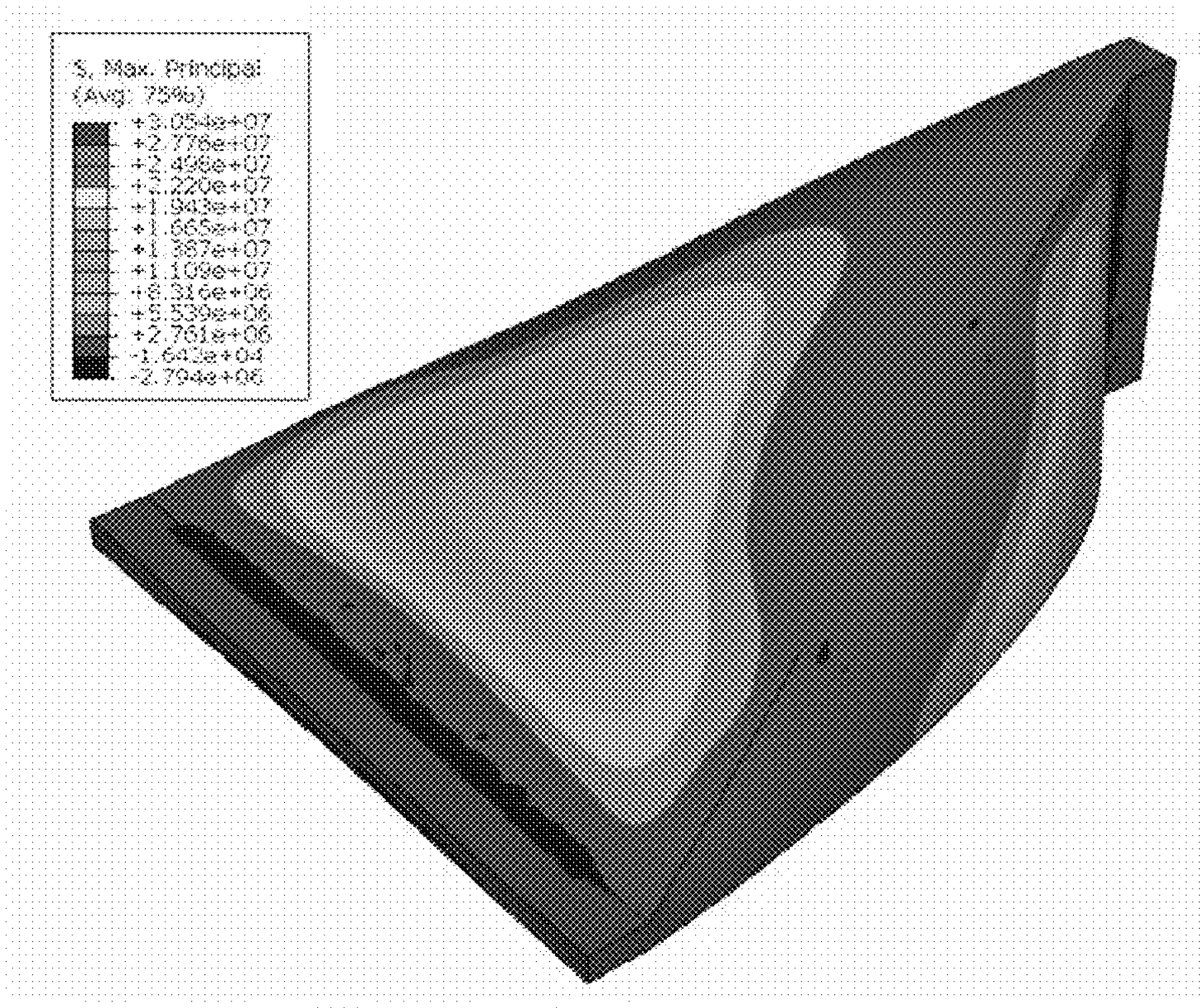
S, Max. Principal
(Avg: 75%)
+3.054e+07
+2.776e+07
+2.498e+07
+2.220e+07
+1.943e+07
+1.665e+07
+1.387e+07
+1.109e+07
+8.316e+06
+5.539e+06
+2.761e+06
-1.643e+04
-2.794e+06

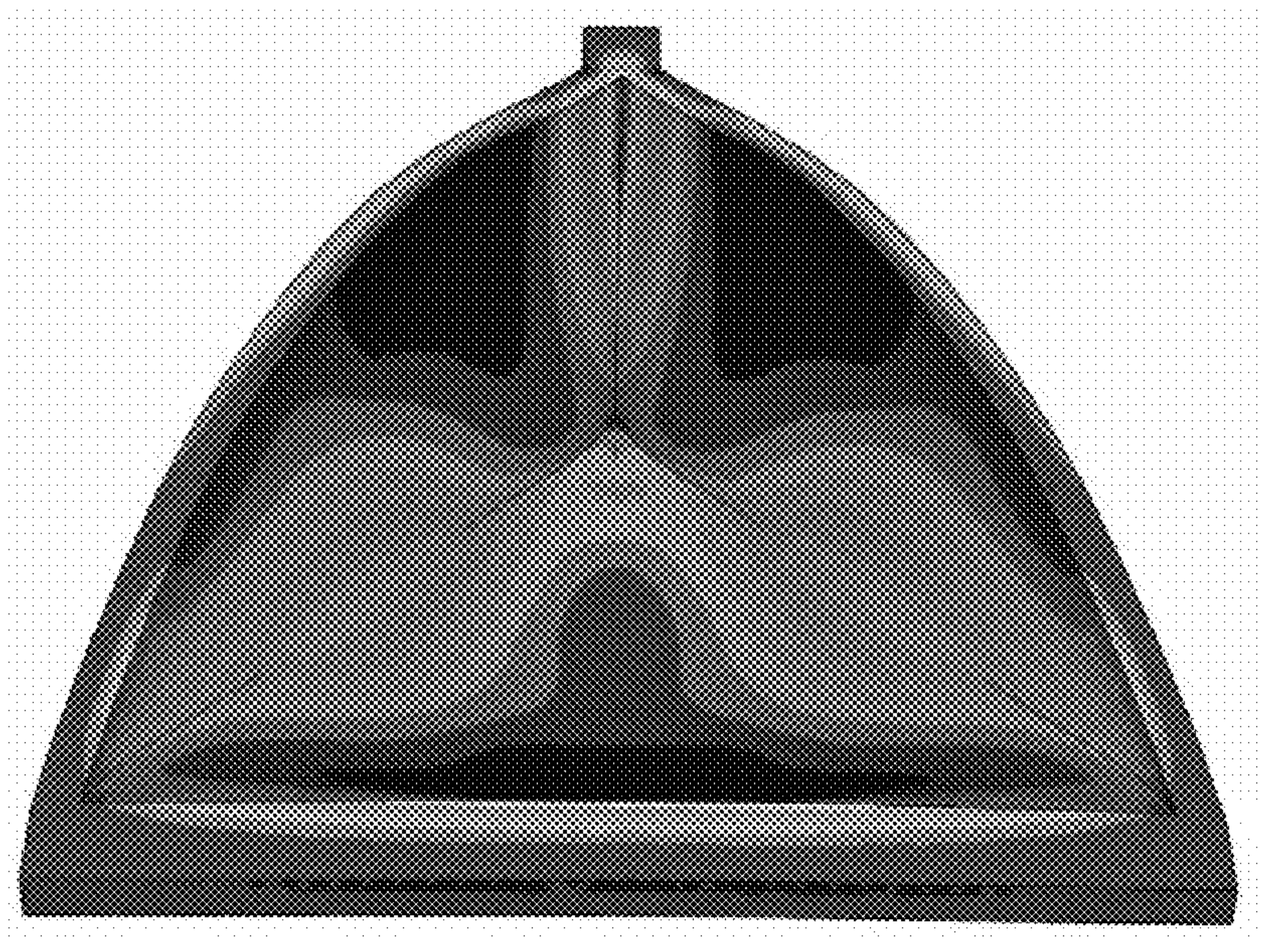

Figure 22

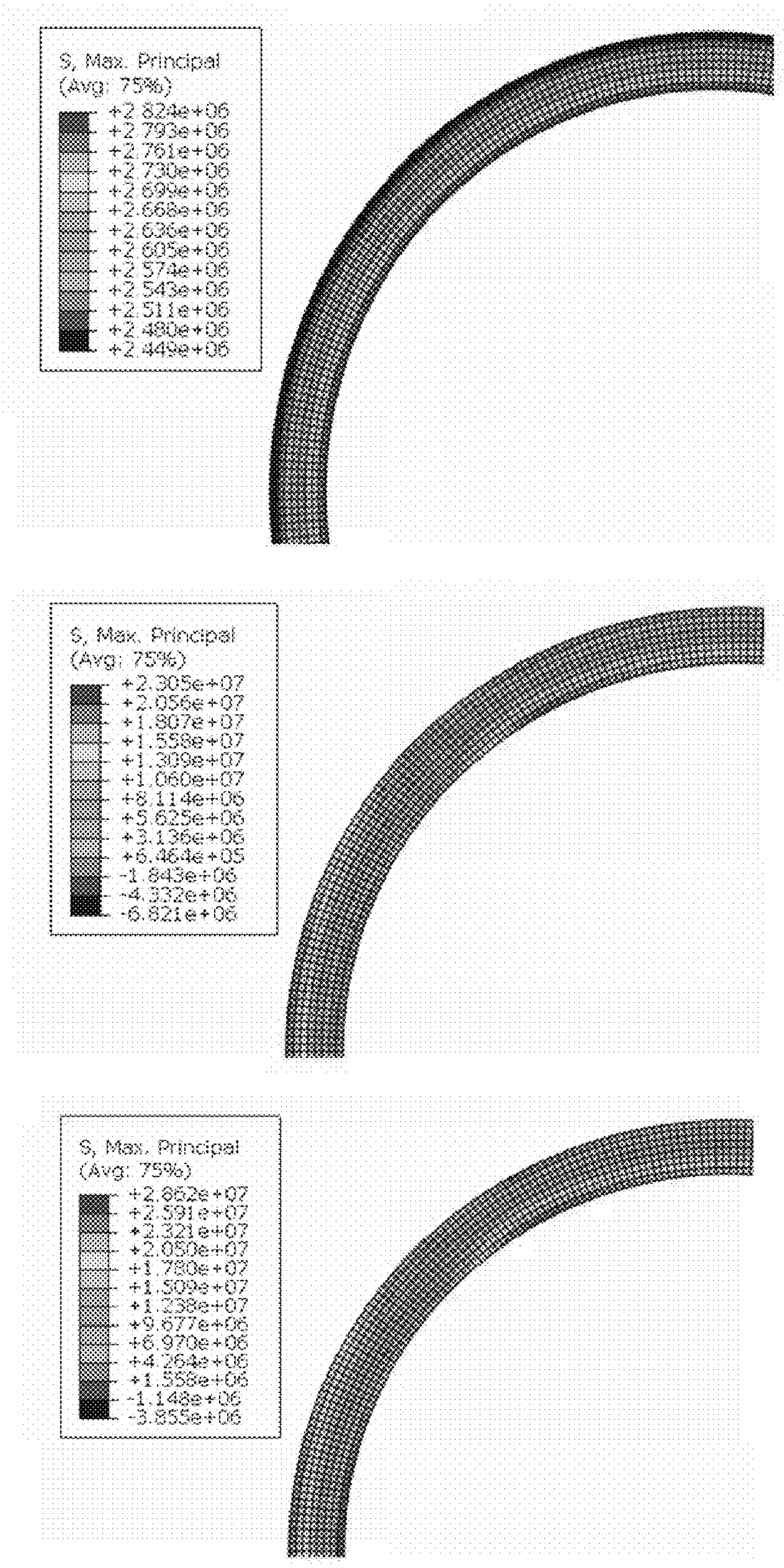
S, Max. Principal
(Avg: 75%)
+2.824e+06
+2.793e+06
+2.761e+06
+2.730e+06
+2.699e+06
+2.668e+06
+2.636e+06
+2.605e+06
+2.574e+06
+2.543e+06
+2.511e+06
+2.480e+06
+2.449e+06
S, Max. Principal
(Avg: 75%)
+2.305e+07
+2.056e+07
+1.807e+07
+1.558e+07
+1.309e+07
+1.060e+07
+8.114e+06
+5.625e+06
+3.136e+06
+6.464e+05
-1.843e+06
-4.332e+06
-6.821e+06
S, Max. Principal
(Avg: 75%)
+2.862e+07
+2.591e+07
+2.321e+07
+2.050e+07
+1.780e+07
+1.509e+07
+1.238e+07
+9.677e+06
+6.970e+06
+4.264e+06
+1.558e+06
-1.148e+06
-3.855e+06

Figure 23

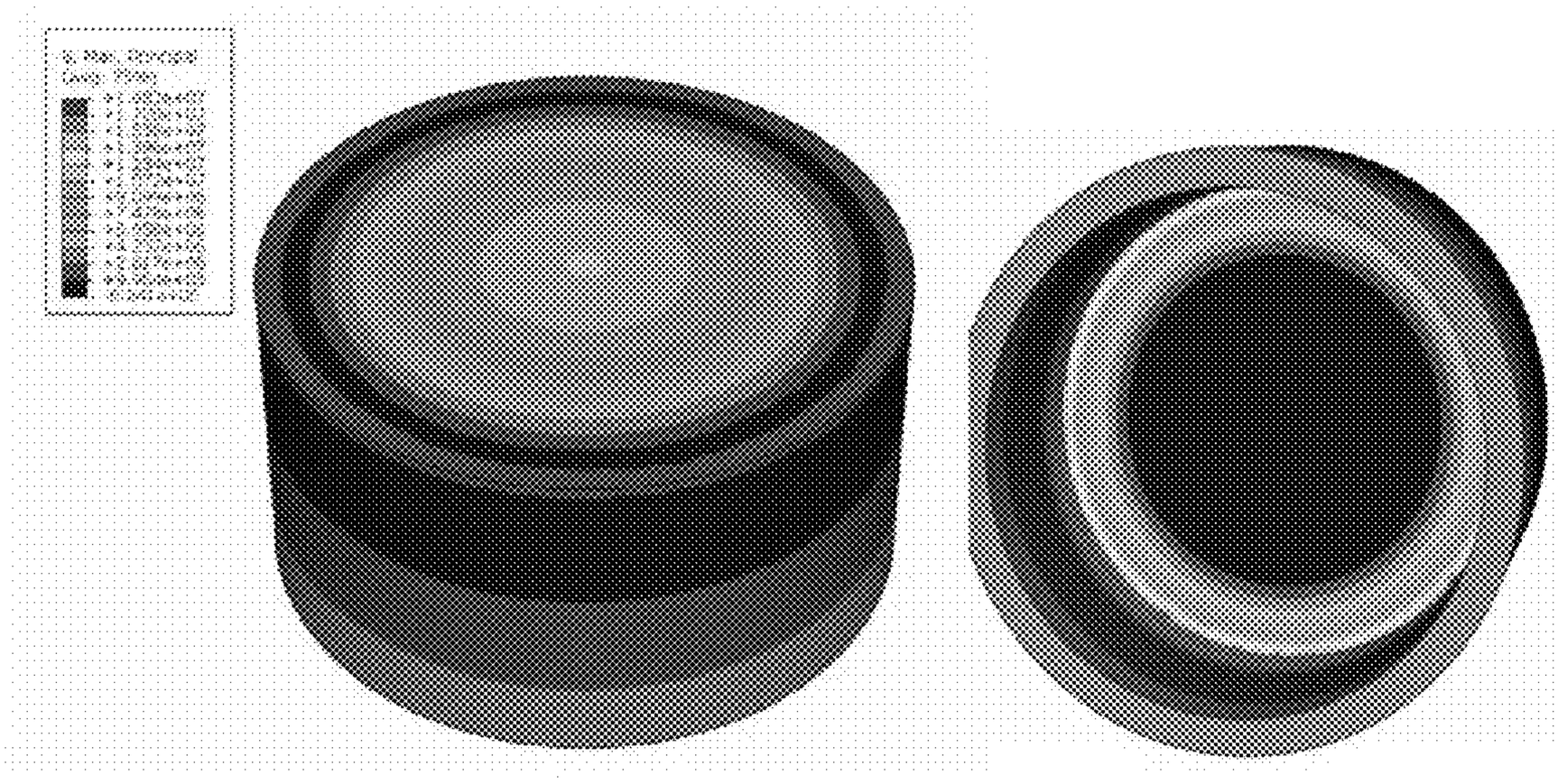

Figure 24

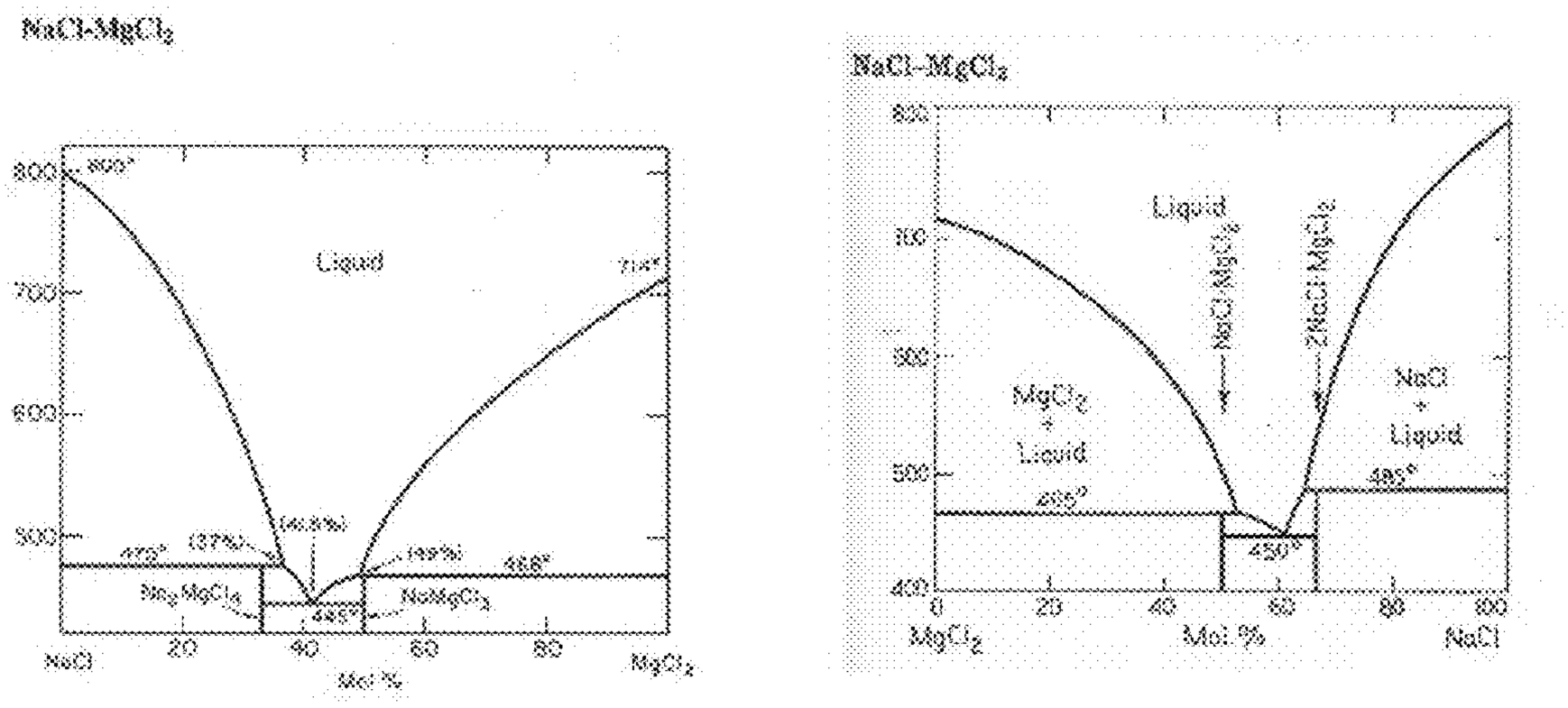
NaCl-MgCl2
800
700
600
500
Liquid
660°
715°
472°
(37%)
(46.8%)
(49%)
466°
Na2MgCl4
NaMgCl3
445°
NaCl
20
40
60
80
MgCl2
Mol %
NaCl-MgCl2
800
700
600
500
400
Liquid
NaCl.MgCl2
2NaCl.MgCl2
MgCl2
+
Liquid
NaCl
+
Liquid
465°
450°
485°
0
20
40
60
80
100
MgCl2
Mol %
NaCl

Figure 25

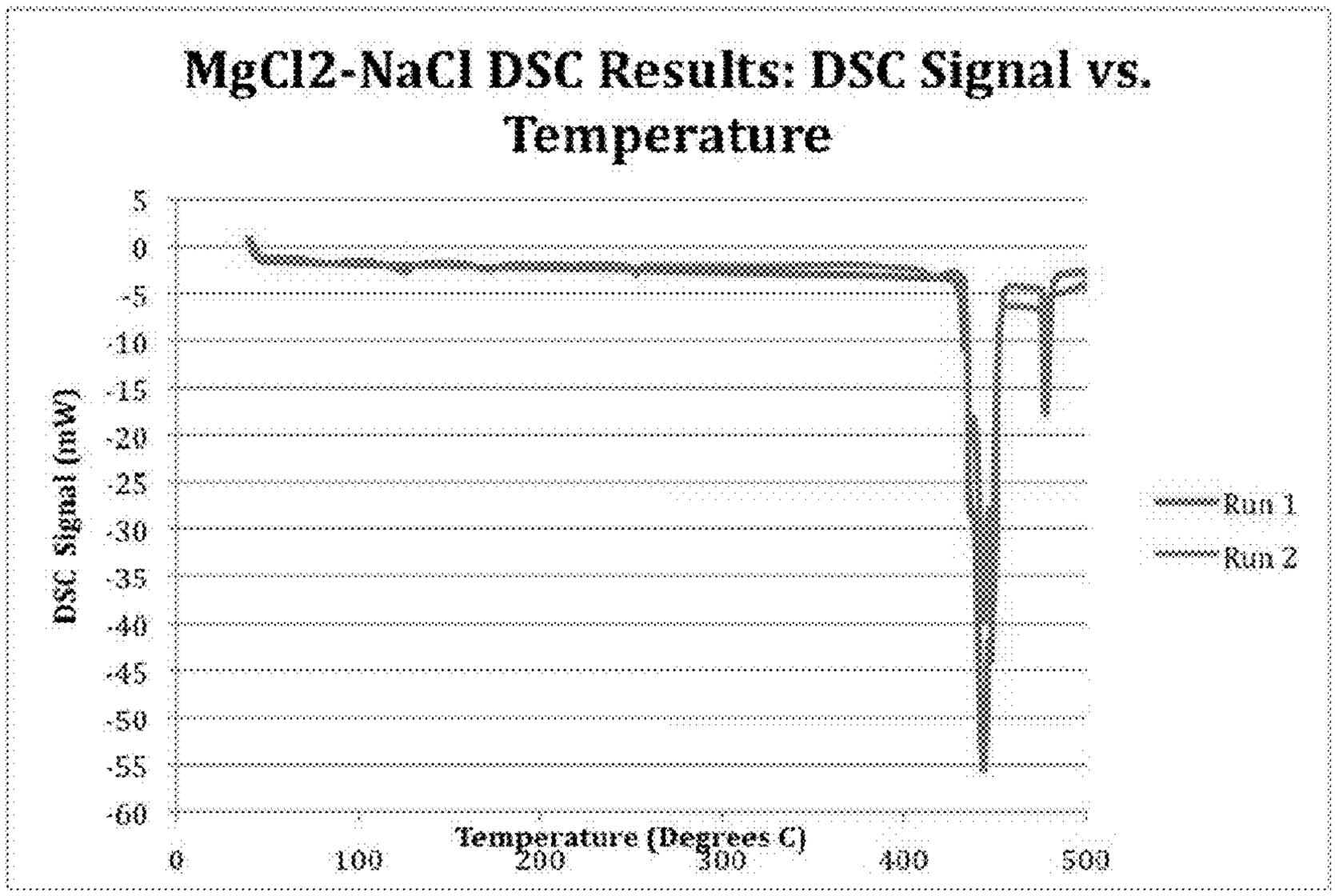

Figure 26

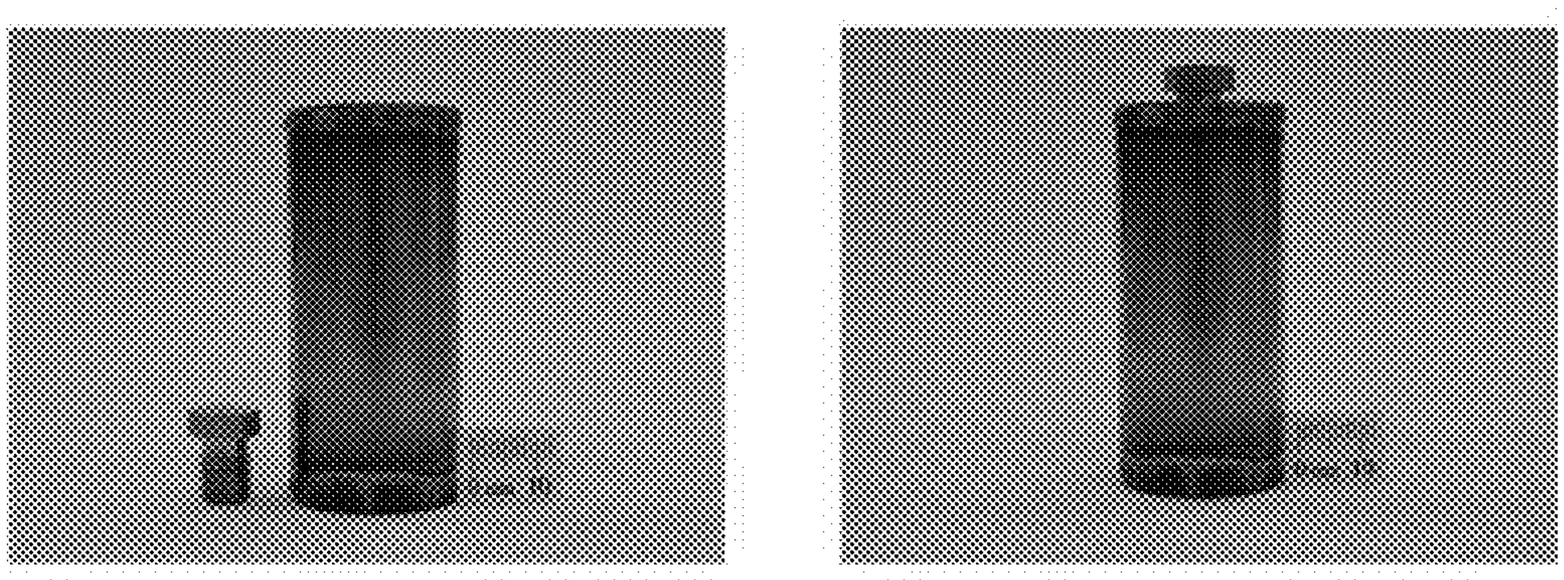

Figure 27

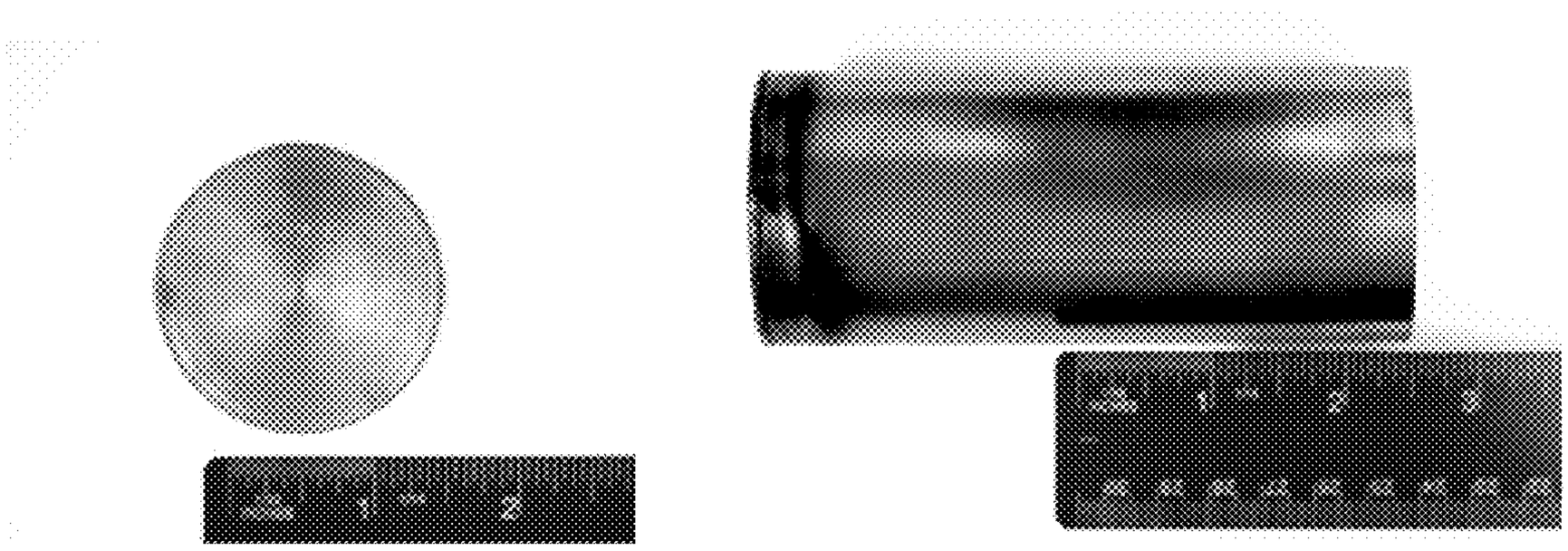

Figure 28

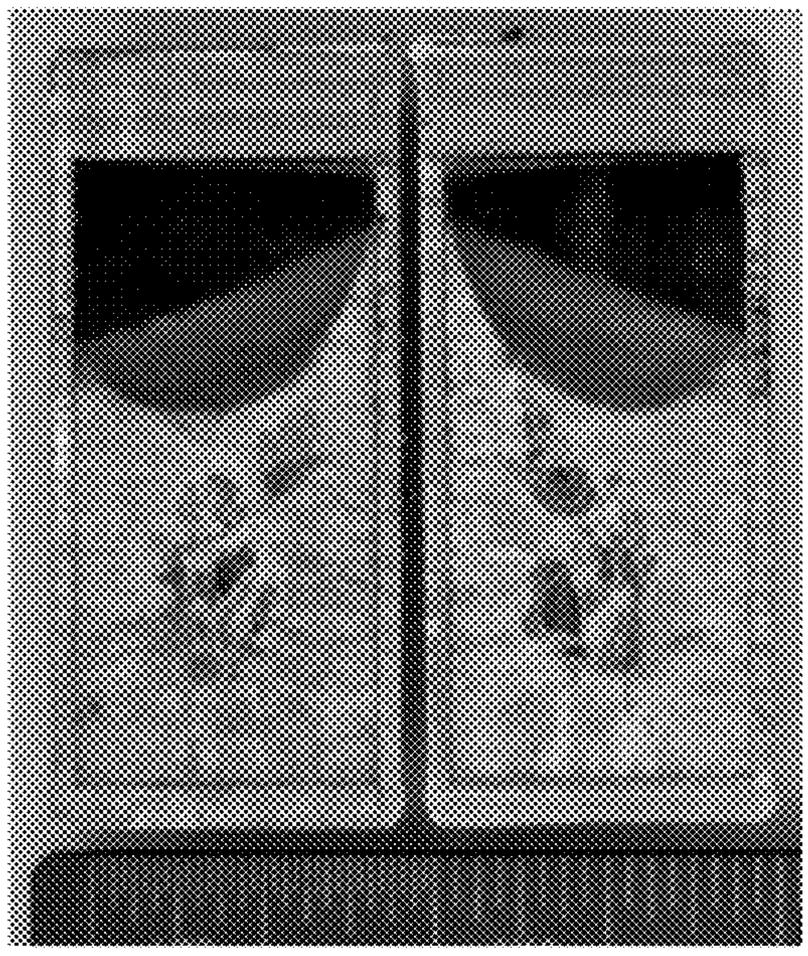

Figure 29

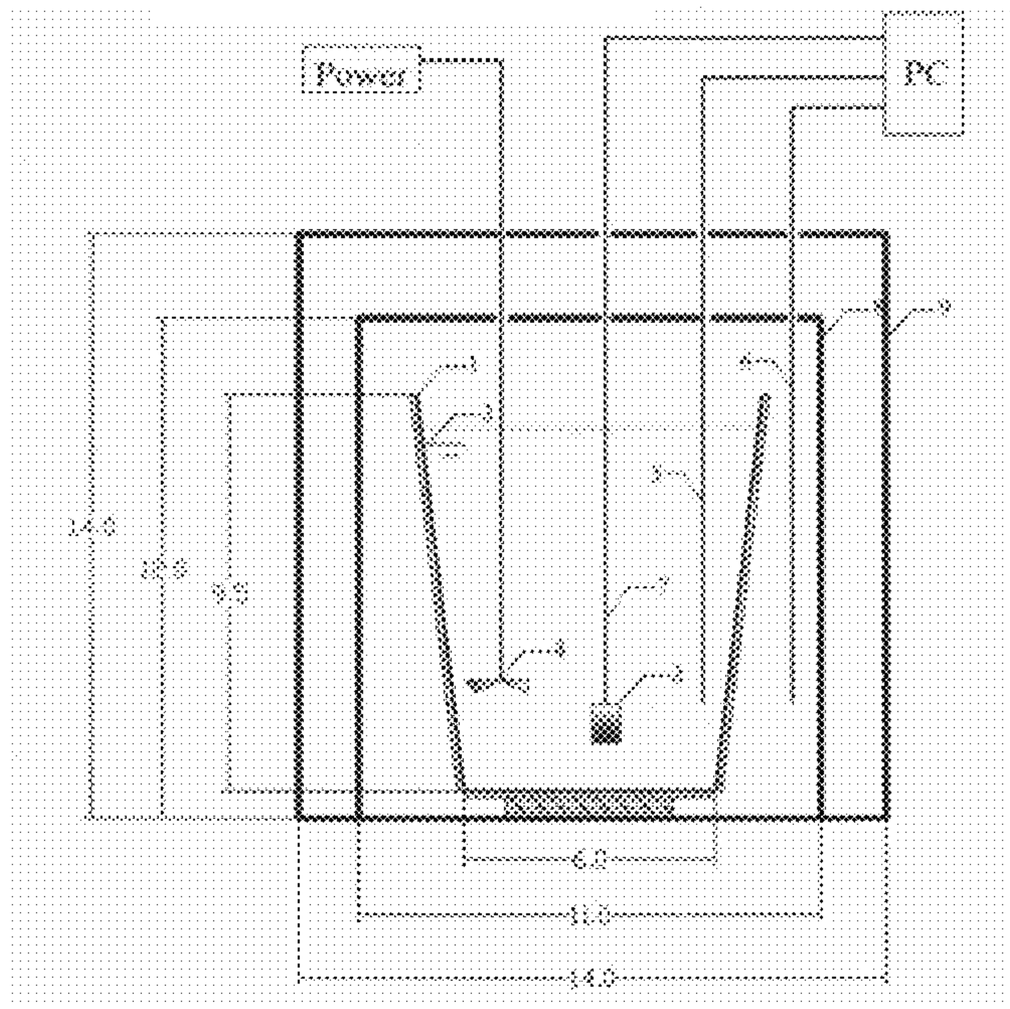

Figure 30

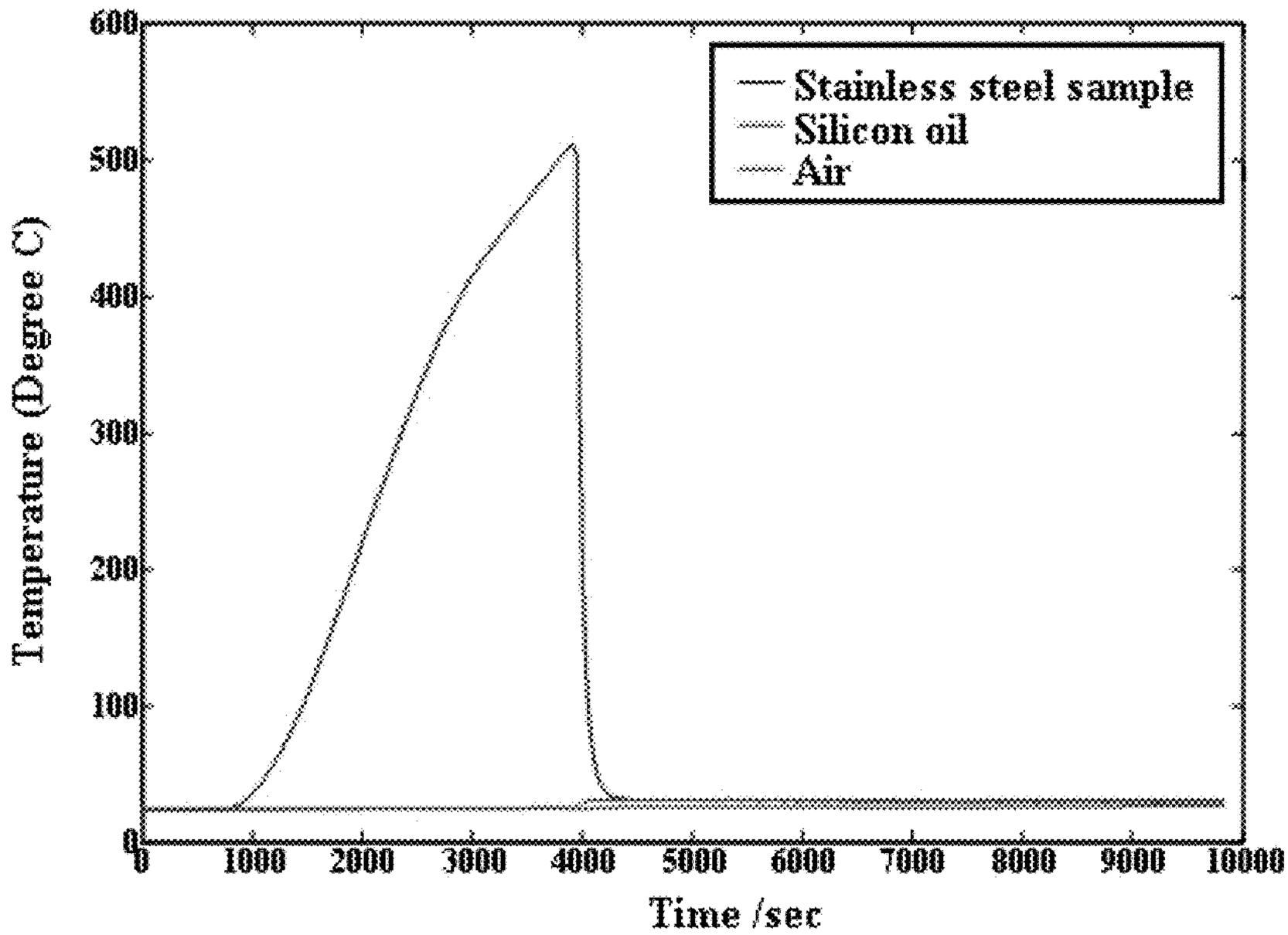

Figure 31

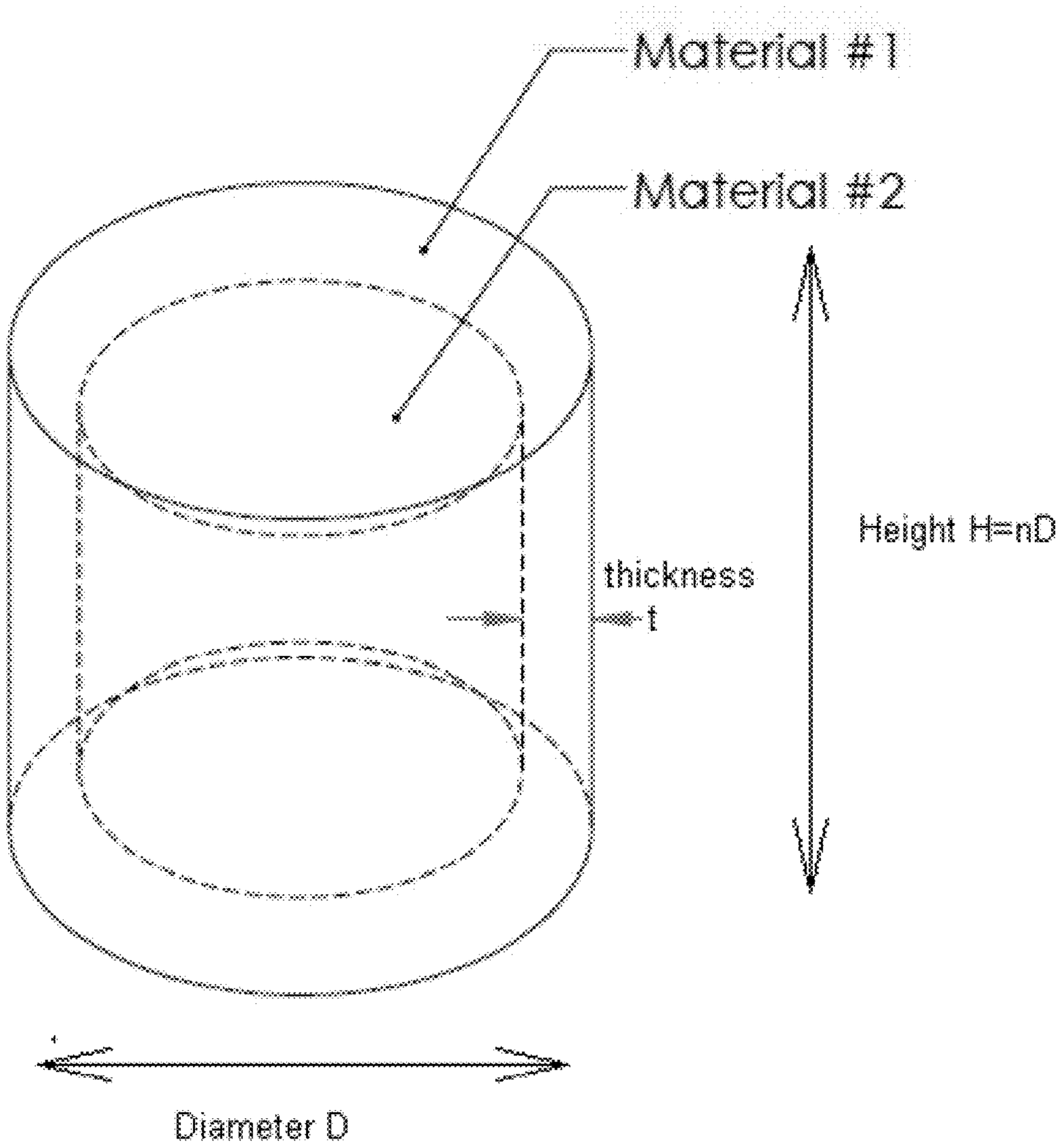

Figure 32

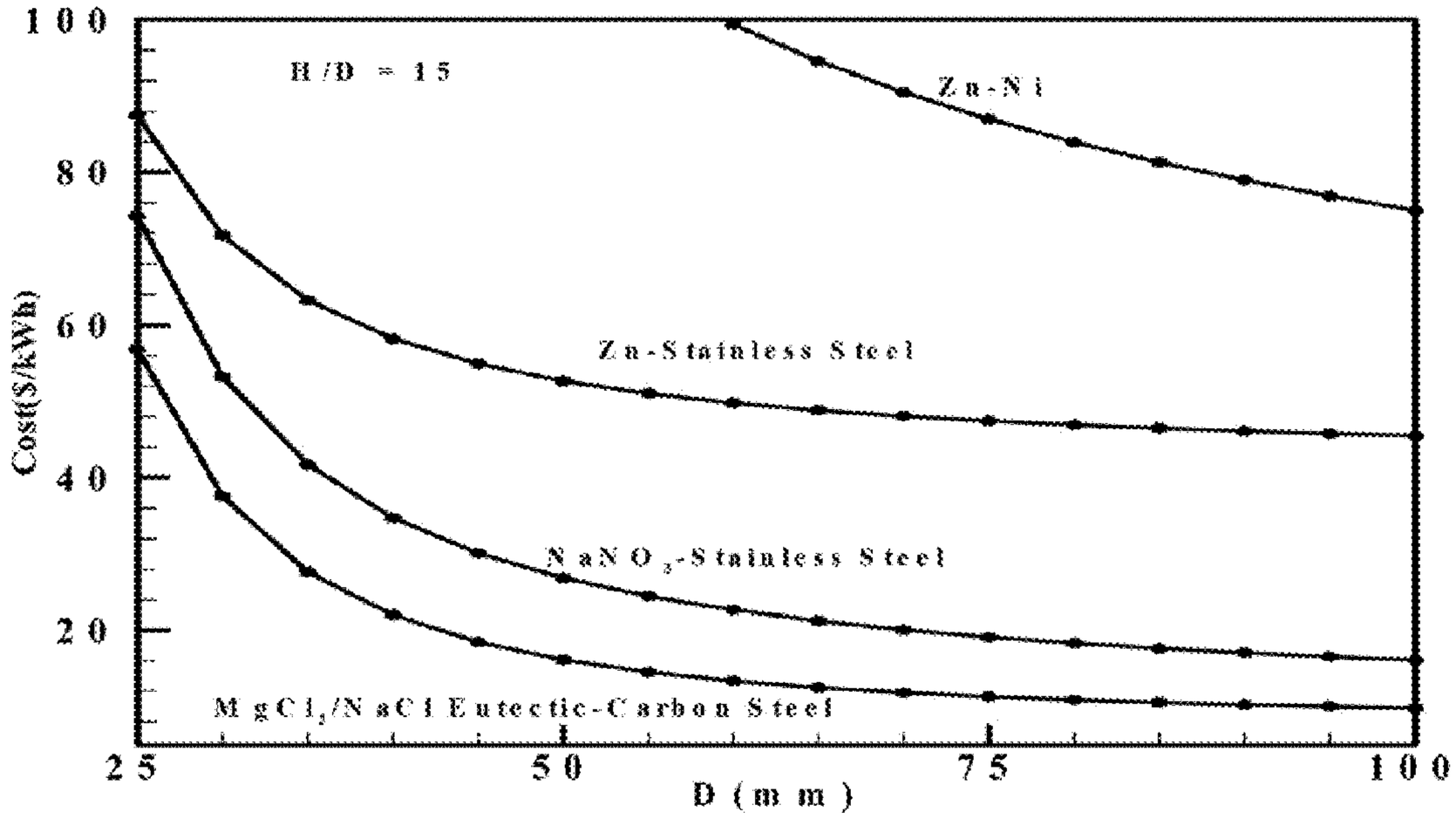
100
80
60
40
20
Cost($/kWh)
H/D = 15
Zn-Ni
Zn-Stainless Steel
NaNO3-Stainless Steel
MgCl2/NaCl Eutectic-Carbon Steel
25
50
75
100
D (mm)

Figure 33

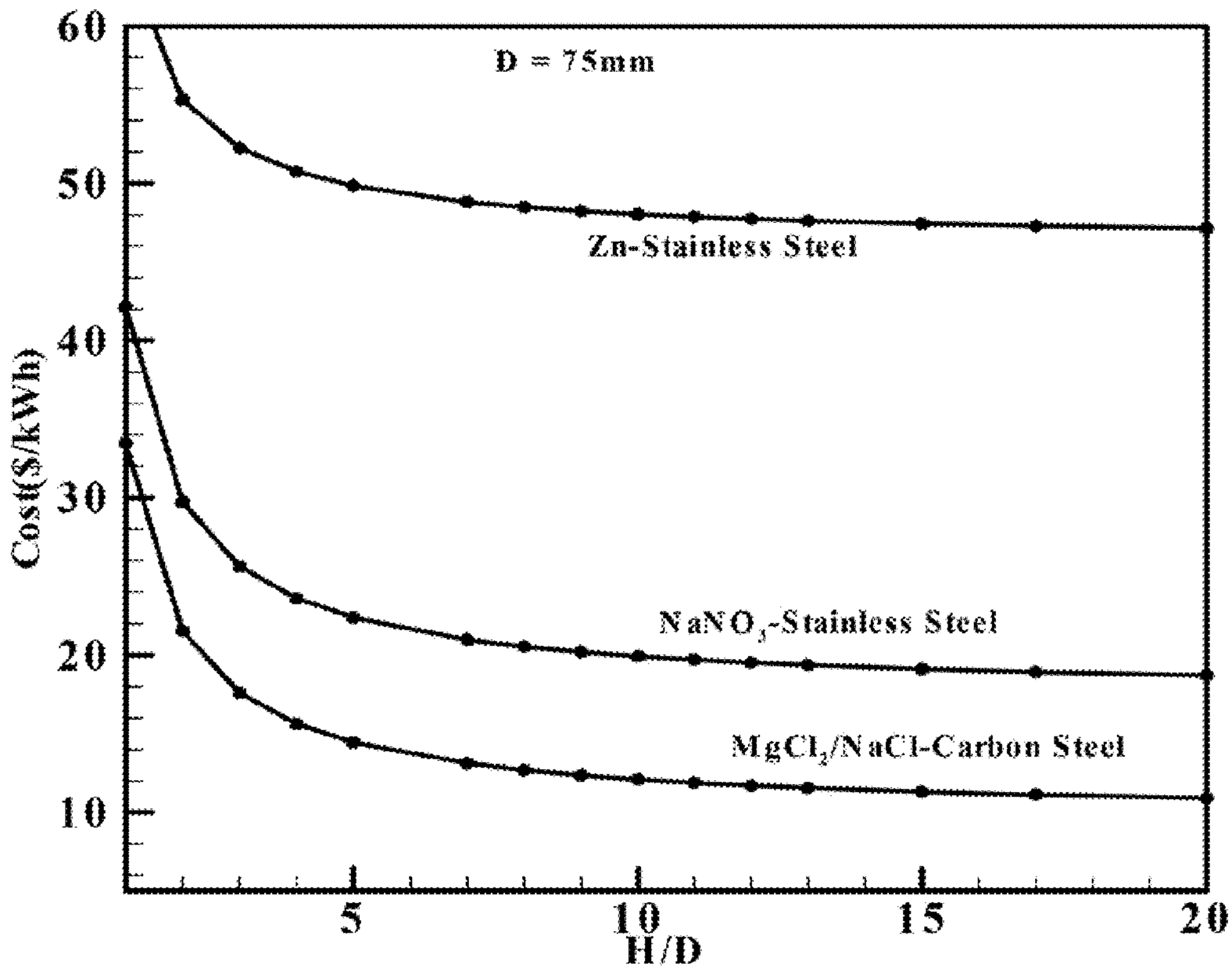
D = 75mm
Zn-Stainless Steel
NaNO3-Stainless Steel
MgCl2/NaCl-Carbon Steel
Cost($/kWh)
60
50
40
30
20
10
5
10
15
20
H/D

Figure 34

ENCAPSULATED PHASE CHANGE APPARATUS FOR THERMAL ENERGY STORAGE

CROSS-REFERENCE TO RELATED APPLICATIONS

[0001] This application claims the priority of U.S. Provisional Patent Application No. 61/326,412, filed on Apr. 21, 2010, which is incorporated herein by reference in its entirety.
[0002] Not Applicable

STATEMENT REGARDING FEDERALLY SPONSORED RESEARCH OR DEVELOPMENT

[0003] This invention was developed with financial support from the Department of Energy, Government Grant Award Number DE-FG36-08G018150. The United States government may have certain rights to the invention.

BACKGROUND

[0004] The inventors have developed new thermal energy storage devices and methods, such as for use in conjunction with energy generation systems, such as solar energy panels and related devices.
[0005] Solar power generation has been proven to be an excellent source of renewable energy. The program entitled "Advanced Heat Transfer Fluids and Novel Thermal Storage Concepts for Concentrating Solar Power Generation" belongs to Renewable Energy Research and Development Division of U.S. DOE Golden Field Office, Golden, Colo. Concentrating Solar Power (CSP) technology is recognized as an attractive option for solar power for plants of 100 MW or greater capacity. Two key needs for this technology are the development of improved heat transfer fluids (HTF) and the development of improved methods for thermal energy storage (TES). This proposal addresses the second need, with the objective of developing a novel TES technology that utilizes phase-change latent heat to increase thermal capacity, and offers energy storage at preselected high temperatures (e.g., such as about 400° C.) to improve thermodynamic efficiency.

SUMMARY

[0006] Provided herein are apparatus and methods for storing thermal energy.
[0007] For example, in one embodiment, an apparatus is provided including at least one phase change material and a capsule containing the at least one phase change material. The capsule may be permanently or temporarily sealed to contain the encapsulation material. The encapsulation material includes at least one material that is chemically and physically distinct from the phase change material. The encapsulation material and phase change material are selected to store and discharge thermal energy at temperatures of greater than 400 degrees without capsule failure.
[0008] In another embodiment, an apparatus is provided for storing thermal energy, the apparatus comprising at least one phase change material, and a capsule containing the at least one phase change material. The capsule comprises a preselected encapsulation material, and the encapsulation material comprises at least one material that is chemically and physically distinct from the phase change material.
[0009] In some embodiments, the capsule comprises an inner chamber for containing the at least one phase change material. The inner chamber may include a void space at a first preselected temperature. That void space may be substantially completely filled with the phase change material when the phase change material reaches a second preselected temperature.

BRIEF DESCRIPTION OF THE DRAWINGS

[0010] The patent or application file contains at least one photograph or drawing executed in color. Copies of this patent or patent application publication with color photograph(s) or drawing(s) will be provided by the U.S. Patent and Trademark Office upon request and payment of the necessary fee.
[0011] FIG. **1** illustrates a cross sectional view of a cylindrical capsule in accordance herewith.
[0012] FIG. **2** illustrates a schematic of a cross section of a spherical capsule in accordance herewith.
[0013] FIG. **3** illustrates a graph of temperature distribution of an exemplary capsule in accordance herewith.
[0014] FIG. **4** illustrates a graph of temperature distribution at the end of a PCM melting process in accordance herewith.
[0015] FIG. **5** illustrates a graph of temperature variations during the charging heat transfer process for a 100 mm diameter cylinder with sodium nitrate PCM and with air as HTF in accordance herewith.
[0016] FIG. **6** illustrates a graph of locations of interface between solid state PCM and liquid state PCM during melting process for a 100 mm diameter cylinder with sodium nitrate PCM and with air as HTF in accordance herewith.
[0017] FIG. **7** illustrates a graph of temperature variations during the discharging heat transfer process for a 100 mm diameter cylinder with sodium nitrate PCM and with air as HTF in accordance herewith.
[0018] FIG. **8** illustrates a graph of locations of interface between solid state PCM and liquid state PCM during discharging (freezing) for a 100 mm diameter cylinder with sodium nitrate PCM and air as HTF in accordance herewith.
[0019] FIG. **9** illustrates a graph of stress-strain relationship assumed with strain hardening in accordance herewith.
[0020] FIG. **10** illustrates stresses, strains and displacements of a 50 micron thick shell encapsulation coating in elastic deformation in accordance herewith.
[0021] FIG. **11** illustrates stresses, strains and displacements of a 100 micron thick shell encapsulation coating in elastic deformation in accordance herewith.
[0022] FIG. **12** illustrates stresses, strains and displacements of a 150 micron thick shell encapsulation coating in elastic deformation in accordance herewith.
[0023] FIG. **13** illustrates stresses, strains and displacements of a 200 micron thick shell encapsulation coating in elastic deformation in accordance herewith.
[0024] FIG. **14** illustrates stresses, strains and displacements of a 250 micron thick shell encapsulation coating in elastic deformation in accordance herewith.
[0025] FIG. **15** illustrates elastic-plastic stresses for spherical shell with pressure for 3 percent strain in accordance herewith.
[0026] FIG. **16** illustrates elastic-plastic strain for spherical shell with pressure in accordance herewith.
[0027] FIG. **17** illustrates a phase diagram of a Ni—Zn binary system in accordance herewith.
[0028] FIG. **18** illustrates alumina silicate ceramic crucibles with test specimens for exposure to liquid zinc at 450° C. in accordance herewith.

[0029] FIG. **19** is an optical photomicrograph that illustrates Differential Interference Contrast (DIC) of a Ni/Zn system as polished using differential interference contrast (The Ni is in the upper left of the picture and the Zn is in the bottom right) in accordance herewith.

[0030] FIG. **20** illustrates stresses for a pressure-only model with a thickness of 250 micron in accordance herewith.

[0031] FIG. **21** illustrates stresses due to a triangular crack (top left), a straight dent (top right), and a thinned part of the nickel shell (bottom) in a 250 micron thick nickel shell in accordance herewith.

[0032] FIG. **22** is an isometric view of maximum principal stresses on crimped cylinder due to 70% initial zinc content loading case (left), view of stresses inside of crimped cylinder due to 70% initial zinc content loading case (right), in accordance herewith.

[0033] FIG. **23** illustrates stress distribution of the 70% initial zinc content pressure only case (left), stress distribution of the 85% (middle), and 86% (right) PCM (zinc) content cases with point loads of 100 particle weights in accordance herewith.

[0034] FIG. **24** illustrates stress distribution on cylinder of aspect ratio 1 for the 70% initial PCM (zinc) content case; (left) stresses on the outside of the cylinder, (right) stresses inside of the cylinder in accordance herewith.

[0035] FIG. **25** are phase diagrams of a binary NaCl—$MgCl_2$ system from two separate sources in accordance herewith.

[0036] FIG. **26** illustrates the comparison of two separate DSC runs to determine the melting point of the 55 wt % $MgCl_2$-45 wt % NaCl eutectic salt. The melting point is determined to be 444° C. in accordance herewith.

[0037] FIG. **27** illustrates stainless steel capsules for calorimetry tests—with and without the NPT pipe plug in accordance herewith.

[0038] FIG. **28** illustrates carbon steel (1018) capsule for use with the eutectic salt in accordance herewith.

[0039] FIG. **29** illustrates sections of a $MgCl_2$—NaCl eutectic EPCM encapsulated with Stainless Steel-304 in accordance herewith.

[0040] FIG. **30** is a schematic of a precision calorimeter designed and built for use in the present work—all units are inches in accordance herewith.

[0041] FIG. **31** illustrates a graph of temperature profiles of sample, silicon oil, and air in accordance herewith.

[0042] FIG. **32** illustrates the geometry of an exemplary capsule in accordance herewith.

[0043] FIG. **33** illustrates a graph of the cost of storage units ($/kWh) as a function of the diameter of the cylindrical shaped capsule in accordance herewith.

[0044] FIG. **34** illustrates a graph of the cost of storage unit ($/kWh) as a function of length of the capsule in accordance herewith.

DETAILED DESCRIPTION

[0045] The methods and apparatus described herein focuses on encapsulated phase-change material (EPCM), such as in either particulate (near spherical) and/or tubular forms, either of which can be assembled into heat exchangers for thermal exchange with HTFs. This work builds upon the team's unique experience for encapsulation of PCM, using an electrochemical coating technique. There are many PCMs suitable for use herein, including Zn, $NaNO_3$, $MgCl_2$, and other materials as well as eutectic mixtures of $MgCl_2$—NaCl, and other materials, with our primary focus on salts. Nickel, carbon steels and stainless steels are among the materials suitable as encapsulation materials. In some embodiments, Nickel is used with Zn. Scoping analysis has shown that nominal dimensions of 1-100 cm are suitable for the EPCM to provide for ease of fabrication and assembly into heat exchangers.

[0046] The inventors have conceived of various thermal energy storage apparatus and methods. They have further established the technical requirements and demonstrated feasibility, along with bench scale testing, of various embodiments. The examples herein prove the usefulness of thermal energy storage systems incorporating encapsulated phase change materials (EPCM) at elevated temperatures (such as up to about ~750° C., for example). Additionally, the testing and engineering results described herein prove the scalability of the technology, and thereby, enable the development of large scale thermal storage systems. To the knowledge of the inventors, the apparatus and methods described herein have not previously been described or demonstrated by others.

[0047] For the encapsulated phase change apparatus described herein, several methodologies and geometries (spherical and cylindrical) are demonstrated having different designs and materials. For example, Zinc (Zn) encapsulated in Nickel (Ni); stainless steel and $NaNO_3$, $MgCl_2$, $MgCl_2$—NaCl eutectic salts encapsulated in carbon steels or stainless steel; and other appropriate material combinations. The technologies developed in this work are designed to enable storage of thermal energy in 100 MW_e solar energy plants for 6 hours or more, at temperatures of up to about 750° C.

[0048] Experimental activities conducted include modeling of the transient heat transfer and associated analysis involving zinc, the zinc being used as a phase change material. Examples included spherical and cylindrical geometry for particles of encapsulated phase change material (EPCM) in capsules. Since the heating of encapsulated PCM can exert significant stress on the encapsulating material, significant effort was put into FEM (Finite Element Analysis), which is a well-established numerical technique for solving differential equations computations using Abaqus™ brand of FEM software to quantify these stresses. Commercializable embodiments of EPCM materials, including the encapsulating of zinc using nickel, were explored in detail. A calorimeter was designed, built, and utilized to evaluate the energy storage properties of the various EPCM embodiments, as well as the surrounding enclosures/tanks holding a plurality of EPCM capsules therein. "Capsule" as used herein is the closed coating or other container that immediately surrounds and/or holds the phase change material ("PCM"). The "encapsulating material" as used herein is the material that makes up the capsule. The capsule may be permanently closed (whether a continuous wall of encapsulating material) or re-closable (e.g. a cap or other removable closure over each opening in the encapsulation material wall.

[0049] The thermal energy performance characteristics, namely energy absorption, energy retention, and energy release, and operational temperature vary from one embodiment of EPCM to the next. Those performance criteria are primarily determined by the selection of the encapsulated material and the selection of the material for the capsule. In some embodiments, suitable phase change materials include $NaNO_3$, KNO_3, $NaNO_3$—KNO_3, $MgCl_2$, $MgCl_2$—NaCl, $MgCl_2$—KCl, NaCl—KCl, inorganic salts, and combinations thereof that exhibit phase change at desirable tempera-

tures compatible with particular heat exchange systems and associated power sources (solar, nuclear, steam, geothermal, etc.). Further, the geometry and relative sizes of the encapsulated materials of the EPCM and the capsule material impact the thermal performance characteristics. Similarly, various thermally induced stresses are associated with the EPCM and any surrounding enclosure system. Several exemplary EPCM have been manufactured and tested by the inventors, each tested using a calorimeter to prove the charging and discharging of energy into and out of the EPCM.

[0050] In one example, eutectic mixtures of $MgCl_2$—NaCl (55-45 w/o) were prepared and the melting point of 444° C. confirmed using DSC. EPCM capsules with that Chloride salt mixture, as well as $NaNO_3$, have been prepared and tested separately and independently in the calorimeter described herein. Calorimetry results confirm the storage capability of the salts and prove the feasibility of charging and discharging of energy into and out of the EPCM capsules.

[0051] Additionally, an economic analysis of the thermal energy storage systems described herein (using the EPCM capsules described above) was conducted. The analysis assumes a 100 MW_e plant storing energy for 6.3 hours. All of the other assumptions used in the analysis are the same as those used in a recent (National Renewable Energy Lab ("NREL") report for a trough plant. The economic analysis confirms that the EPCM systems, based on current designs, can store thermal energy in salts at about $20.29/kWh. That cost is well below the publicly stated Department of Energy (hereinafter, "DOE") goal of $40/kWh for new, alternative energy storage systems.

[0052] The following accomplishments and examples have been demonstrated by the inventors. First, the inventors have formulated details of desirable heat transfer in various EPCM, including phase change characteristics. Potential stresses in the encapsulating material for various geometries have been quantified, including those associated with the stacking of EPCM pellets in a bed for heat storage. Encapsulation capabilities of the commercial Nickel forming houses have been evaluated. Further, encapsulation of Zinc using Nickel and stainless steel tubes has been evaluated for stresses as well as phase formations. A calorimeter to quantify the energy storage in an EPCM pellet has been designed, analyzed and built. Measurements of energy stored and retrieved using precision calorimetry of the EPCM have been completed and prove that thermal energy can be stored. Additionally, heat transfer fluids (HTF) compatible with the EPCM materials herein include silicones, biphenyls, eutectic salt mixtures such as $NaNO_3$—KNO_3, $NaNO_3$—KNO_3—$LiNO_3$, and combinations thereof. Other HTF will be evident based upon their compatibility with operating temperatures in particular heat transfer and storage systems and use (charging, discharging of thermal energy) requirements.

[0053] The following examples are exemplary of the various embodiments of thermal transfer and storage apparatus and methods.

EXAMPLE 1

[0054] We have been successful in preparing $MgCl_2$—NaCl eutectic PCM with a melting point of 444° C. We have manufactured cylindrical EPCM capsules with $MgCl_2$—NaCl eutectic salt mixture encapsulated in stainless steel (304) and carbon steel (1018) cylinders. FIG. **1** shows a section of the EPCM $MgCl_2$—NaCl eutectic with stainless steel encapsulation. As shown in FIG. **1**, which is a cross-sectional view of an exemplary EPCM apparatus, a void space is purposefully provided within the encapsulated space for managing stresses related to expansion of the encapsulated material and any air or gas therein.

EXAMPLE 2

[0055] Thermal energy storage capabilities of $MgCl_2$—NaCl eutectic mixture has been proven by conducting calorimetry of heated EPCM cylinders to temperatures above the melting temperatures of the PCM and recovering the energy by quenching it in silicon fluid.

EXAMPLE 3

[0056] We have manufactured cylindrical EPCM capsules with $NaNO_3$ salt as PCM with a melting point of 308° C. encapsulated in stainless steel (304). Thermal energy storage capabilities of $NaNO_3$ has been proven by conducting calorimetry of heated EPCM $NaNO_3$ cylinders to temperatures above the melting temperatures of the PCM and recovering the energy by quenching it in silicon fluid.

TABLE A

Thermal Energy Storage Calorimetry Results for $MgCl_2$—NaCl Eutectic-Carbon Steel EPCM (1"Dia × 2" EPCM Capsule)

Cycling Number	Energy Transferred to Silicone Oil (kJ)	Energy from Capsule (kJ)	Energy from Eutectic (kJ)	Reference Energy from Eutectic (kJ)	Fraction of Reference Energy from Eutectic
Expt 1	41.6	21.4	20.2	23.8	0.85
Expt 2	41.8	21.7	20.1	24.4	0.82
Expt 3	41.1	21.2	19.9	23.4	0.85
Expt 4	40.9	21.1	19.8	23.2	0.85
Expt 5 (8 hrs)	42.6	21.6	21.0	24.1	0.87
Expt 6	38.7	21.5	17.2	19.8	0.87
Expt 7	38.9	21.7	17.2	20.1	0.86
Expt 8 (8 hrs)	39.0	21.8	17.2	20.2	0.85

TABLE B

Thermal Energy Storage Calorimetry Results for NaNO3-Stainless Steel and Carbon steel EPCM (2"Dia × 5" EPCM Capsule)

Cycling Number	Energy Transferred to Silicone Oil (kJ)	Energy from Capsule (kJ)	Energy from NaNO3 (kJ)	Reference Energy from NaNO3 (kJ)	Fraction of Reference Energy from Eutectic
Expt 1	215	63.5	152	167	0.91
Expt 2	222	64.5	158	168	0.94
Expt 3	222	65.3	156	169	0.92
Expt 4	214	60.0	154	160	0.96

[0057] The repeatability of the energy stored by the PCM (percentages ~85% and ~92%) is surprising and remarkable. The percentages are not 100% only because the thermal properties of these materials are not well established in the temperature ranges of interest. Establishment of thermal properties is an ongoing study.

[0058] A cost analysis of thermal energy storage systems that use Zinc, $MgCl_2$—NaCl eutectics and $NaNO_3$ as PCM has been conducted. The cost analysis is for a 100 MW_e plant and for 6.3 hours of energy storage. The assumptions used for this analysis are the same as those used by NREL and presented in an NREL report. The Thermal Energy Storage system that uses salts in EPCM combinations are well under the DOE goal of $40/kWh at about $27 and $20/kWh$_e$. The storage system using zinc-stainless steel will cost a little over the DOE goal.

TABLE C

Cost of the storage unit ($/kWh) for different combinations of PCM and encapsulation materials for D = 75 mm and H/D = 15 and t = 1.5 mm

PCM-Shell Combination	Zn—Ni	Zn-Stainless Steel	$NaNO_3$-Stainless Steel	MgCl2/NaCl Eutectic - Carbon Steel
Cost ($/kWh)	$93.08	$53.55	$26.62	$20.29

[0059] A preferred EPCM geometry, based on heat transfer considerations, stress analysis, large-scale fabrication (millions of EPCM capsules) and cost analysis, incorporates a large aspect ratio cylinder (L/D of cylinder ~15) of 75 mm diameter containing a salt as the PCM. By way of further example, it is expected that thermal energy storage for any of the PCM materials proposed herein will be adequate when using an appropriate encapsulation consisting of a long cylinder-like structure, with management of hot air flow in proximity to the capsule and/or its surrounding tanks or container (s).

Modeling of Heat Transfer

[0060] To store energy in the EPCM material, the convective heat transfer from the solar heat transfer fluid (HTF) to the EPCM through the encapsulation needs to be efficient. HTF at known flow, temperature and thus heat transfer coefficient is assumed to be available. Conduction heat transfer in spherical pellets is considered. Though closed form solutions are available for this transient heat transfer, since melting of the Zinc PCM and front tracking are essential for the problem on hand, a numerical formulation is provided in spherical coordinates. Diffusion of heat through the encapsulation is included in the formulation.

[0061] Conduction heat transfer in spherical and cylindrical pellets is considered herein. Numerical results for transient heat transfer for spherical geometry are presented below. The formulation includes conduction as well as phase change. Initially, to estimate the order of magnitudes, lumped mass analysis was conducted. Space-dependent and time dependent results are briefly discussed herein.

[0062] As shown in FIG. **2**, the heat transfer in a spherical shell with multiple materials is a moving boundary problem, and it is nonlinear in nature.

Example Calculations of FIG. 2. Spherical Geometry of Particle.

[0063] The equation governing the unsteady heat diffusion in each layer of the exemplary sphere of FIG. **2** is of the form:

$$\rho_j c_j \frac{\partial T_j}{\partial t} = k_j \frac{1}{r^2} \frac{\partial}{\partial r}\left(r^2 \frac{\partial T_j}{\partial r}\right), \; j = 1, 2, \text{ and } 3$$

where ρ_j is density; c_j is specific heat; k_j is thermal conductivity; T_j is temperature distribution in each layer; r is the radial distance; t is the time. Furthermore, the suffixes j equals 1, 2, or 3 for the thin layered shell (nickel or stainless steel), liquid phase, or solid phase of the phase change material, respectively. Appropriate boundary and initial conditions are used. The solid temperature is scaled with the inlet fluid temperature (~450° C.).

[0064] Boundary Conditions for the heat transfer into or out of the spherical or cylindrical pellet are:

$$-k_1 \frac{\partial T_1}{\partial r} = h(T_s - T_f), \text{ at } r = R_1$$

$$k_1 \frac{\partial T_1}{\partial r} = k_2 \frac{\partial T_2}{\partial r}, \text{ and } T_1 = T_2, \text{ at } r = R_2;$$

$$-k_2 \frac{\partial T_2}{\partial n} = -k_3 \frac{\partial T_3}{\partial n} + L\rho_2 V_n, \text{ and } T_2 = T_3 = T_m;$$

$$\frac{\partial T_3}{\partial r} = 0, \text{ at } r = 0.$$

where h is convective heat transfer coefficient; R_1 is the radius of the whole particle; R_2 is the radius of the phase change material part; T_s is the temperature at r=R_1; T_f is the temperature of heat transfer fluid; T_m is the melting temperature of phase change material; L is latent heat of phase change materials; V_n is the velocity of the interface movement in the normal direction; n is the normal direction of the interface movement. Initially, T(r,0)=T_0, which is constant.

[0065] Dimensions of an exemplary EPCM pellet. 25 mm (1") diameter Zinc-Ni (or Stainless Steel) cylindrical and spherical pellets are considered. The size has been treated as an independent variable. 1.6 mm (1/16") Thickness for Stainless Steel Layer is used in the encapsulating material. Two Heat Transfer Fluids (hereinafter, "HTF") are considered—air and VP-1 (though VP-1 cannot be used at the temperatures of interest here, a VP-1 like liquid capable of 550° C., designated as VP-1 is used for the current calculations).

[0066] Examples of normalized zinc temperature as a function of time and space are indicated in the graph of FIG. **3**, which shows temperature distribution at about 9 seconds. FIG. **4** illustrates temperature distribution at the end of melting process (t=15 s).

[0067] Extensive computational results have been generated to be able to generalize the heat transfer of interest. The goal here is to be able to get energy into the zinc in about 8 hours with the potential to give up the energy to the heat transfer fluid in approximately 16 hours. The overall times for the melting of zinc and to store the latent heat of melting depends on the size of the zinc EPCM pellet and conduction and convective heat transfer. To get an estimate of the heat transfer times for the charging process (based on numerical simulations), the melting times for the zinc PCM for 25 mm pellets are given below.

TABLE D

Diffusion and Melting Times of zinc in the EPCM Capsule 25 mm in Dia.

Process	Heat Transfer Fluid	Geometry	Time
Diffusion and Melting Process	Air	Sphere	21.6 minutes
		Cylinder	41 minutes
	VP-1 like fluid capable of 550° C.	Sphere	2.1 minutes
		Cylinder	3.9 minutes

Modeling Heat Transfer Related to Use of Salts as the PCM.

[0068] Exemplary salt phase change materials (PCM) include $MgCl_2$—NaCl eutectic mixture, as well as $NaNO_3$. The results of these exemplary salt PCMs can be compared to the Zinc-Stainless Steel EPCM. However, the charging times are functions of material properties as well as inlet HTF temperature used as the boundary condition for the charging process.

[0069] Extensive heat transfer computations based on first principles (with equations and boundary conditions) as described above in salts being used as phase change materials have been conducted. The heat transfer fluid, HTF (Air or VP-1 like fluid capable of 550° C.) boundary conditions establish the nature of energy input to the PCM. The tables below present the total times for phase change in the PCM with radial heat transfer into the cylindrical EPCM capsule. For each PCM, an appropriate encapsulating material has been used with appropriate thermal properties forming the EPCM. The times for the charging (energy into PCM) and discharging (energy out of the PCM and into the HTF) are presented. The times for the phase change are presented as functions of EPCM capsule radius, PCM in use for Air and VP-1 like fluid capable of 550° C. Data for air presented here, as for reference, though air is not likely to be used as a HTF in the field. For all the cases shown below, an overall 150 K temperature difference is chosen between the inlet and outlet for the HTF.

[0070] Radial and temporal temperature variations for the capsule are presented in the figures herein. The governing equations and boundary conditions are very similar to the ones described above. Since the 100 mm diameter cylinder EPCMs are likely to have the longest times for charging (energy stored into PCM) and discharging (energy to HTF), the temperature profiles are presented for these in the graphs of FIGS. **5-8**.

[0071] The time it takes for the radial diffusion through and melting of all the PCM is presented in the Tables below as functions of EPCM capsule diameter during the charging (energy into the PCM) process. The heat transfer fluid that brings thermal energy to the PCM can be any suitable HTF for the operating temperature of the system. In some embodiments, the HTF is air. In other embodiments, it is a liquid such as a VP-1 like fluid liquid. "VP-1" is a brand of heat transfer fluid that is a Biphenyl Heat Transfer Fluid currently used in Trough solar plants but is limited to 390° C. As used herein, "VP-1 like" means the HTF possesses a high capacity for absorbing and transferring thermal energy, without degradation of its chemical structure and desirable chemical and physical properties. By way of non-limiting example, such desirable properties include chemical inertness, flowability, and viscosity of 750° C. Air is compatible and will be used in future thermal energy storage system experiments. Another compatible liquid-state HTF is XL-1.

[0072] A preferred EPCM configuration is a long (L/D ~15) aspect ratio cylinder, such as a 75 mm diameter and 1125 mm long EPCM module filled with PCM. The charging time for the $MgCl_2$—NaCl eutectic is longer than those for $NaNO_3$ primarily because the HTF temperature is much closer to the phase change temperature (444° C.) of the eutectic temperature. These times as well as the axial progression of the freeze front (and energy retrieval rate from PCM) can be controlled with judicious choices of HTF flow parameters.

Charging Process:

[0073]

TABLE E

Total Heat Transfer Times for Charging Process (Minutes) in a Cylindrical EPCM Capsule Using Air as Heat Transfer Fluid

Diameter	Eutectic Salt/Carbon Steel Capsule	Sodium Nitrate/ Stainless Steel Capsule
10 mm	7.1 min	5.8 min
25 mm	34.5 min	25.7 min
50 mm	109 min	78.3 min
75 mm	214 min	152 min
100 mm	350 min	245 min

TABLE F

Total Heat Transfer Times for Charging Process (Minutes) in a Cylindrical EPCM Capsule Using VP-1 like fluid as HTF capable of 550° C.

Diameter	Eutectic Salt/Carbon Steel Capsule	Sodium Nitrate/ Stainless Steel Capsule
10 mm	1.1 min	0.7 min
25 mm	9.4 min	5.1 min
50 mm	40.5 min	22.5 min
75 mm	93.3 min	52.3 min
100 mm	167 min	94.5 min

Discharging Process:

[0074]

TABLE G

Total Heat Transfer Times for Discharging Process (Minutes) in a Cylindrical EPCM Capsule Using Air as Heat Transfer Fluid

Diameter	Eutectic Salt/Carbon Steel Capsule	Sodium Nitrate/ Stainless Steel Capsule
10 mm	4.8 min	8.2 min
25 mm	16.8 min	41.8 min
50 mm	44.6 min	145 min
75 mm	79.6 min	300 min
100 mm	120 min	502 min

TABLE H

Total Heat Transfer Times for Discharging Process (Minutes) in a Cylindrical EPCM Capsule Using VP-1 like fluid HTF capable of 550° C.

Diameter	Eutectic Salt/Carbon Steel Capsule	Sodium Nitrate/ Stainless Steel Capsule
10 mm	0.3 min	1.8 min
25 mm	1.2 min	16.6 min
50 mm	4.5 min	73.7 min
75 mm	9.8 min	171 min
100 mm	17.1 min	309 min

[0075] From the times presented, it is seen that the discharge time of 309 minutes is approaching the 6.3-hour storage anticipated, although these results can be engineered to be different with a judicious choice of flow rates and inlet temperatures. Though these times as well as the axial progression of the freeze front (and energy retrieval rate from PCM) can be controlled with a judicious choice of HTF flow parameters, 75 diameter capsules are currently considered the more conservative design.

[0076] Modeling of Heat Transfer. Heat transfer modeling of the EPCM for various PCM and encapsulation materials has been completed for phase change and melt front propagation in the capsules. The analysis yielded results as well as tools that can be used for optimization of heat transfer in the future. It is seen that for all anticipated solar thermal energy storage scenarios considered here, heat transfer and melting or freezing of the EPCM are not likely to be the limiting criteria. The heat transfer modeling and methods are important tools for predicting the anticipated behavior of PCM in the EPCM in the context of desirable HTF. The examples chosen here in no way limit the methods and techniques to the much higher 750° C. that the current storage methods can be applied to with the use of $MgCl_2$ filled EPCM.

[0077] Selection/Fabrication of Exemplary EPCM. The encapsulating material of EPCM pellet is required to withstand stresses associated with thermal expansion, volume change by phase change of the PCM-Zinc, $MgCl_2$—NaCl eutectic, or $NaNO_3$ salts. Cost analysis will play a big role in selecting the PCM to be used and the choice of encapsulating material will depend on compatibility between the phase change material and the encapsulating material. Based on material compatibility considerations, it is anticipated zinc can be encapsulated with 316 stainless steel or nickel, the chloride salts are best encapsulated with 1018 carbon steel, and sodium nitrate does well with 316 stainless steel. The stress analysis and shape of the encapsulated phase change material (EPCM) capsules are scalable and thus the present discussion related to stress analysis and encapsulation is done with regard to nickel with the resulting conclusions having broader implications.

[0078] The EPCM capsules will have to withstand the stresses due to volume increase of PCM as well as external forces such as those due to stacking, local crimping or denting of the encapsulation material. As the zinc is heated and melts, there will be volume increase subjecting the encapsulating zinc to elastic as well as plastic stresses. Elastic stress analysis has been conducted using closed form solutions and Elastic/Plastic stress analysis using Abaqus has been conducted. This stress analysis determines the thickness of the encapsulating material.

[0079] The material selections for the proposed EPCM systems were done after an exhaustive search of literature from purely theoretical considerations. The validity and practicality of those considerations are tested by shape the encapsulating material for the EPCM. The actual form/shape of the EPCM will be determined after further research—for example, the size and wall thickness of the encapsulation from stress analysis as well as what is feasible in the industry. Actually, large-scale manufacturability will be a key criterion in making this choice. We started with the analysis of the near spherical Zn—Ni system and then applied the findings to the more complex shapes as necessary, but always keeping cost as an important deciding parameter.

[0080] Material Properties and Assumptions. The material properties of the nickel shell are shown in the Table below.

TABLE I

Properties of Nickel

Density	8880	kg/m^3
Modulus of Elasticity	207	GPa
Yield Strength	59	MPa
Poisson's Ratio	0.31	
CTE	13.1	μm/m-° C.
Specific Heat Capacity	460	J/kg-° C.
Thermal Conductivity	60.7	W/m-K

[0081] Strain hardening was assumed at 30° from the perfectly plastic case; therefore, the stress-strain relationship looks as shown below. This assumption was made because reliable data could not be found for the plastic deformation of nickel. The present assumption hopefully is more conservative than the perfectly plastic case and, thus, should be safer and appropriate.

[0082] Stresses for Ni thicknesses of 50 to 250 micron spherical shells are considered with elastic as well as plastic strain. The results (e.g., FIGS. **14-16**, et al.) are for elastic case of a spherical shell. The results are obtained using FEM analysis using Abaqus program.

[0083] As the zinc liquefies and expands by about ten percent in volume, the expansion of the zinc inside the nickel shell could have estimated 3% strain due to (~10% volumetric expansion) the thermal expansion of the zinc. This involves elastic-plastic deformation and is analyzed using Abaqus. Since this strain was initiated with equivalent forces inside the sphere, the model could be simplified by simply exerting an internal pressure inside the nickel shell until it reaches a value of 3% strain. The axisymmetric case was used for this model. The differences in the stresses at 3% strain for the

different shell thicknesses were minimal, showing that the shell will ideally be able to stretch to 3% strain regardless of thickness. The figures show the maximum principal stresses and strains from the 250-micron thickness case of the spherical shell, the deformation of the figures is multiplied by a factor of 2.209 and to exaggerate the effect of the internal pressure. Results for these plastic deformations are given in FIGS. **15** and **16**.

[0084] The above results indicate that 250-micron Ni shells could withstand the expansion forces involved. Preliminary indications are that we will need at least 250 microns of Ni thickness. The ability of the commercial manufacturers to generate 250 microns or thicker shells for encapsulation has been investigated in detail and it appears that at present commercial manufacturers cannot generate such 250-micron thick encapsulations. Additionally, encapsulation of Zn with stainless steel or Nickel may have considerations dealing with the formation of intermetallic compounds between the PCM and encapsulating material and issues related to that are discussed in the next sub-section.

[0085] The encapsulation details are discussed in more detail in the next section with an alternative and more economical approach to fabricating the Zn—Ni EPCM capsules or rods. Encapsulation of PCM in the form cylinders with thickness sufficient to withstand anticipated stresses could be the most economical way of making EPCM. The preferred encapsulating material is stainless steel for Chloride and Nitrate salts, and carbon steel for chloride eutectics.

[0086] Intermetallic phase formations and related solutions. The melting and solidification of the zinc inside the metal encapsulation material is somewhat analogous to galvanizing, wherein a metal is exposed to molten zinc and coated with it as the zinc freezes. The galvanization process results in the formation of binary phases with the substrates exposed to diffusion in the liquid zinc [1-5]. A couple of relevant papers that describe the interaction of liquid zinc and stainless steel and nickel provide us some guidance in this regard. Unlike in an ordinary galvanizing, the phase change material (PCM) in the thermal energy storage system will undergo multiple melting/solidification cycles. A measurement system to better understand the phase formations is described below.

Solutions

[0087] The formation of these phases will depend on the amount of metal that can be diffused across the layers of interest. If a phase that does not melt at the operating temperature is formed, the diffusion through that solid phase will be several orders of magnitude smaller. This is the approach that this work is taking to form phases that have much higher melting points than the operating temperature of 450° C. Thus, we would like to condition each of the cylinders so that there is a very small layer of intermetallics that will severely slow or stop further diffusion between the liquid zinc and substrate. Conditioning will involve heating complete cylinders (containing zinc and completely sealed) to the system's operating temperature of 450° C. and holding for a designated time, then cooling the cylinders to room temperature. A series of small intermetallic layers should form that will not melt upon reheating the cylinders. The outermost layer should be comprised of a large amount of zinc and a much smaller amount of some alloying element coming from the containing material. This layer should limit further diffusion upon reheating and re-melting.

[0088] The Ni—Zn binary phase (FIG. **17**) indicates just such feasibility. For Zn percentages of about 85 and 90 percent, g and d phase that can be formed have melting temperatures of about 490° C. and 881° C. We hope to take advantage of this feature by the formation of the g and d phases inside the EPCM pellet with a brief exposure of molten zinc to the nickel encapsulation.

Material Selection—(Ni, SS316L, Ti-6-4, 1018, Cu, Grey Cast Iron)

[0089] Six different types of material were selected to encapsulate the zinc. The materials are nickel, stainless steel 316L, titanium-6 aluminum-4 vanadium, 1018 plain carbon steel, copper, and grey cast iron. These materials were selected based upon literature, materials that are galvanized, common engineering materials, general availability, and their high melting points. Aluminum alloys were also considered, but were discounted because of their relatively low melting temperatures (~600-660° C.) and their strength at 450° C. decreases significantly. Inconel type-high temperature Ni based alloys are also being considered.

Material Testing (Rods in Liquid Zn)

[0090] The interactions of the six encapsulating materials with liquid zinc were tested. A custom nine-well crucible was fabricated to hold all of the test specimens. 99.997% pure zinc inserts were machined to fit in each well of the crucible and one, two inch long, 0.5 inch in diameter rod of each material was fit into the zinc insert as shown in FIG. **18**. The test apparatus was placed in an L&L Special Furnace and heated to 450° C. where it was held for eight hours then cooled to room temperature in the furnace.

Analysis of Phase Formation Tests

[0091] Each of the six specimens were sectioned, mounted, and metallographically prepared for light optical and electron microscopy. Examination by light optical microscopy showed that intermetallic layers formed in each specimen between the rod and the zinc (FIG. **15** for Zn—Ni). The layer thicknesses ranged from 200 um-300 um in the nickel/Zn specimen to 3000 um in the grey cast iron/Zn specimen. The iron based specimens showed signs of in homogeneous and non-uniform layer growth. Stainless steel 316L demonstrated the least uniform layer growth. The nickel/Zn, copper/Zn, and Ti-6-4/Zn specimens demonstrated the most layer growth. These specimens also formed the most amounts of layers.

[0092] Energy Dispersive Spectroscopy (EDS) was performed on the copper/Zn and nickel/Zn specimens using a Hitachi 4300 Scanning Electron Microscope equipped with an EDAX system. Line scans were made across the intermetallic layers of each specimen extending from the copper or nickel rod into the zinc. The plots of K alpha peak intensity versus distance show that there are discreet peak intensity steps at the interfaces of each layer. This suggests that there are corresponding compositional changes at the interfaces.

[0093] Electron Probe Microanalysis (EPMA) was then performed on the SS316L/Zn and Ni/Zn specimens to determine the compositions in weight percent of the intermetallic layers and this confirmed the presence of the thin layers of various phases. It was found that the composition across an individual layer was relatively constant.

[0094] Three to four intermetallic layers were present in the Ni/Zn specimen as evident in DIC Figures and EPMA mea-

surement confirmed this observation. Only very small changes in concentration were observed traversing across each layer. Significant changes in concentration were present on either side of an interface as seen in FIG. **19**. As mentioned above, take advantage of the thin layers of phases formed that have much higher temperature than an anticipated operating temperature of a heat storage or heat transfer system.

[0095] Selection of Materials for Salt-based EPCM. Salts are suspected of being quite corrosive in the presence of air/Oxygen under normal circumstances and even more so at high temperatures if proper material choices are not made. The choice of material to encapsulate $MgCl_2$—NaCl eutectic and $NaNO_3$ is based on past experiences. Stainless steel-304 is known to have good compatibility with Nitrate salts. This is known from its use for Thermocline tanks that contain $NaNO_3$—KNO_3 eutectics in solar industry. Stainless steel-304 as well as carbon steel-1018 have been used for the encapsulation of $MgCl_2$—NaCl eutectic. Stainless steel-304 appears to work well (with no air/Oxygen) and we expect carbon steel-1018 also to be compatible if care is taken to avoid air/Oxygen inside the capsule where the chlorides are in contact with the encapsulating materials. The inventors contemplate studying the long-term corrosion and compatibility of the salts with the corresponding encapsulating materials.

[0096] Selection of Materials for Fabrication of EPCM. Methods for the encapsulation of Zinc using Nickel were analyzed based on state-of-the-art of the electroless process and manufacturing capabilities of the industry. Encapsulation shape and thickness were optimized and cylindrical capsules (25 to 100 mm dia.) with long lengths (L/D>10) were determined to be the best. Current industrial state-of-the-art does not permit large-scale economical means of generating electroless layers of the desired thickness (>250 to 500 microns). Encapsulation of PCM in welded cylindrical shells has been determined to be the most economical way of manufacturing EPCM. The thickness of the encapsulation (~1.5 mm) is determined from weldability and stress criteria. This will generate safe encapsulation of PCM and economical EPCM for thermal energy storage particularly in large quantities. Stainless for $NaNO_3$ and stainless steel and carbon steels are seen to be acceptable as encapsulation materials for the $NaNO_3$ and $MgCl_2$—NaCl eutectic PCM.

[0097] Fabrication of Sample EPCM. As the PCM is heated and melts, there will be significant volume increase subjecting the encapsulating PCM to elastic as well as plastic stresses. These stresses depend on the geometry, amount of air in the pellet and material properties. The actual form/shape of the EPCM is determined using potential stresses in the nickel encapsulation based on stress analysis described in an earlier section, e.g., the size and wall thickness of the encapsulation based on FEM stress analysis. The phase formations for the PCM-Encapsulation combination (e.g., Zn—Ni) need to be taken into account. Large-scale manufacturability will be an additional key criterion in making the choices for the EPCM system for thermal energy storage. The current emphasis is on the development of cylindrical Zn—Ni EPCM pellets keeping cost as an important deciding parameter.

[0098] Material Properties and Assumptions. The below discussion related to stresses in and the strength of the encapsulation is given with Nickel as the example material. The resulting discussion and results are applicable to other encapsulating materials just as well in a broad sense.

[0099] The material properties for the nickel, shell or encapsulation material, used herein have been discussed in a previous section. Strain hardening was assumed at 30° off the perfectly plastic case for stress-strain relationship. This assumption enables a more conservative design. Three different designs for the Ni—Zn ECPM containment vessels encapsulating the PCM have been investigated. The investigated shapes are spherical nickel shell, stainless steel cylindrical shell with crimped and welded ends, and a stainless steel cylinder with caps welded on the ends.

[0100] The spherical nickel shell design enables the largest possible surface area-to-volume ratio and maximizes heat transfer. In the electroless process the nickel shell is formed by electrically covering zinc spheres with a nickel. Very little void space (also referred to as "air gap") is provided or assumed in the EPCM. Zinc would substantially completely fill the nickel shell and the thermal expansion of the zinc over the melting process would cause the nickel sphere to experience a strain value of 3% for an overall 10% expansion of the PCM. The stresses in the nickel shell resulting from the expansion of the zinc, along with the effects of any imperfections in the nickel shell and external point loads have been investigated. Stress distributions for some of the cases investigated are shown in FIGS. **20** and **21**.

[0101] The 250 micron thick nickel shell, the thickest shell simulated in these examples, does not seem to be sufficient because the stresses resulting from point forces, dents, and thinning in the shell reach values of approximately 80 MPa. Furthermore, a crack in the outside of the shell could cause stresses surpassing 100 MPa. In each of the simulations only one of these problems is taken into account, whereas in the actual part, multiple inconsistencies and forces will be present. Modeling only a single crack, dent, thinned area, or point force into account does not show what will happen if all of these effects are acting together. If the spherical shell has a crack in it, then thinning of the shell as it plastically deforms while a point force is pushing on the shell at another point, the shell will definitely fail. Also the shell cannot be guaranteed to be manufactured perfectly; therefore, it is likely that imperfections such as thinner sections in the shell are a possibility. Even if the shell is manufactured perfectly, dents, cracks, and scratches could be formed on the shell when the balls are poured into the container for the actual system.

[0102] Electroless Coating Manufacturing of EPCM. The electroless process is usually a batch process used mainly for small quantities of the substrate material to be coated. Though Zinc is expensive, it is currently our primary material of choice. A continuous electroless technology is envisioned here. The proposed process will use a mesh type belt which will agitate Zn balls in electrolyte allowing them the most uniform coating possible. The speed of the electroless process is an extremely important process parameter and will be controlled by the speed of the belt (closed loop process control). Chemical composition of the electrolyte used in the electroless process needs to be controlled, and during the process, electrolyte needs to be replenished to maintain constant composition. The belt will be made of a material that does not impede the electroless deposition and does not accept Nickel coating. These requirements are not very complicated in principal, but on the other hand, it needs attention to detail and cost considerations as the systems are scaled up for the uniform Nickel deposition on Zn balls. The 229 million kg of Zinc in the form of 8 million 0.01 m balls will need to be coated with about 10 microns thickness of Nickel layer.

This will entail the use of five 10 m×1 m×0.25 m tanks; the process control system to complete this process in about 2 months. The cost of the tanks, controls and the Nickel in the form of electrolyte to coat the balls will cost approximately $200K, which is not prohibitively expensive for the benefits anticipated here.

[0103] The secondary PCM of choice are the eutectic salt mixtures ($MgCl_2$—NaCl 38 wt %-62 wt %) that are likely to be quite inexpensive but may have a short service life due to potential segregation of the two media. They will be encapsulated in 2.5 m long, 0.02 m (2 to 5 cm) diameter tubes made of metallic corrosion resistant material such as stainless steel. The total 33,000 m3 of salt mixtures needed (for the 26 Tera J) will be melted and injected into 2.5 m long tubing, which will be first flattened and joined by the homogenous welding process. In order to make this approach economically attractive the rolled 0.001 m thick sheet of 316 stainless steel will be split into tapes, which will then be roll formed and welded to produce the welded tube of 0.02 m diameter. After molten salt injection, the top end of the tube will be flattened and welded to ensure encapsulation of the salt mixture. The custom made robotic welding equipment, cost of salts and welding tube fabrication is estimated to be about $4 million (not part of current project budget) and thus this project will only look into the design of such systems.

[0104] Crimped Cylinder. The crimped and welded stainless steel cylinder design is considered as a potential geometry for encapsulating the PCM. It enables easy large-scale manufacture and provides large surface area-to-volume ratio. The encapsulation was formed by crimping and welding one end of a cylinder, filling approximately 80% of the cylinder with zinc powder, and then crimping and welding the other end of the cylinder. The stresses on the inside of the vessel at the point where the weld is located were investigated because this is where the stress magnitude is largest. The stresses are highest at the weld line because the sharp corner created by the crimping process creates an area of point loading and a stress concentration. See FIG. **22**.

[0105] The stresses in the crimped cylinder will be in the elastic range for the cases of 70%, 80%, and 85% initial zinc content at a temperature of 450° C., with the compressive stresses shown on the inside of the crimped cylinder and tensile stresses shown on the outside of the crimped cylinder. The stresses calculated using the pressures found with the combined gas law for the 70%, 80%, and 85% initial zinc content cases are 0.37, 0.58 and 1.31 MPa, respectively. The stresses found on the outside of the crimped cylinder at the seam at the end of the crimped and welded section of the crimped cylinder are compressive because the crimped and welded section does not expand outwards due to the internal pressure like the rest of the crimped cylinder does; therefore, as the crimped cylinder expands, it pushes on that seam, pulling on it on the inside and pushing on it on the outside.

[0106] At 86% initial zinc filling the internal pressure is 2.03 MPa, and the stresses in the crimped cylinder will be higher than the yield strength of the type 316L stainless steel, which is 125.8 MPa at 450° C. When plastic deformation was taken into account, the difference between the elastic and plastic models was found to be extremely small because at such a small amount of plastic strain, the stresses will always be relatively the same.

[0107] The maximum stress values occur on the inside of the weld lines of the crimped cylinder because the internal pressure becomes a line load on the seam of this section. The stresses in the rest of the crimped cylinder are well below the stresses at these maximum points and the maximum stresses are also much lower than the failure stress, which is 423 MPa.

[0108] The crimped cylinder would be the perfect container to use in the thermal energy storage system; provided the stainless steel container can be filled with zinc easily. This could be done by filling the cylinder crimped on one side with molten PCM and then welding the other end after the PCM has solidified. Another way to fill the crimped cylinder would be with small (5 mm or 0.25") solid pieces of zinc. The crimped cylinder geometry is a viable encapsulation method.

[0109] Capped Cylinder (welded cylinder). The capped stainless steel cylinder design made use of traditional machining processes and the strength of the cylinder in the hoop-wise direction. One cap is initially welded onto the cylinder, and then a rod of zinc is inserted into the cylinder, which is followed by the welding of the second cap. Void space was left between the zinc rod and the steel cylinder so that air pressures inside of the part could be controlled and do not reach levels that will cause failure in the part. The stresses were investigated on the inside of the cylinder around the corner where the weld line of the cap is located. The stress concentrations caused by the point loading on the outside of the cylinder when the cylinders are stacked in the full system were also investigated.

[0110] A two-dimensional model of the cylinder showed that an infinitely long cylinder would not be subject to failure by the stresses caused by each of the different loading cases. The addition of point loads shows that the stack size could be over 1,500 cylinders without causing the hoop stresses to reach the ultimate stress of the material. The actual forces will be less since real loading will be non-point type and precautions can be taken to ensure that there are no more than about 1,000 cylinders exert weight onto the lower cylinders. The side forces caused by the expansion of the cylinders adjacent to the cylinder in question or the edge of the system could be ignored because they will not be very large compared to the points loads caused by the weight of the balls. Also, in the actual system, the cylinders will not be perfectly stacked as shown in the model; rather, they will be poured into the system and will arrange themselves randomly. An aspect ratio close to one would ensure that the distribution is random. Other considerations may also govern the aspect ratio of the EPCM cylinders. As explained later, manufacturing cost considerations could favor long aspect ratio EPCM cylinders proving for a rod bundle geometry for the thermocline as opposed to a packed bed.

[0111] A three-dimensional model of the cylinder shows that the stainless steel cylinder will be able to handle the stresses caused by the expansion of the zinc in the axial direction, the tangential direction and the area directly surrounding the inside corner of the welded cap. The weld at the cap of the cylinder was assumed to be perfect in this model, where the weld creates a continuous part, without any change of material properties. Any zinc that contaminates the weld would weaken the weld. During the welding process, melted zinc can possibly form cyanide; therefore, safety precautions must be taken. The capped cylindrical geometry and container made of 304L stainless steel for the encapsulation of zinc as the phase change material appears to be the most viable option for thermal energy storage. It can withstand the

stresses caused by the internal pressure and also the external loads applied on it by the surrounding cylinders in the system.

Fabrication of Sample EPCM.

[0112] $MgCl_2$—NaCl Eutectic and $NaNO_3$ Salts. The melting temperatures of NaCl or $MgCl_2$ are 804° C. and 714° C., respectively. These temperatures are well beyond the current range of interest for thermal energy storage. Fortunately, the eutectic composition of 55 wt % $MgCl_2$-45 wt % NaCl has a melting point (444° C.) that is very near the temperatures of interest here. The phase diagrams for these chloride salts from two references are included in the figures below. Thermal energy storage and retrieval at 444° C. with $MgCl_2$—NaCl eutectic as phase change material (PCM) can enable very good efficiency for the Rankine cycle.

[0113] We have completed a significant amount of work related to the manufacture of $NaNO_3$ EPCM and proof of their ability for thermal energy storage. $NaNO_3$ has been used in the solar industry for thermal energy storage but usually using sensible heat only. $NaNO_3$ has a significant heat of fusion and thus in the present work, $NaNO_3$ is used as a phase change material enabling significant savings in the overall cost of thermal energy storage systems. The steps for the successful use of the salts for thermal energy storage will include the preparation of the $MgCl_2$—NaCl eutectic or preparation of $NaNO_3$, manufacture of the salt based EPCM with appropriate encapsulating materials, and the testing of the EPCM for storage and retrieval of thermal energy. These steps are described below.

[0114] Initial eutectic salt synthesis. To prepare the chloride eutectic, 99.0% GR ACS grade NaCl and 99% Anhydrous $MgCl_2$ (manufacturers: EMD and Alfa Aesar, respectively), two solid crystalline powders were mixed in an alumina crucible with an Ar blanket. The powder mixture was heated to 500° C. (well below the respective melting points of 804° C. and 714° C.) and allowed to soak at this temperature for an hour, above the eutectic temperature (445° C.$<T_e<$450° C.—based on the phase diagrams). The eutectic was formed under these conditions resulting in crystalline powder. The resulting eutectic has a melting point of 444° C. as proven below.

[0115] Proof of Eutectic Composition. Differential Scanning calorimetry (DSC) was used to determine the melting point of the synthesized $MgCl_2$—NaCl eutectic salt. The results of the DSC measurements are quite consistent with the data in the phase diagrams shown above. The melting point, determined by peak analysis was found to be approximately 444° C. which is within 1° C. of the published/reported value of 445° C. The DSC scans for the chloride eutectic are shown in FIG. **26**.

[0116] Manufacture of EPCM Cylinders for the $MgCl_2$—NaCl Eutectic and $NaNO_3$ Salts. Several cylindrical capsules to contain the PCM salts have been made. Stainless steel capsules with dimensions: D1"×H2" and 0.065" wall thickness were made with two different caps welded to the open ends of a SS304 tube. In another design, one cap was made with a (tapered) threaded hole to allow for a 1/16 NPT pipe plug. This opening allows the PCM salt (in powder form) to be poured into the capsule. This was done to avoid heating $NaNO_3$ to weld temperatures, which is considered potentially dangerous.

[0117] NaCl and $MgCl_2$ solid crystalline powders were mixed together in the eutectic ratio (55 wt % $MgCl_2$ to 45 wt % NaCl) and heated to 550° C. and allowed to completely melt. The molten salt eutectic was poured into the carbon steel cylinder. The cylinders were filled only to a predetermined 'fill-line' to ensure sufficient space for the expansion of the PCM in the capsules.

[0118] $MgCl_2$—NaCl eutectic encapsulated cylindrical capsules were made with stainless steel (304) as well as carbon steel (1018) encapsulation to look into compatibility issues. To increase the proportion of the mass of PCM compared to the encapsulation, and to test EPCM cylinders that are likely to be used in the field, some larger diameter (3" dia.) and longer capsules were also made and tested.

[0119] The sealed EPCM capsules made with the procedures described above and containing known amount of one of the salts was used for calorimetry to prove the energy storage capabilities of the salts.

[0120] FIG. **29** shows sections of a $MgCl_2$—NaCl eutectic EPCM cylinder with stainless steel encapsulation. The void in the EPCM is purposeful for managing stresses related to expansion. The cross section of the $MgCl_2$—NaCl eutectic EPCM cylinder indicates that the chloride eutectic is good status and so is the stainless steel encapsulation. The sectioning of this cylinder was done after nearly 50 hours of repeated heating and cooling (thermal energy charging into and discharging out) of the cylinder and contents. Further study of this issue is needed.

[0121] Fabrication of Sample EPCM. Elongated cylinders have been determined to be the best shape for EPCM based on several competing criteria. Several cylindrical EPCM capsules of various PCM (Zinc, $MgCl_2$—NaCl eutectic and $NaNO_3$) with appropriate encapsulation materials have been made with diameters of 25 to 100 mm and with lengths up to 125 mm. Thermal energy storage capabilities of the various PCM are tested using the sample EPCM.

[0122] Calorimetric Measurements. The first thermodynamic experiments to evaluate the encapsulated phase change material consist of calorimetric measurements to establish the amount of energy storage that can be actually realized in a single unit of the encapsulated assembly.

[0123] These calorimetric experiments will determine the enthalpy change of the EPCM when it is cooled from ~450° C. (above the melting point of PCM) to ambient room temperature. Thus, energy storage will include sensible heat of solid PCM as well as latent heat of PCM, and sensible heat of liquid PCM as well as sensible heating of encapsulation material. A search for calorimeter suitable for this purpose did not reveal any off-shelf instrument with sufficient accuracy. Therefore, we have designed a calorimeter, of "drop" type, which should provide the desired level of accuracy. FIG. **29** presents a sketch of this calorimeter system. A thin metal container with various layers of thermal insulation is loaded with silicon oil (Siltherm 800 from Dynalene, Inc.), serving as the heat sink. A test unit of the encapsulated PCM is preheated in an oven to the starting temperature of 450° C. , then immersed in the silicon oil. Measurement of the subsequent change in oil temperature permits determination of the enthalpy change of the EPCM sample. Judicious care is required to guard against parasitic heat loss and to correct for mixing power input. A schematic of the precision calorimeter is shown in FIG. **30**.

Calorimeter parts are indicated as --	
1-	Stainless steel container
2-	Sample
3-	Silicon oil
4-	Mixer
5, 6-	Thermistor
7-	Thermocouple
8-	shielding cylinder#1
9-	shielding cylinder #2

[0124] We used about 1.5 gallons of silicon oil (Dynalene Siltherm 800) in the conical stainless steel flask as the working fluid to absorb the heat from the sample. The silicon oil is an excellent liquid with high conductivity coefficient, and its flash point is 315° C., which contributes to ignorable evaporation mass loss in the experiment. A mixer is used to stir the oil when sample is dipped into it in order to get a uniform temperature quickly. Outside of the container, we attach shielding to control heat losses. A PC-DAQ system is used to record the temperature profiles of the sample, silicon oil and ambient air as a function of time.

[0125] The initial sample tested is a cylindrical stainless steel with dimensions of D=0.998"×H=1.828". Samples of EPCM are also tested. The sample is heated to 500° C., and quickly immersed into the silicon oil. FIG. **31** shows the temperature history of the sample, silicon oil and air in the experiment.

[0126] From FIG. **32**, we can see that it just takes a few minutes for the silicon oil and sample to reach equilibrium temperature and decrease together because of the heat loss to the environment. Using an overall energy balance including all energy inputs (mixer power input, etc.) and outputs (heat losses etc.), the actual energy given up by the solid or EPCM is to the silicon oil evaluated. The calorimetry proves the thermal energy storage capability of a single EPCM pellet, and the packed bed experiment to be done in phase 2 will prove the thermal energy storage capabilities of a large mass of phase change material.

[0127] Thermal Energy Storage capabilities of $MgCl_2$—NaCl and $NaNO_3$. Encapsulated phase change material (EPCM) capsules were tested using calorimetry to quantify the energy storage capabilities of the PCM. The calorimeter used for this purpose has been designed and built specifically for this purpose and has been described in the previous section.

[0128] The test procedure consisted of heating the EPCM cylinders in a furnace with tight temperature controls. The cylinders were heated to a temperature well above the melting temperature (thus storing sensible and latent heat) and held for a significant amount of time for steady temperature measurements. The cylinders were quenched in the calorimeter silicon fluid and the energy stored was evaluated based on the temperature increase of the fluid and well-established heat loss data. The overall heat balance is verified to be within 2%.

[0129] Lack of reliable and consistent set of thermal properties of the phase change materials as functions of temperature turned out to be a major difficulty in evaluating the calorimeter data. The most consistent data available has been used here. It is important to note the consistency of the data presented below and its repeatability rather than delve on the fact that the fraction of energy from the PCM calculated is not unity.

TABLE J

Thermal Energy Storage Calorimetry Results for $MgCl_2$—NaCl Eutectic-Stainless Steel and Carbon Steel EPCM

Cycling Number	Energy Transferred to Silicone Oil (kJ)	Energy from Capsule (kJ)	Energy from Eutectic (kJ)	Theoretical Energy from Eutectic (kJ)	Fraction of Theoretical Energy from Eutectic
Expt 1	41.6	21.4	20.2	23.8	0.85
Expt 2	41.8	21.7	20.1	24.4	0.82
Expt 3	41.1	21.2	19.9	23.4	0.85
Expt 4	40.9	21.1	19.8	23.2	0.85
Expt 5 (8 hrs)	42.6	21.6	21.0	24.1	0.87
Expt 6	38.7	21.5	17.2	19.8	0.87
Expt 7	38.9	21.7	17.2	20.1	0.86
Expt 8 (8 hrs)	39.0	21.8	17.2	20.2	0.85

1"Dia × 2" EPCM Capsule

TABLE K

Thermal Energy Storage Calorimetry Results for $NaNO_3$-Stailess Steel EPCM (2"Dia × 5" EPCM Capsule)

Cycling Number	Energy Transferred to Silicone Oil (kJ)	Energy from Capsule (kJ)	Energy from NaNO3 (kJ)	Theoretical Energy from NaNO3 (kJ)	Fraction of Theoretical Energy from Eutectic
Expt 1	215	63.5	152	167	0.91
Expt 2	222	64.5	158	168	0.94
Expt 3	222	65.3	156	169	0.92
Expt 4	214	60.0	154	160	0.96

2"Dia × 5" EPCM Capsule

[0130] The repeatability of the energy stored by the PCM (percentages ~85% and ~92%) is remarkable and the uncertainties in overall energy balance for these experiments are about 2%. To repeat a predicament related to material properties mentioned earlier, the percentages reported are not 100% only because the properties of these materials are not well established in the temperature ranges of interest.

[0131] Calorimetric Measurements. An inexpensive precision calorimeter has been designed and built for testing thermal storage capabilities of the EPCM since none were available for purchase. Encapsulated phase change material (EPCM) cylindrical capsules consisting of Zn, $MgCl_2$—NaCl eutectic and $NaNO_3$ have been manufactured. The encapsulation materials used are stainless steel or carbon steel as appropriate. Calorimetry of Zn, $MgCl_2$—NaCl eutectic and $NaNO_3$ EPCM cylinders have proven the thermal storage and retrieval capabilities of these materials successfully and with repeatability.

[0132] Cost Analysis of Thermal Energy Storage System. Cost analysis of thermal energy storage is described here. The cost analysis has been performed for a 100 MWe plant to have 6.3 hours of thermal storage capability to determine the viability of EPCM based thermal storage systems. The cost analysis has used exactly the same assumptions made by NREL scientists and includes separate cost analyses for Zn, $MgCl_2$—NaCl eutectic and $NaNO_3$ EPCM cylinders used in a large thermal energy storage system (Thermocline). Solar power plant data used here are from two NREL Reports—Nexant NREL/SR-550-40163, July, 2006 and "Parabolic Trough Reference Plant for Cost Modeling with the Solar Advisor Model," NREL Reference subcontractor Report, DRAFT May 11, 2010.

[0133] Cost analysis is based EPCM cylindrical shaped capsules that can be manufactured in large-scale with welding. As described earlier in the report, cylindrical EPCM capsules are the most practical based on stress analysis, also. As a result, the discussion below is related to the cost analysis of cylindrical capsules. Some of the details of the cost analysis are described below followed by the variation of cost of thermal energy storage ($/kWh).

[0134] The analysis for various phase change materials and encapsulation materials is presented here for various diameters and lengths of the capsules. Manufacturing of cylindrical EPCM capsules with large length to diameter ratio turns out to be more cost effective since that involves smaller manufacturing costs. The cost analysis is presented for wall thickness t=1.5 mm. The geometry of the capsule is shown in the figure below.

[0135] Costs are calculated on what it costs to make the EPCM capsules and how many are needed to be in a tank with an appropriate pump etc. (fixed costs).

[0136] Volume of individual capsule,

$$V_{cap} = \frac{\pi D^2 H}{4}$$

[0137] D is the diameter of the capsule, H is the length of the capsule. With t as the wall thickness of the shell the volume occupied by the PCM is

$$V_{enc} = \frac{\pi}{4}(D-2t)^2(H-2t)$$

[0138] The cap that is welded at each end of the capsule is considered to have a wall thickness of t as well. The result of the cost analysis is presented for the diameter of the capsule varying from 25 mm to 100 mm and the length of the capsule varying from 1×D to 20×D.

[0139] The thermal energy stored by the individual capsule, Q_{cap}, can be calculated as

$$Q_{cap}=Q_{pcm}+Q_{encl}$$

[0140] Where the energy stored by phase change material is Q_{pcm} and the energy stored by encapsulation material is Q_{enc}

$$Q_{pcm}=\rho_{pcm}V_{pcm}(cp_{pcm,s}(T_m-T_{min})+cp_{pcm,l}(T_{max}-T_m)+L)$$

and

$$Q_{enc}=\rho_{enc}V_{enc}cp_{enc}(T_m-T_{min}).$$

[0141] Here ρ_{pcm} and ρ_{enc} are the density of the PCM and encapsulation materials, cp_{pcm} and cp_{enc} are the specific heat capacities of the PCM and encapsulation materials and L is the latent heat of fusion. For PCM, the heat capacity of the solid and liquid phase may be different. T_m is the melting temperature of the PCM and T_{max} and T_{min} are the maximum and minimum operating temperature of the storage unit. The material properties of PCM and encapsulation materials considered in the present study are given in the Table below.

TABLE L

Physical properties of PCM and encapsulation materials

	Zinc		Eutectic-Salt		$NaNO_3$		Stainless	Carbon	
Materials	Solid	Liquid	Solid	Liquid	Solid	Liquid	Steel	Steel	Nickel
Density (kg/m^3)	7140		2160		2257		8003	7860	8908
Specific Heat (kJ/kgK)	0.48	0.39	0.86	0.86	1.67	1.78	0.48	0.48	0.44
Latent heat (kj/kg)	112		329		173				
Melting Temperature (° C.)	419		459		308				

[0142] The number of EPCM capsules, N, needed to store 300 MW_{th} (~100 MW_e) for 6.3 hours can then be determined

$$N = \frac{Q_{total}}{Q_{cap}}, \text{ with } Q_{total} = 300{,}000 * 6.3 * 3{,}600$$

[0143] The total cost of the thermal energy storage system (Thermocline unit) is determined from the cost of material making up the capsule (PCM and encapsulation), the cost of manufacturing of the capsule and fixed cost. The fixed cost includes the cost of tanks, heat exchanger, pumps, pipes and controller. The cost of material is calculated as

$$Cost_{mat}=mass_{pcm}*price_{pcm}+mass_{enc}*price_{enc}$$

[0144] Here $mass_{pcm}$ and $mass_{enc}$ are the total mass of the PCM and encapsulation in the storage unit and $price_{pcm}$ and $price_{enc}$ are the price of PCM and encapsulation material. The prices of PCM and encapsulation material are given in the Table below.

TABLE M

Material and tubing costs

Materials	Zinc	Eutectic Salt	$NaNO_3$	Stainless Steel	Carbon Steel	Nickel
Material Price ($/kg)	$2.13	$0.35	$0.62	$3.69	$0.74	$24.21
Tubing Price ($/kg)				$0.50	$0.34	$ 1.00

[0145] The cost of manufacturing of capsules is calculated as

$$Cost_{man}=N*price_{cap}+mass_{enc}*price_{tubing}$$

[0146] where N is the number of capsule, $price_{cap}$ is the cost of welding caps of each capsule and $price_{tubing}$ is the price of encapsulation tubes. The price of tubing for encapsulation materials used in this work is listed in the Table above.

[0147] The fixed cost is determined as the cost of pipes, pumps, controllers, heat exchangers and tanks. The cost of such components excluding the cost of tanks is $2,638,000 (as given in the Nexant NREL report). The cost of tank is determined from the total volume as

$$Cost_{tan\ k} = \frac{V_{total}}{V_{existing}} Cost_{existing}$$

[0148] It is assumed that the cost of tank is proportional to its volume. $V_{existing}$, the volume of the tank of the existing solar power system, and $Cost_{existing}$, the cost of tank in the existing solar power system, are taken from the reference.

$$V_{total} = \frac{N * V_{cap}}{1 - \text{void}}$$

[0149] where 'void' is determined from the arrangement of the capsules in the vessel. The center-to-center spacing between the capsules is taken to be 1.4 D.

[0150] The result of cost analysis is presented in FIG. **33** as a function of the diameter of the cylindrical shaped capsule for H/D of 15 for various combinations of PCM and encapsulation material. The cost ($/kWh) decreases significantly as the size of capsules increases. The eutectic salt and $NaNO_3$ are cost-effective PCM material; they easily met the DOE's target of the $40/kWh. Zinc in a large size capsule with stainless steel encapsulation material is slightly above the cost target.

[0151] The EPCM thermal energy storage system cost is shown in Figure above as a function of length/diameter (H/D) for different combinations of PCM and encapsulation material for D=75 mm. The longer capsules provide more cost-effective storage unit for any combinations of PCM and encapsulation material.

[0152] The cost of the thermal energy storage unit with the costs broken down are shown in the Table below—for material costs, manufacturing costs and fixed costs which include the cost of pipes, pumps, controllers, heat exchangers, tanks, etc. The cost of such components excluding the cost of tanks ($2,638,000) are the same as those used in the Nexant NREL report (reference listed at end).

TABLE N

The breakup of the total cost of the storage unit ($/kWh) for different combinations of EPCM and for D = 75 mm and H/D = 15. The costs categorized as material, manufacturing and fixed (heat exchanger/pumps/tanks etc).

PCM-Shell Combination	Zn—Ni	Zn-Stainless Steel	NaNO3-Stainless Steel	MgCl2/NaCl Eutectic-Carbon Steel
Material Cost ($/kWhth)	80.50	41.97	11.17	4.13
Manufacturing Cost ($/kWhth)	2.87	1.86	2.20	2.38
Tank, Pump and Balancing Cost ($/kWhth)	9.70	9.70	10.82	11.92

[0153] The total cost of EPCM thermal storage system for D=75 mm and H/D=15 is shown in the Table below for the material, manufacturing and fixed costs indicated in the Table above.

TABLE O

The cost of the storage unit ($/kWh) for different combinations of PCM and encapsulation materials for D = 75 mm and Length of capsule 15 D.

PCM-Shell Combination	Zn—Ni	Zn-Stainless Steel	$NaNO_3$-Stainless Steel	$MgCl_2$/NaCl Eutectic-Carbon Steel
Cost ($/kWh)	$93.08	$53.55	$26.62	$20.29

[0154] The Thermal Energy Storage system that uses salts in EPCM combinations are well under the DOE goal of $40/kWh at $27 and $20/$kWh_e$. The storage system using zinc-stainless steel will cost a little over the DOE goal.

[0155] Manufacture Cost of TES. A cost analysis has been performed for a 100 MW_e plant to have 6.3 hours of thermal storage capability to determine the viability of EPCM based thermal storage systems. The cost analysis has used exactly the same assumptions made by NREL scientists. A separate cost evaluation will be conducted for both the Zinc and salt systems. A summary of the analysis is given below.

[0156] Preliminary analysis indicates that the EPCM cost decreases by a factor of 2 for L/D from 1 to 10. Ideal L/D for EPCM capsules is likely to be between 10 and 15.

[0157] The total cost of the thermal energy storage system that includes the cost of the materials, manufacturing costs and costs associated with pumps, tanks, heat exchanger, etc. are shown in the Table below for capsule diameter D=75 mm and length/diameter, H/D=15.

TABLE P

The cost of the storage unit ($/kWh) for different combinations of PCM and encapsulation materials for D = 75 mm and Length of capsule 15 D.

PCM-Shell Combination	Zn—Ni	Zn-Stainless Steel	$NaNO_3$-Stainless Steel	$MgCl_2$/NaCl Eutectic-Carbon Steel
Cost ($/kWh)	$93.08	$53.55	$26.62	$20.29

[0158] The above cost analysis indicates the advantages of large diameters and long aspect ratios (L/D of cylinder) of EPCM. It is apparent salts are likely to make better PCM and cost per kWh to use Zinc may be high. The use of salts as PCM for thermal energy storage can be quite economical and could cost much less expensive than currently used two tank thermoclines that use sensible heat only.

[0159] Determination of the optimum thickness of the Nickel to withstand the anticipated stresses is a critical step. This in turn depends on the diameter of the Zinc pellets which will be based on heat transfer considerations. Additionally, the eutectic behavior of the NaCl and $MgCl_2$ salts will also determine the path for further action. The EPCM based thermal storage system(s) must have potential to cost less than $\$40/kWh_{th}$ in order to be considered viable.

[0160] The best EPCM geometry for economical and effective thermal energy storage is a long cylinder (with L/D ~10 or larger). Cylindrical encapsulated phase change material (EPCM) capsules with Zinc, $MgCl_2$—NaCl eutectic and $NaNO_3$ as phase change material (PCM) have been manufactured. Zinc, $MgCl_2$—NaCl eutectic and $NaNO_3$ EPCM capsules have been tested in a precision calorimeter made for this purpose to test their efficacy for thermal energy storage. All the three PCM (Zn, $MgCl_2$—NaCl eutectic and $NaNO_3$) tested in this project have been shown to store thermal energy well though with different caveats, advantages and disadvantages. Salts used as PCM can have costs significantly below DOE goal of $\$40/kWh_{th}$ and can be much better than current thermoclines that use sensible heat only for thermal energy storage.

[0161] Preliminary designs for testing the PCM currently under consideration are flexible enough to accommodate any of the three PCM described considered above.

[0162] Manufacture Cost of TES. A cost analysis will be performed to determine the viability of EPCM based thermal storage systems. A separate cost evaluation will be conducted for both the Zinc and salt systems.

[0163] The electroless process is usually a batch process used mainly for small quantities of the substrate material to be coated. Though Zinc is expensive, it is currently our primary material of choice. A continuous electroless technology is envisioned here. The proposed process will use a mesh type belt which will agitate Zn balls in electrolyte allowing them the most uniform coating possible. The speed of the electroless process is an extremely important process parameter and will be controlled by the speed of the belt (closed loop process control). Chemical composition of the electrolyte used in the electroless process needs to be controlled and during the process electrolyte needs to be replenished to maintain constant composition. The belt will be made of a material that does not impede the electroless deposition and does not accept Nickel coating. These requirements are not very complicated in principal but, on the other hand, it needs attention to detail and cost considerations as the systems are scaled up for the uniform Nickel deposition on Zn balls. The 229 million kg of Zinc in the form of 8 million 0.01 m balls will need to be coated with about 10 microns thickness of Nickel layer. This will entail the use of five 10 m×1 m×0.25 m tanks, the process control system to complete this process in about 2 months. The cost of the tanks, controls and the Nickel in the form of electrolyte to coat the balls will cost approximately $200K, which is not prohibitively expensive for the benefits anticipated here.

[0164] The secondary PCM of choice are the eutectic salt mixtures ($MgCl_2$—NaCl 38 w %-62 w %) that are likely to be quite inexpensive but may have a short service life due to potential segregation of the two media. They will be encapsulated in 2.5 m long, 0.02 m (2 to 5 cm) diameter tubes made of metallic corrosion resistant material such as stainless steel. The total 33,000 m3 of salt mixtures needed (for the 26 Tera J) will be melted and injected into 2.5 m long tubing, which will be first flattened and joined by the homogenous welding process. In order to make this approach economically attractive, the rolled 0.001 m thick sheet of 316 stainless steel will be split into tapes, which will then be roll formed and welded to produce the welded tube of 0.02 m diameter. After molten salt injection, the top end of the tube will be flattened and welded to ensure encapsulation of the salt mixture. The custom made robotic welding equipment, cost of salts and welding tube fabrication is estimated to be about $4 million (not part of current project budget) and thus this project will only look into the design of such systems. In some embodiments, a plurality of sealed (or resealable) EPCM units are provided to form a thermal energy storage system to operate at multiple temperatures leading to higher exergy capabilities and lower entropy production. Such multiple sealed EPCM units are particularly desirable for partial load operations, and also for sudden changes from energy storage mode to a discharge mode, and vice-versa.

[0165] EPCM Heat Transfer Experiment. An experiment for to quantitatively demonstrate the feasibility of the use of EPCM for the storage of thermal energy will be conducted. The experimental arrangements will consist of three tanks each approximately 0.2 m dia and 0.1 m height. All the tanks will be insulated and the middle tank will be capable of housing different EPCM, Zinc or MgCl2—NaCl with appropriate encapsulating material (Ni or stainless steel, respectively). The total amount of PCM in the middle tank will be about 1.5 Kg (~375 balls) as a packed bed corresponding to around 170 kJ of heat of fusion. Including the sensible heat to be supplied for a charge/discharge experiment that lasts about 60 minutes.

[0166] Air mass fluxes of about 6 Kg/hr (~3.5 SCFM) will be heated to 450° C. in the bottom tank and used to charge the EPCM with thermal energy. During the charge, the PCM changes into the liquid phase thus storing thermal energy. During the discharge process, air through the top tank will be used to remove the energy from the EPCM. The air flow rate and temperatures of the fluid and EPCM bed (or tubes) at

several points in the experiment will be recorded to quantify the energy flow rates and storage precisely using a LabView DAQ system. The transient data for such bed behavior will characterize the bed behavior and may lead to design changes.

[0167] Scale up Heat Transfer Design. The decision process for this proposal is very much based on the potential for the scale up of technologies developed here for large scale implementation of thermal energy storage—for a 100 MWe plant with storage for 24 hours. A review of the past efforts in this area reveals failures in two arena; not being able to store energy at low entropy high temperature (exergy) conditions and not being able to scale up to power plant size applications due to various technical problems.

[0168] The efficiency of the large (26 Tera J) storage system can be discussed in the context of the percentage of energy available during the recovery (discharge) process. The overall efficiency of the storage system is limited by the amount and percentage of heat losses from the outer surfaces of the storage systems to the ambient. The storage systems under consideration will be huge to be able to store 26 Tera J of energy (100 MWe for 24 h or more hours). The amount (mass and volume) of Zinc or salts needed for such storage is huge of the order of 200 million tons. The storage heat exchangers are also going to be quite large of the order of several 30 m×30 m devices. Though the surface areas for the heat losses will be large, with insulation, the surface temperatures will not be high. The storage system at this cost enables the use of solar energy 24 hours a day. The high temperatures (420° C.) that the proposed EPCM operates will enable the generation of superheated steam at 420° C. instead of 380° C. and that in turn will improve plant thermodynamic efficiency by 0.41% with a corresponding decrease in the cost of electricity of $0.0012/kWh.

[0169] Scale up Design. During this stage of the work, processes and procedures for scale up of manufacturing EPCMs will be developed. Some basic ideas for such designs are presented here. This will lead to the design of full size fabrication process for the selected material. Fabrication processes such as tube and extruded can, powder consolidation and laser welding will be evaluated for this application.

[0170] Future Experiments and Activities. The heat transfer into the zinc and the stresses in the encapsulating material will be taken into account in finalizing the EPCM design. Methods described for the encapsulation of zinc will be used to manufacture EPCM in the shops at Lehigh University in sufficient quantities to do heat transfer measurements in a packed bed full of EPCM with hot air (450° C.) to charge the bed material and cooler (300° C.) air to discharge the bed energy. A one dimensional analysis of heat transfer in a bed will be conducted to establish the operating regimes of the bed and ensure that the experiments at Lehigh represent actual field experience. An air flow experiment with packed bed of EPCM pellets will be conducted to establish proof of the concept proposed for this project. The cost analysis of the EPCM based thermal storage system(s) performed in Phase 1 will be updated based on the Phase 2 results and current commodity prices. Performance of EPCM in the bed will prove/disprove the proposed hypothesis and may require design changes to EPCM. The EPCM based thermal storage system(s) must have potential to cost less than $40/kWhth in order to be considered viable. The cost analysis of the EPCM based thermal storage system(s) performed is somewhat dependent upon then-existing material and energy capture and generation costs and prices.

[0171] For sake of completeness, the figures attached and made part hereof are described herein. FIG. **1** illustrates a cross-sectional view of a cylindrical capsule in accordance herewith. FIG. **2** illustrates a schematic of a cross section of a spherical capsule in accordance herewith. FIG. **3** illustrates a graph of temperature distribution of an exemplary capsule in accordance herewith. FIG. **4** illustrates a graph of temperature distribution at the end of a PCM melting process in accordance herewith. FIG. **5** illustrates a graph of temperature variations during the charging heat transfer process for a 100 mm diameter cylinder with sodium nitrate PCM and with air as HTF in accordance herewith. FIG. **6** illustrates a graph of locations of interface between solid state PCM and liquid state PCM during melting process for a 100 mm diameter cylinder with sodium nitrate PCM and with air as HTF in accordance herewith. FIG. **7** illustrates a graph of temperature variations during the discharging heat transfer process for a 100 mm diameter cylinder with sodium nitrate PCM and with air as HTF in accordance herewith. FIG. **8** illustrates a graph of locations of interface between solid state PCM and liquid state PCM during discharging (freezing) for a 100 mm diameter cylinder with sodium nitrate PCM and air as HTF in accordance herewith. FIG. **9** illustrates a graph of stress-strain relationship assumed with strain hardening in accordance herewith. FIG. **10** illustrates stresses, strains and displacements of a 50 micron thick shell encapsulation coating in elastic deformation in accordance herewith. FIG. **11** illustrates stresses, strains and displacements of a 100 micron thick shell encapsulation coating in elastic deformation in accordance herewith. FIG. **12** illustrates stresses, strains and displacements of a 150 micron thick shell encapsulation coating in elastic deformation in accordance herewith. FIG. **13** illustrates stresses, strains and displacements of a 200 micron thick shell encapsulation coating in elastic deformation in accordance herewith. FIG. **14** illustrates stresses, strains and displacements of a 250 micron thick shell encapsulation coating in elastic deformation in accordance herewith. FIG. **15** illustrates elastic-plastic stresses for spherical shell with pressure for 3 percent strain in accordance herewith. FIG. **16** illustrates elastic-plastic strain for spherical shell with pressure in accordance herewith. FIG. **17** illustrates a phase diagram of a Ni—Zn binary system in accordance herewith. FIG. **18** illustrates alumina silicate ceramic crucibles with test specimens for exposure to liquid zinc at 450° C. in accordance herewith. FIG. **19** is an optical photomicrograph that illustrates Differential Interference Contrast (DIC) of a Ni/Zn system as polished using differential interference contrast (The Ni is in the upper left of the picture and the Zn is in the bottom right) in accordance herewith. FIG. **20** illustrates stresses for a pressure-only model with a thickness of 250 micron in accordance herewith. FIG. **21** illustrates stresses due to a triangular crack (top), a straight dent (middle), and a thinned part of the nickel shell (bottom) in a 250 micron thick nickel shell in accordance herewith. FIG. **22** is an isometric view of maximum principal stresses on crimped cylinder due to 70% initial zinc content loading case (left), view of stresses inside of crimped cylinder due to 70% initial zinc content loading case (right), in accordance herewith. FIG. **23** illustrates stress distribution of the 70% initial zinc content pressure only case (left), stress distribution of the 85% (middle), and 86% (right) PCM (zinc) content cases with point loads of

100 particle weights in accordance herewith. FIG. **24** illustrates stress distribution on cylinder of aspect ratio 1 for the 70% initial PCM (zinc) content case; (left) stresses on the outside of the cylinder, (right) stresses inside of the cylinder in accordance herewith. FIG. **25** are phase diagrams of a binary NaCl—$MgCl_2$ system from two separate sources in accordance herewith. FIG. **26** illustrates the comparison of two separate DSC runs to determine the melting point of the 55 wt % $MgCl_2$-45 wt % NaCl eutectic salt. The melting point is determined to be 444° C. in accordance herewith. FIG. **27** illustrates stainless steel capsules for calorimetry tests—with and without the NPT pipe plug in accordance herewith. FIG. **28** illustrates carbon steel (1018) capsule for use with the eutectic salt in accordance herewith. FIG. **29** illustrates sections of a $MgCl_2$—NaCl eutectic EPCM encapsulated with Stainless Steel-304 in accordance herewith. FIG. **30** is a schematic of a precision calorimeter designed and built for use in the present work—all units are inches in accordance herewith. FIG. **31** illustrates a graph of temperature profiles of sample, silicon oil, and air in accordance herewith. FIG. **32** illustrates the geometry of an exemplary capsule in accordance herewith. FIG. **33** illustrates a graph of the cost of storage units ($/kWh) as a function of the diameter of the cylindrical shaped capsule in accordance herewith. FIG. **34** illustrates a graph of the cost of storage unit ($/kWh) as a function of length of the capsule in accordance herewith.

[0172] While this description is made with reference to exemplary embodiments, it will be understood by those skilled in the art that various changes may be made and equivalents may be substituted for elements thereof without departing from the scope. In addition, many modifications may be made to adapt a particular situation or material to the teachings hereof without departing from the essential scope. Also, in the description there have been disclosed exemplary embodiments and, although specific terms may have been employed, they are unless otherwise stated used in a generic and descriptive sense only and not for purposes of limitation, the scope of the claims therefore not being so limited. Moreover, one skilled in the art will appreciate that certain steps of the methods discussed herein may be sequenced in alternative order or steps may be combined. Therefore, it is intended that the appended claims not be limited to the particular embodiment disclosed herein.

1. An apparatus for storing thermal energy, the apparatus comprising:

at least one phase change material;

a capsule containing the at least one phase change material, wherein the capsule comprises an encapsulation material, and wherein the encapsulation material comprises at least one material that is chemically and physically distinct from the phase change material, and wherein the encapsulation material and phase change material are selected to store and discharge thermal energy at temperatures of greater than 450° C. without capsule failure.

2. The apparatus of claim **1**, wherein the capsule comprises an inner chamber for containing the at least one phase change material.

3. The apparatus of claim **1**, wherein the capsule comprises a layer of encapsulation material deposited onto the surface of the phase change material.

4. The apparatus of claim **2**, wherein the inner chamber is substantially completely filled with the phase change material when the phase change material reaches a first preselected operating temperature.

5. The apparatus of claim **4**, wherein the inner chamber is filled to less than about 90 percent of its volume by the phase change material at the first preselected temperature.

6. The apparatus of claim **5**, wherein the preselected temperature is at least about 308° C.

7. The apparatus of claim **5**, wherein the preselected temperature is at least about 444° C.

8. The apparatus of claim **5**, wherein the preselected temperature is about 725° C.

9. The apparatus of claim **5**, wherein the inner chamber is not substantially completely filled with the phase change material when the phase change material reaches a second preselected temperature, the second preselected temperature being lower than the first preselected temperature.

10. The apparatus of claim **1**, wherein the phase change material comprises Zinc, and wherein the encapsulation material comprises Nickel.

11. The apparatus of claim **1**, wherein the phase change material comprises at least one of stainless steel and $MgCl_2$—NaCl eutectic salts, and wherein the encapsulation material comprises at least one of carbon steel or stainless steel.

12. The apparatus of claim **1**, wherein the phase change material comprises at least one of $NaNO_3$, KNO_3, $NaNO_3$—KNO_3, $MgCl_2$, $MgCl_2$—NaCl, $MgCl_2$—KCl, NaCl-KCl, and combinations thereof.

13. The apparatus of claim **9**, wherein a plurality of capsules are provided to form a thermal energy storage system.

14. The apparatus of claim **13**, wherein the thermal energy storage system further comprises at least one fluid in thermal contact with the plurality of capsules, wherein the fluid serves conduct heat from an energy source to the capsules, thereby heating the phase change material to at least the first preselected temperature.

15. The apparatus of claim **14**, wherein the fluid is selected from the group consisting of air, silicones, biphenyls, eutectic salt mixtures such as $NaNO_3$—KNO_3, $NaNO_3$—KNO_3—$LiNO_3$, and combinations thereof.

16. The apparatus of claim **15**, wherein the phase change material, encapsulation material, and heat transfer fluid are selected and arranged to enable storage of thermal energy for at least 6 hours at temperatures of at least about 450° C.

17. The apparatus of claim **16**, wherein the thermal energy comprises energy generated from at least one energy source, the energy source comprising at least one of solar, wind, geothermal, and nuclear, and combinations thereof.

18. The apparatus of claim **17**, wherein the efficiency of the system permits storage of thermal energy at less than about $40 kWh.

19. The apparatus of claim **1**, wherein the capsule comprises an opening that can be operated to adjust the amount of phase change material contained therein.

20. The apparatus of claim **1**, wherein the capsule includes a void space that is determined based upon the thermal and physical properties of the phase change material, the thermal and physical properties of the encapsulation material, and the geometric shape of the capsule.

* * * * *